A STUDY ON SEISMIC STABILITY OF MSW LANDFILLS

Thesis Submitted to AcSIR for the Award of

Degree of

MASTER OF TECHNOLOGY

in

BUILDING ENGINEERING AND DISASTER MITIGATION

by

ANNAPAREDDY VENKATA SIVA RAMAKRISHNA

30EE15A01003

Under the Guidance of

Dr. Anindya Pain
Dr. Shantanu Sarkar

CSIR – Central Building Research Institute
Roorkee-247667

May 2017

CERTIFICATE

This is to certify that the work incorporated in this M.Tech thesis entitled "*A study on seismic stability of MSW landfills*" submitted by Mr. Annapareddy Venkata Siva Ramakrishna to Academy of Scientific and Innovative Research (AcSIR) in fulfilment of the requirement for the award of the Degree of *Master of Technology*, embodies original research work under our guidance.

We further certify that this work has not been submitted to any other university or institution in the part or full for the award of any degree or diploma. Research material obtained from other sources has been duly acknowledged in the thesis. Any text, illustration, table etc., used in the thesis from other sources, have been duly cited and acknowledged.

A. V. S. RamaKrishna
M.Tech Student
AcSIR

Dr. Anindya Pain
Assistant Professor
GE Group
CSIR-CBRI

Dr. S. Sarkar
Professor
GE Group
CSIR-CBRI

ACKNOWLEDGEMENTS

Date: 15th May 2017

Place: Roorkee

A.V.S.Ramakrishna

ABSTRACT

Rapid population growth and urbanization in the developing countries like India had increased the municipal solid waste (MSW) generation in enormous quantities. Engineered landfill is a common technique for the disposal of municipal solid waste, with least damage to the environment as well as public health. As the modern landfills are capable of generating energy from waste, the study on their stability got importance in the recent decades. The failure of landfill causes a severe damage to the environment and public health. A very limited number of numerical and analytical studies are available on the stability of MSW landfills under static and dynamic conditions.

In the present study, robust closed form solutions are developed to compute the acceleration profiles, factor of safety and yield acceleration coefficient of MSW landfills resting on different types of foundation. The effect of inhomogeneity of landfill material is also considered in the present study. In the present study, both linear and equivalent linear analyses are carried out. The acceleration (surface/input) ratios computed in the present study are in good agreement with the DEEPSOIL results. From parametric study, it is observed that the landfill is vulnerable to seismic damage for low frequency input motions. At low frequencies the seismic inertia force at all depths are in phase. The seismic force acting in landfill mass is reducing at higher frequencies. At higher frequencies landfill mass is entering into higher modes of vibration, where some portion of landfill is moving in one direction and the remaining portion is moving in opposite direction. The maximum shear strain generated at low frequencies is significantly higher compared to high frequencies.

The results from present study also showed that the foundation material has a significant effect on the seismic stability of MSW landfills. Obtained results are compared and validated with the similar existing literature. Present method is further validated against a well-documented failure case history under static condition. In addition, an extensive parametric study are carried out to know the effect of all other parameters on the stability of MSW landfills

CONTENTS

LIST OF FIGURES

LIST OF TABLES

ABBREVIATIONS

CCL: Compacted Clay Liner

CFR: Code of Federal Regulations

CPCB: Central Pollution Control Board

CSS: Cyclic Simple Shear

CTX: Cyclic Triaxial

MAM: Microtremor Analysis Method

MASW: Multichannel Analysis of Surface Waves

MHA: Maximum Horizontal Accelerations

MSW: Municipal Solid Waste

OII: Operating Industries Inc.

PI: Plasticity Index

SASW: Spectral Analysis of Surface Waves

SWM: Solid Waste Management

TPD: Tons per Day

NOTATIONS

The following symbols are used in the present work of this thesis.

$a_h(z,t)$	Horizontal acceleration in the waste fill at depth z and time t
G	Shear modulus of solid waste
G^*	Complex shear modulus of solid waste
k^*	Complex wave number
g	Acceleration due to gravity
B	Top width of landfill
H, H_1	Height of landfill components
z	Depth from the top of the landfill
MSW	Municipal Solid Waste
E_{Ha}, E_{Hp}	Horizontal force acting on active and passive wedge at the interface respectively
E_a, E_p	Resultant interwedge force acting on active and passive wedge respectively
E_{Va}, E_{Vp}	Vertical force acting on the side of interface between active and passive wedge respectively
FS	Factor of safety of entire waste mass
FS_a, FS_p	Factor of safety at the base of active and passive wedge respectively
$FS_{min}, FS_{max}, FS_{avg}$	Minimum, maximum and average factor of safety against translational failure
FS_V	Factor of safety at the interface between active and passive wedge
F_a, F_p	Frictional forces developed at base of active and passive wedge respectively
N_a, N_p	Normal reaction at the base of active and passive wedge respectively
k_h	Seismic acceleration coefficient in horizontal directions
k_y	Yield acceleration coefficient
$Q_{Ha},$ and Q_{Hp}	Horizontal inertia forces on active and passive wedges respectively
t	Time
T	Period of lateral shaking
V_s	Shear wave velocity

γ_s	Shear strain
γ_{sw}	Unit weight of MSW
ρ_{sw}	Solid waste density
T	Shear stress
δ_a, δ_p	Interface friction angles at the base of active and passive wedges respectively
ϕ_{sw}	Internal friction angle of solid waste
ξ	Damping Ratio
ω	Angular frequency of motion = $2\pi/T$
η_{sw}	Viscosity of the solid waste
W_a, W_p, W_t	Weight of active wedge, passive wedge and combined weight of both wedges respectively
α	Front slope angle
β	Back slope angle
k	Wave number

1.1 General

Rapid urbanization and sustained development in living standards are the reasons for the generation of huge amounts of municipal solid waste (MSW). According to the information provided by central pollution control board (CPCB), 1, 27,486 TPD (Tons per day) municipal solid wastes are generated in India during 2011-12. Out of which, 89,334 TPD (70%) of MSW is collected and 15,881 TPD (12.45%) is treated. Therefore, there is a need of proper waste management and disposal systems. Presently three methods are in use for MSW treatment and disposal namely; incineration, composting, and landfills (Huang and Fan, 2016). Landfills is the most acceptable method of MSW disposal in most of the countries, as it provides a more convenient and economical way of MSW disposal. Engineered landfills controls the harmful effects by solid waste on humans and environment. But, in the developing countries like India, MSW is still disposing as uncontrolled waste dumps (Reddy and Basha, 2014). Recently, Government of India had announced programs like Swachh Baharat Abhiyan and development of 100 smart cities. To attain such goal, a proper waste management system is required. Recently, Ministry of Environment, Forest and Climate Change (2016), India has set the new rules for solid waste management (SWM) in India. According to the new rules all the local bodies (Municipal corporations, Nagar nigams, Nagar panchayats, Censes towns, Notified areas and Notified industrial townships) should setup the SWM facilities such as waste processing units, sanitary landfills etc. within the time bound mentioned in the SWM, 2016 rules. The modern engineered landfill consists of four main components bottom liner system, leachate collection system, gas collection system, and final cover system. More waste generation and increased land values made the engineers to design higher and higher landfills with very steeper slopes to increase waste filling capacity per unit area. The stability of these landfills is important for continues functioning of leachate and gas collection systems under both static and dynamic conditions.

Several landfill failures case histories may be found in the literature, these data would be helpful to understand the modes and causes of landfill failures (some of the case histories of major landfill failures are explained below). The stability of landfills depends on dynamic

properties of waste mass, landfill geometry, pore pressures generated by leachate and gas, weather conditions, etc.

The subtitle D (40 CFR Part 258, Criteria of Municipal Solid Waste Landfills) of U.S. Federal Resource Conservation and Recovery Act says that. Unless the landfill is designed to resist seismic effects, it is not allowed to locate in seismic impact zone. "seismic impact zone is defined as an area with 10% or greater probability that the maximum horizontal acceleration (MHA) in lithified earth material will exceed 0.1g in 250 years" (Qian and Koerner, 2010).

1.1.1 Case Histories of Major Landfill Failures

Several landfill failures are reported in literature that includes both uncontrolled dumps and engineered landfills. Both rotational and translational failures had occurred and these recorded failures helps to know the effect of different parameters on the stability of landfills. Some of the major landfill failures are briefly descried.

The failure of Unlined MSW Landfill in North America occurred in 1984, which was constructed on saturated fine-grained soil. The mode of failure was the rotational failure through the waste mass involving a quantity of about 110,000 m^3 of solid waste. The identified cause of failure was the immediate raise in the water level within the waste mass due the occurrence of 3 days continues rainfall (Divinoff et al., 1986; Erdogan et al., 1986). The failure of Kettleman Hills Waste Landfill occurred on March 19, 1988. The mode of failure was translational failure along the composite liner system. Very low interface shear strength between waste mass and geo-synthetic materials within the liner system triggered the failure (Mitchell et al., 1990). The failure of Umraniye-Hekimbasi Landfill in Istanbul, Turkey occurred in 1993. The rotational failure plane passed through the waste mass as shown in Fig. 1.1. The quantity of waste mass involved in this failure was approximately 12,000 m^3. The cause of failure was reported as; the gas liberated from the landfill combined with the air and reached to an explosive composition. The sliding of waste mass was initiated due to heavy rainfall and accelerated by explosion (Kocasoy and Curi, 1995).
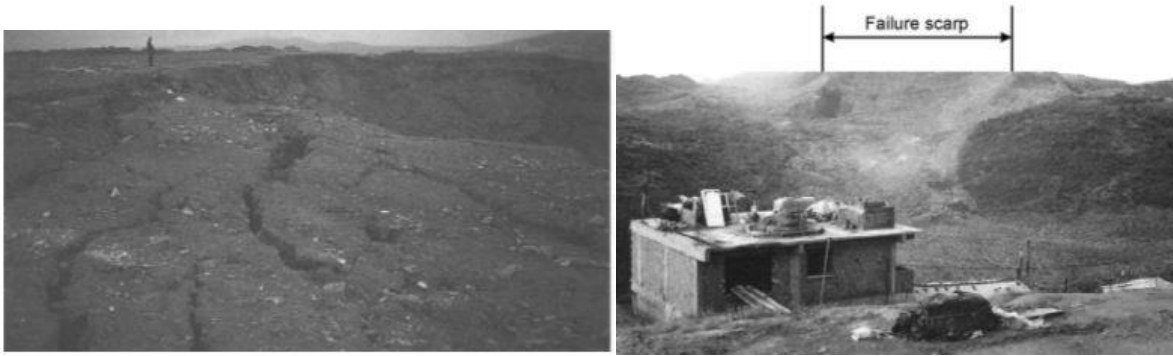
Fig. 1.1 Umraniye-hekimbasi landfill failure in Istanbul, Turkey (Blight, 2008)

The failure of an engineered landfill lined with geo-membrane clay liner in Europe occurred in 1994 involving approximately 60,000 m^3 of solid waste. The translational failure of the landfill occurred along the interface between the geo-membrane and compacted clay layer (CCL). It was reported that the failure causes a displacement of 6.0 m at the top the landfill. The occurrence of failure is due to the excessive wetness at the interface component of geo-membrane − CCL liner system (Ouvry et al., 1995; Koerner and Soong, 2000). The failure of Bulbul Landfill in Durban, South Africa was occurred on September 8, 1997 following rotational mode of failure within the solid waste as shown in Fig. 1.2. The amount of waste mass involved in failure is approximately 180,000 m^3. The reported cause of failure was the development of excess pore pressures due to the accumulation of leachate and water through heavy rainfall (Brink et al., 1999, Blight, 2004).

Fig. 1.2 Failure of bulbul landfill in Durban, South Africa (Blight, 2008)

The failure of a lined landfill in South America occurred in 1997 following a translational mode of failure involving a solid waste of approximately 1,200,000 m^3. It was reported that the failure surface passed through the interface between sand and geo-membrane. The most

likely cause of failure was the increased levels of leachate within the waste mass (Koerner and Soong, 2000). Leuwigajah Landfill in Bandung, Indonesia failed in 2005. The rotational failure involved approximately 2,700,000 m^3 of solid waste. The cause of failure reported in the literature was the development of water pressure in the foundation soil due to heavy rainfall (Koelsch et al., 2005). Xerolakka canyon Landfill in Greece failed in 2010 and involved solid waste of approximately 12,000 m^3. The reasons for the failure were reported as, poor compaction of waste and the absence of daily soil cover, steep slope of the landfill, very high percolation of water through the waste mass during rainfall due to the absence of soil cover and generation of gas pressure within the waste mass (Athanasopoulos et al., 2013).

1.1.2 Seismically Induced Landfill Failures

The earthquakes occurred in the recent years have provided valuable information on the seismic performance of well instrumented landfills. During Northridge earthquake twenty-two landfills, were subjected to ground motions more than 0.05g, out of which eight landfills were geosynthetic-lined landfills (Augello et al., 1995). The observed damages include damage to the cover liners, cracks at the interface between waste mass and ground surface, and changes in landfill geometry (e.g. Cracking to the cover soil was observed at Chiquita Canyon Landfill, California). The cracking may be attributed to the difference in the dynamic properties of weak waste and stiff adjacent ground (Bray et al., 1998).

Fig. 1.3 Liquefaction of Sand at landfill site in Kobe, Japan (Bray et al., 1998)

Gas liners of several landfills were damaged due to earthquake. Gas collection system stops functioning at the instance when gas liners are damaged. Stopping gas collection systems for even short duration may lead to fire or a big explosion.

After Kobe earthquake in Japan, two landfills that were located at a distance of 12 and 20 km from the epicenter of the Kobe earthquake were surveyed. And reported one of the landfill foundations was subjected to sand liquefaction as shown in Fig.1.3 (Akai et al., 1995).

1.1.3 Slope Stability of Landfills under Seismic Condition

Dynamic properties of MSW landfill is needed for carrying out the stability analysis under seismic condition. Dynamic properties of MSW include unit weight, shear and primary wave velocities, shear strength parameters, modulus reduction curve and damping ratio curve. Stability of landfills needs to be addressed during and after landfill operations. The typical failure modes of landfill are listed below (Reddy and Basha, 2014);

- Sliding failure of leachate collection system
- Sliding failure of Final cover system
- Rotational Failure through waste mass, liner, and subsoil
- Rotational failure within the waste mass
- Translational failure along the liner system

The analysis of translational failure of landfills may be carried out using two-part wedge (Qian et al., 2003, Qian and Koerner, 2004) and three-part wedge model (Qian and Koerner, 2010, Feng et al., 2010).

1.1.4 Site Response Analysis of Landfills

The site response analysis is very important to understand the seismic response of the landfills. Seismic response of landfills depends on the dynamic characteristics of MSW and the dynamic properties of the foundation soil. The methods available for the site response analysis are linear, equivalent-linear and non-linear. Commercial software's like SHAKE, DEEPSOIL are used for the site response analysis of landfills.

1.2 Objective of the present study

To develop a robust closed-form solution for the evaluation of seismic stability of municipal solid waste landfills that satisfies the boundary conditions.

1.3 Organization of the Thesis

The thesis has been organized in 6 chapters. In this chapter, a brief introduction on the chosen research topic is given and the objective of the present research work has been defined.

Chapter 2 presents the review of literature on the dynamic properties of MSW such as unit weight, shear wave velocity, primary wave velocity, shear strength parameters, normalized shear modulus and material damping ratio. Literature review on translational failure analysis of MSW landfills, translational failure analysis of landfills with engineered berm and site response analysis of MSW landfills are also presented in chapter 2. This review of literature has helped in identifying the research gaps and planning for the present study.

Chapter 3 describes the proposed modified pseudo-dynamic method for the seismic translational failure of MSW landfills. Expressions for computation of acceleration ratio, factor of safety and seismic yield acceleration coefficient for a typical side-hill type MSW landfill are given. The results for both linear and equivalent linear analysis are presented. The acceleration ratios are compared and validated with the DEEPSOIL results. The factor of safety and yield acceleration coefficients for different combination of input parameters are presented in the form of graphs and tables. The present results are validated by comparing with the similar existing literature and a failure case history from literature under static condition.

Chapter 4 describes the effect of the use of unit weight and shear wave velocity profiles in the computation of acceleration profiles and factor of safety of MSW landfills. The acceleration profiles and the factor of safety values calculated by using unit weight and shear wave velocity profiles in the proposed method. The results are presented in the graphical and tabular forms for different combination of input parameters.

Chapter 5 describes the effect of local site condition on the seismic stability of MSW landfills. Expressions for computation of acceleration ratio and factor of safety for a MSW landfill resting on a foundation soil are given. The results for both linear and equivalent linear analysis are presented. The acceleration ratios are compared and validated with the DEEPSOIL results. The factor of safety for different foundation types and for different combination of input parameters is presented in the form of graphs and tables. The present results are validated by comparing with the similar existing literature.

Chapter 6 repots the conclusions that are drawn from the present research, limitation of the present methodology and the scope for future studies.

2.1 General

The review of literature on the dynamic properties of MSW such as unit weight, shear wave velocity, primary wave velocity, shear strength parameters, normalized shear modulus and material damping ratio are presented in the tabular forms. Literature review on translational failure analysis of MSW landfills, translational failure analysis of landfills with engineered berm and site response analysis of MSW landfills are also presented.

2.2 Dynamic Properties of Municipal Solid Waste (MSW)

The dynamic properties of MSW are very much important to understand the behaviour of engineered landfills or waste dumps during earthquakes. Earthquake damages the landfills by inducing large strains in the MSW. The dynamic properties of MSW are needed for the analysis and design of landfills under seismic conditions. The most important dynamic properties that have direct impact on the response of landfills under seismic conditions are unit weight, shear strength properties, shear wave and primary wave velocities, normalized shear modulus, and damping properties of MSW.

2.2.1 Unit Weight (γ_{sw})

The unit weight of MSW is highly variable from landfill to landfill because of its heterogeneity. It is needed in almost all engineering analysis and design of landfill systems. Unit weight varies along the depth of the landfill as function of waste composition, level of composition, thickness of soil cover and effective overburden stress. So, a characteristic MSW unit weight profile should be used, not the constant average unit weight. The unit weight of MSW also varies with the age of the landfill because of the decomposition of the organic matter and settlement of landfill. The unit weight values of MSW given by different authors are summarized in Table 2.1. The hyperbolic model for unit weight of MSW, which varies with depth maybe expressed as, (Zekkos et al., 2006).

$$\gamma = \gamma_i + \frac{z}{\alpha + \beta z} \tag{2.1}$$

where, γ_i= near-surface in place unit weight (kN/m^3),

z = depth (m) from the top surface,

α (m^4/kN) and β (m^3/kN) = model parameters.

Choudhury and Savoikar (2009a) developed a model for unit of MSW using the data available in literature with the help of curve fitting techniques. The mathematical expression for model is as follows,

$$\gamma_{sw} = \frac{14.46}{\left(1+e^{6.06-0.207z}\right)^{0.064}}$$

(2.2)

where, z = depth from the top surface. The effect of leachate recirculation, saturated waste, and waste degradation on unit weight of MSW are largely unknown (Zekkos et al., 2006).

Table 2.1: Unit weight of MSW for different landfills reported in literature

Reference	Reported unit weight values and remarks
Wiermer (1982)	Unit weight of 6 kN/m^3 at shallow depths and 10 kN/m^3 at greater depths (>20 m).
Henke (1985)	A landfill with MSW and industrial waste had a unit weight of 15.8 kN/m^3.
Landva and Clark (1986)	The unit weight of MSW including soil cover is ranged between 8.1 and 17 kN/m^3.
Pagotto and Rimoldi (1987)	Unit weight of a landfill in Modena (Italy) is 10 kN/m^3.
Shumann (1989)	Density of a landfill containing MSW, construction waste, and excavation waste is 16 kN/ m^3.
Sharma et al. (1990)	Richmond landfill in California had a density of 7.4 kN/m^3, calculated from weighing data and volume change records.
Richardson and Reynolds (1991)	A 12m high landfill had an average density of 12.5 kN/m^3, calculated using test pit method.
Cowland et al. (1993)	Average density of 13 kN/m^3 for 40 m high landfill and 15 kN/m^{3}for 100 m high landfill. Hong Kong landfill had a unit weight of 11.5 kN/m^3, calculated using weight and volume of MSW.

Sanchez-Alciturria et al. (1993)	Meruello landfill in Spain had a density of 11.5 kN/m^3.
Fasset et al. (1994)	Unit weight of MSW ranges from 3 to 16 kN/m^3 depending on level of compaction mentioned below. Poor compaction – 3 to 9 kN/m^3. Medium compaction – 5 to 8 kN/m^3. Good compaction – 9 to 10.5 kN/m^3.
Withiam et al. (1995)	Average unit weight of 11 to 13 kN/^{3} for Dekorte Park landfill in New Jersey, measured using test pits, weight and volume records.
Kavazanjian et al. (1995) and Kavazanjian (2001)	Unit weight varies from 10 to 13 kN/m^3 at surface and 13 to 16 kN/m^3 at a depth of 30 m, measured using the correlation with shear wave velocity; A typical unit weight profile having 12 to 16 kN/m^3 at surface and 14 to 17 kN/m^3 at a depth of 60 with a standard deviation of ± 1.
Machado et al. (1996)	Muribeca landfill in Brazil had a density of $14 - 19$ kN/m^3, measured from water replacement method.
Shimizu (1997)	Density of 7 to 10 kN/m^3 for Port Harbour landfill in Japan.
Konig and Jessberger (1997)	Unit weight of 3 kN/m^3 for uncompacted refuse and 17 kN/m^3 for compacted refuse.
Oweis and Khera (1998)	Unit weight ranges from 9.5 to 17.5 kN/m^3 measured using a bucket auger of 300 mm diameter.
Matasovic and Kavazanjian (1998)	Unit weight varies between 12 to 21 kN/m^3 for OII landfill measured using auger boring, with most values lies between $14 - 18$ kN/m^3.
Watts and Charles (1999)	Density of MSW for three different landfills in UK: Bulk density of 18 kN/m^3 for old landfill in London. Bulk density of 18 kN/m^3 for old MSW landfill in Redditch. Bulk density of 5.4–6.3 kN/m^3 for old MSW landfill at Liverpool.
Zornberg et al. (1999)	Azusa landfill had a unit weight values ranges from 10–5 kN/m^3, measured using 750 mm borehole drilled with bucket auger.
Stark et al. (2000)	Total unit weight of MSW used in the slope stability analysis of Rumpke landfill is 10.2 kN/m^3.
Gomes et al. (2002)	Unit weight for fresh waste is 11.3 kN/m^3 and old waste is 11.6

	kN/m^3, estimated using test pit and borehole techniques respectively.
Pereira et al. (2002)	Unit weight of MSW for Valdemingomez landfill is 5 kN/m^3, estimated using test pit technique.
Caicedo et al. (2002)	The unit weight of MSW for Dona Juana landfill in Colombia is 9.1 kN/m^3.
Geosyntec Consultants (2003)	Unit weight of MSW for 0–3 m is 5–10 kN/m^3; for 3–6 m is 7–17 kN/m^3; and for depths greater than 6 m is 7.7–15.5 kN/m^3 having an average value of 11.3 kN/m^3, using in-situ unit weight tests.
Zekkos et al. (2006)	Unit weight of MSW for 37 different landfills are lied between 3 to 20 kN/m^3.
Zekkos et al. (2008)	Unit weight of 10 kN/m^3 at near ground surface and 16 kN/m^3 at depth, using boreholes for Tri-Cities landfill in Fremont, San Francisco.
Ramaiah et al. (2014)	Bulk unit weight of 11.41 kN/m^3 for Ghazipur landfill in Delhi, India and is estimated by water displacement method.
Ramaiah et al. (2016a)	Bulk unit weight of 10.5 kN/m^3 (Test Pit-1) and 13.5 kN/m^3 (Test Pit-2) for Okhla landfill in Delhi, India.
Abreu et al. (2016)	Unit weight ranges between 9 to 15 kN/m^3 for Sao Carlos sanitary landfill,

2.2.2 Shear (Vs) and Primary (Vp) Wave Velocities

Shear wave velocity is an important property that relates the small-strain shear modulus (G_{max}) and mass density (ρ) using the theory of elasticity. Shear wave velocity reflects the stiffness and density of MSW. It can be measured using several methods such as, seismic refraction (Kholmatov et al., 2007), seismic dilatometer (Castelli et al., 2012), down-hole (Houston et al., 1995), cross-hole (Singh and Murphy, 1990), suspension logging (Matasovic and Kavazanjian, 1998). In addition, surface wave methods includes spectral analysis of surface waves method (SASW) (Kavazanjian et al., 1996), and multichannel analysis of surface waves method (MASW) (Del Grecoetal, 2007). Out of all the above methods, surface wave methods are widely used to determine the shear wave velocity. The shear wave velocity reported by different researchers for different MSW landfills around the world are listed in Table 2.2. The model for shear wave velocity of MSW along the depth of landfill, developed

by Choudhury and Savoikar (2009b) using data of different landfills reported in literature is mentioned below,

$$V_s = \frac{111 + 9.82z^{0.77}}{1 + 0.0012z^{0.77}}$$

(2.3)

Where, z = depth from the top surface. Zekkos et al. (2014) developed an empirical model in hyperbolic form; the mathematical expression is mentioned below,

$$V_s = V_{si} + \frac{z}{\alpha_{V_s} + \beta_{V_s} \times z}$$

(2.4)

where, V_{si} = shear wave velocity at the ground surface;

α_{V_s} and β_{V_s} = model parameters.

Ramaiah et al. (2016b) developed an empirical model for the estimation of V_s at different depths of MSW landfill, using statistical analysis of 146 in-situ MSW V_s profiles from 37 landfill sites from all over the world. The proposed model is mentioned in equation (2.5).

$$V_s = a + bz$$

(2.5)

where, a and b are the intercept and slope of the linear model respectively. The above model is valid up to a maximum depth of 30 m.

Table 2.2: Shear wave velocity values reported by different researchers

Reference	Shear wave velocity ranges, and landfill location	Method
Woodward Clyde Consultants (1987)	Average velocity of 206–244 m/s for OII landfill, California, USA	Seismic refraction
Earth Technology (1988)	A velocity profile varies from 240 m/s at 6 m depth to 270 m/s at 14 m depth for Puente Hills landfill, California, USA	Cross-hole method
Sharma et al. (1990)	198 m/s for a depth of 15.3 m from top of landfill at Richmond, California, USA	Down-hole
Carey et al. (1993)	185 – 478 m/s for Brookhaven landfill, New York	Cross-hole
Kavazanjian et al. (1994)	80 m/s at ground surface and 300 m/s at 30 m	SASW

	depth for landfills in Southern California	
Houston et al. (1995)	124 – 229 m/s up to a depth of 10 m for Northwest regional landfill, Arizona	Down-hole
Kavazanjian et al. (1995)	80 – 300 m/s up to a depth of 75 m for Azuza landfill, California, USA	SASW
Rix et al. (1998)	120 – 165 m/s up to a depth of 25 m for Bolton road landfill, Georgia	SASW
Cuellar et al. (1998)	80 – 170 m/s up to a depth of 15 m for Villalba landfill, Madrid, Spain	SASW
Carvalho (1999)	92 -208 m/s up to a depth of 28 m for Bandeirantes landfill, Sao Paulo, Brazil	Cross-hole and Down-hole
Lin et al. (2004)	85 – 235 m/s up to a depth of 30 m for Tri-Cities landfill, California	SASW
Matasovic and Kavazanjian (2006)	130 – 240 m/s up to depth of 30 m for Olympic View landfill, Washington, USA	SASW
Del Greco et al. (2007)	100 – 180 m/s up to a depth of 22 m for new waste and 120 – 240 m/s for old waste of Alice Castello landfill, Italy	Seismic refraction and SASW
Zalachoris (2010)	82 – 137 m/s up to a depth of 20 m for Austin Community landfill, Texas	SASW
Sahadewa et al. (2011)	98 – 169 m/s up to a depth of 15 m for Arbor Hills landfill, Michigan	MASW
Carpenter et al. (2013)	105 – 180 m/s up to depth of 13 m for Orchard Hill landfill, USA	MASW
Sahadewa et al. (2014)	110 – 250 m/s for Austin Community landfill, Texas	Cross-hole and Down-hole
Konstantaki et al. (2015)	120 – 260 m/s for Wieringermieer landfill, Netherlands	Seismic reflection and MASW
Ramaiah et al. (2016a)	160 – 175 m/s up to a depth of 20 m for Okhla landfill, Delhi, India	SASW, MASW, and

	145 – 165 m/s up to a depth of 20 m for Ghazipur landfill located in Delhi, India	MAM
Abreu et al. (2016)	92 – 214 m/s for Sao Carlos Sanitary landfill, Brazil	Cross-hole method
Anbazhagan et al. (2016)	Profile varied from 53 m/s at surface to 522 m/s at 70 m depth for Mavallipura landfill, Bangalore, India	MASW

The study on primary wave velocity of MSW landfills is very limited. The methods that are used for the determination shear wave velocity can also give primary wave velocity. The values of primary wave velocity reported by different researchers are given in Table 2.3. The value of V_p is very much dependent on the degree of saturation of MSW (Valle-Molina and Stokoe, 2012).

Abreu et al. (2016) reported Poisson's ratio value for MSW landfill in Brazilian landfill is varied from 0.24 to 0.42 up to a depth of 20 m. Average value of 0.35 is reported with a standard deviation of 0.05.

Table 2.3: Primary wave velocity values reported in literature

Reference	Primary Wave Velocity Ranges and Landfill Location	Method
Sharma et al. (1990)	717 m/s at a depth of 15.3 m for Richmond landfill, California	Down-hole
Houston et al. (1995)	235 – 346 m/s for a depth ranges from 1.5 – 10 m, Northwest Regional landfill at Arizona in USA	Down-hole
Carvalho (1999)	195 – 400 m/s up to a depth of 28 m for Bandeirantes landfill at Sao Paulo in Brazil	Cross-hole and Down-hole
Cossu et al. (2005)	350 – 1500 m/s for Italian landfill	Seismic refraction
Del Greco et al. (2007)	300 – 600 m/s for new waste and 300 – 1200 m/s for old waste up to a depth of 20 m at Alice Castello landfill in Italy	Seismic refraction
Zalachoris (2010)	195 – 260 m/s for Austin Community landfill in Texas, USA	Down-hole

Carpenter et al. (2013)	350 – 643 m/s for Orchard Hills landfill in Illinois, USA	Seismic refraction and direct wave measurements
Sahadewa et al. (2014)	300 – 510 m/s for Austin Community landfill in Texas, USA	Cross-hole and Down-hole
Abreu et al. (2016)	197 – 451 m/s for Sao Carlos landfill in Brazil	Cross-hole

2.2.3 Shear Strength Parameters (c and ϕ)

Shear strength of MSW is very important to know the stability of landfills. A very wide range of shear strength parameters of MSW are reported in the literature because of the dependency on many factors such as waste composition, type of waste, age, level of decomposition, moisture conditions, overburden pressure, state of compaction, etc. Testing MSW to get shear strength is difficult due to the heterogeneous composition, difficulty in sampling, handling of large particle sizes, and time dependent properties such as unit weight, decomposition, and age (Stark et al., 2008).

Effective stress parameters are used in both static and seismic slope stability analysis, because due to the high permeability of MSW shear induced pore pressures are not significant. But, in some situations such as open dumps and bioreactor landfills, MSW may get saturated, in such conditions undrained shear strength parameters may be used. The shear strength parameters suggested by different researchers are reported in Table 2.4.MSW requires large shear strain or displacement to attain peak shear strength because of the reinforcing effect of plastics, fabrics, ropes etc. (Stark et al., 2000). To have a better compatibility of stress-strain behaviour with underlying geosynthetic interfaces and foundation soil, a shear displacement of 25 mm and an axial strain of 10% are recommended (Eid et al., 2000). The shear strength envelope of MSW recommended by Zekkos (2005) is as,

$$\tau = c + \sigma'_n \cdot \tan \phi' \tag{2.6}$$

where, c = 15 kPa, σ'_n = effective normal stress, ϕ' = effective friction angle. Zekkos et al. (2007) failure criterion is based up on the ratio of major and minor principal stresses, denoted by K_o. The suggested failure criterion is for K_o = 0.3 and an additional axial strain of 5%.

Stark et al. (2008) proposed a bilinear shear strength envelope for landfills having depth greater than or equal to 32 m, the expression for the bilinear envelope is mentioned in equation (2.7)

$$\tau = 15 + 0.61\sigma_n' - 0.00002\left(\sigma_n'\right)^2 \tag{2.7}$$

Chouksey and Babu (2015) proposed a constitutive model for strength characteristics of MSW by including different mechanisms such as immediate compression, creep effect, and effect of biodegradation with time.

Ramaiah et al. (2014) reported undrained shear strength parameters for MSW collected from Delhi landfill site. The reported undrained shear strength values are $c = 1.6$ and $\phi = 52.6°$ for the failure criteria of $K_o = 0.5 + 5\%$, $c = 0$ and $\phi = 67.5°$ for the failure criteria of $K_o = 0.5 + 10\%$, and $c = 1.6$ and $\phi = 57°$ for the failure criteria of $K_o = 1 + 10\%$. These values are significantly greater than the values under drained condition, and the difference may be attributed to high compressibility of MSW.

Table 2.4: Drained shear strength parameter values reported in literature

Reference	Condition	Shear Strength Parameters	
		c' (kPa)	ϕ' (°)
Kavazanjian et al. (1995)	Normal stress, 0 – 30	24	0
	Normal stress, 30 – 300	0	33
Van Impe (1998)	Normal stress, 0 – 20	20	0
	Normal stress, 20 – 60	0	38
	Normal stress > 60	≥ 20	30
Eid et al. (2000)	Normal stress < 350	25	35
Dixon and Jones (2005)	----	5	25
Stark et al. (2008)	Normal stress < 200	6	35
	Normal stress $\geq$ 200	30	30
Bray et al. (2009)	----	15	36
Mohurd (2012)	Depth < 10 m	15 – 30	12 – 25
	Depth $\geq$ 10 m	0 – 10	25 – 33

2.2.4 *Normalized Shear Modulus (G/G_{max})*

The strain dependent normalized shear modulus (G/G_{max}) relation is very important input in dynamic analysis of MSW landfills. It depends on factors like, confining stress, time of confinement, waste composition, frequency of loading, and unit weight. Zekkos et al. (2008) performed large scale cyclic triaxial tests on MSW from Tri-Cities landfill and studied on different parameters that affect the normalized shear modulus profile, the researchers had concluded that waste composition and confining stress have significant effect but, for unit weight, loading frequency, and confinement time have negligible effect. Based on the laboratory data, the researchers had suggested a hyperbolic model, and is expressed as,

$$\frac{G}{G_{max}} = \frac{1}{1+(\gamma/\alpha)^{\beta}} \qquad (2.8)$$

where, G = secant shear modulus; G_{max} = small-strain shear modulus; γ = shear strain and α, β = are model parameters that are primarily depends on confining stress and specimen composition.

Information on normalized shear modulus by different researchers is given in Table 2.5. Choudhury and Savoikar (2009b) generated a generalized mathematical model based on the data available in the literature, using mathematical techniques such as curve-fitting and the proposed mathematical expression is,

$$\frac{G}{G_{max}} = \frac{1}{1+7.85\gamma_{u}^{0.95}} \qquad (2.9)$$

where, γ_u = percentage cyclic shear strain.

Ramaiah et al. (2016) stated that stiffness of MSW is increased with increasing confining stress and cyclic degradation due to generation of excess pore pressure is negligible for the samples collected from Okhla dump site in Delhi.

Table 2.5: Information on modulus reduction profiles of MSW reported in literature

Reference	Proposed modulus reduction curve
Singh and Murphy (1990)	Modulus reduction curve based on the curves for peat and clay

Idriss et al. (1995)	Modulus reduction curve for OII landfill based on back analysis
Kavazanjian and Matasovic (1995)	Modulus reduction curve for OII landfill based on non-linear time domain analysis of Northridge and Landers earthquakes data, using modified Kondner-Zelasko model.
Matasovic and Kavazanjian (1998)	Modulus reduction curve for OII landfill based on field and lab testing and back analysis of QUAD4M software.
Geosyntec Consultants (2003)	Modulus reduction curve of OII landfill, based on back analysis of earthquake response
Thusyanthan et al. (2006)	Modulus reduction curve for a model MSW using centrifuge testing
Zekkos et al. (2008)	Modulus reduction curve for MSW collected from Tri-Cities landfill, based on large scale cyclic triaxial testing (CTX)
Choudhury and Savoikar (2009b)	Modulus reduction curve for MSW based on the data available in literature using best curve-fitting methods
Yuan et al. (2011)	Modulus reduction curves for different compositions and different compaction efforts for a MSW collected from Tri-Cities landfill in Fremont, using large-scale cyclic simple shear testing (CSS)
Ramaiah et al. (2016)	Modulus Reduction curve for MSW of Delhi dump site, using large-scale undrained cyclic triaxial testing (CTX)
Peng and Hou (2016)	Modulus reduction curve for model MSW using centrifuge model testing
Anbazhagan et al. (2016)	Modulus reduction curve for MSW landfill in Bangalore, using cyclic triaxial testing

2.2.5 *Material Damping Ratio (ξ)*

The strain dependent damping ratio is also required for the dynamic analysis of MSW landfills. Material damping ratio profile of MSW is effected by waste composition, confining stress, unit weight, and confinement time and is less effected by frequency of loading Zekkos et al. (2008). The generalized mathematical expression for the strain dependent damping ratio

given by Choudhury and Savoikar (2009b) based on the data available in literature using curve-fitting techniques is,

$$\xi = 30\left(1 - e^{-1.4\gamma_u^{0.36}}\right)$$

(2.10)

where, γ_u = percentage cyclic shear strain.

Information on material damping ratio reported by different researchers is summarized in Table 2.6. Anbazhagan et al. (2016) reported higher damping values for MSW of Bangalore landfill because of the presence of large amount biodegradable waste.

Table 2.6: Information on material damping ratio reported by different researchers

Reference	Proposed damping ratio curve
Singh and Murphy (1990)	Damping ratio curve based on the curves for peat and clay
Idriss et al. (1995)	Damping ratio curve for OII landfill based on back analysis
Kavazanjian and Matasovic (1995)	Damping ratio curve for OII landfill based on non-linear time domain analysis of Northridge and Landers earthquakes data, using modified Kondner-Zelasko model.
Matasovic and Kavazanjian (1998)	Damping ratio curve for OII landfill based on field and lab testing and back analysis of QUAD4M software.
Geosyntec Consultants (2003)	Damping ratio curve of OII landfill, based on back analysis of earthquake response
Thusyanthan et al. (2006)	Damping ratio curve for a model MSW using centrifuge testing
Zekkos et al. (2008)	Damping ratio curve for MSW collected from Tri-Cities landfill, based on large scale cyclic triaxial testing (CTX)
Choudhury and Savoikar (2009b)	Damping ratio curve for MSW based on the data available in literature using best curve-fitting methods
Yuan et al. (2011)	Damping ratio curves for different compositions and different compaction efforts for a MSW collected from Tri-Cities landfill in Fremont, using large-scale cyclic simple shear testing (CSS)
Ramaiah et al. (2016)	Damping ratio curve for MSW of Delhi dump site, using large-scale undrained cyclic triaxial testing (CTX)

Peng and Hou (2016)	Damping ratio curve for model MSW using centrifuge model testing
Anbazhagan et al. (2016)	Damping ratio curve for MSW landfill in Bangalore, large-scale cyclic triaxial testing (CTX)

2.3 Translational Failure Analysis of MSW Landfills

Failure of landfill slope may occur at any stage during operation and after closure of landfill. Several landfill failures occurred along the liner system and within the waste mass. Major two types of landfill failures are rotational and translational failures. Using of rotational failure analysis of landfill within the waste mass rather than translational failure analysis within liner system overestimates the stability (Mitchell et al., 1990). Translational failure can occur along, within, or beneath the liner system as shown in Fig 2.1. Such failures are observed in both clay-lined and geosynthetic-lined landfills (Koerner and Soong, 2000, Qian et al., 2003, Qian and Koerner, 2004).

Qian et al. (2003) developed a two-part wedge method using static approach (i.e., considering equilibrium of forces) for translational failure analysis of MSW landfills. This method gives lower and upper bound solutions for the stability of landfill (i.e., minimum factor of safety (FS_{min}) and maximum factor of safety (FS_{max})), the magnitude and direction of the resultant force at the interface between two wedges can be calculated. This method included the internal friction angle of MSW in the translational failure analysis of landfills. The method ensures that the interface factor of safety (FS) between active and passive wedges should not be less than unity, and the waste mass will slide along the predetermined failure planes. The effect of different parameters on the FS was studied. The results obtained using this method is in good agreement with results of PCSTABL6 computer code. The maximum difference between FS_{true} and FS_{avg} may be obtained, and the difference should be within 5%. Design of waste filling sequence may also be done.

Qian and Koerner (2004) modified the equations of two-part wedge analysis by incorporating apparent cohesion of MSW and liner components. Qian (2008) again modified the equations by adding pore pressures generated due to excessive leachate levels over liner system.

Static method overestimates the FS for the landfills situated in seismic risk zones, where seismic forces play a vital role on the stability of landfill.
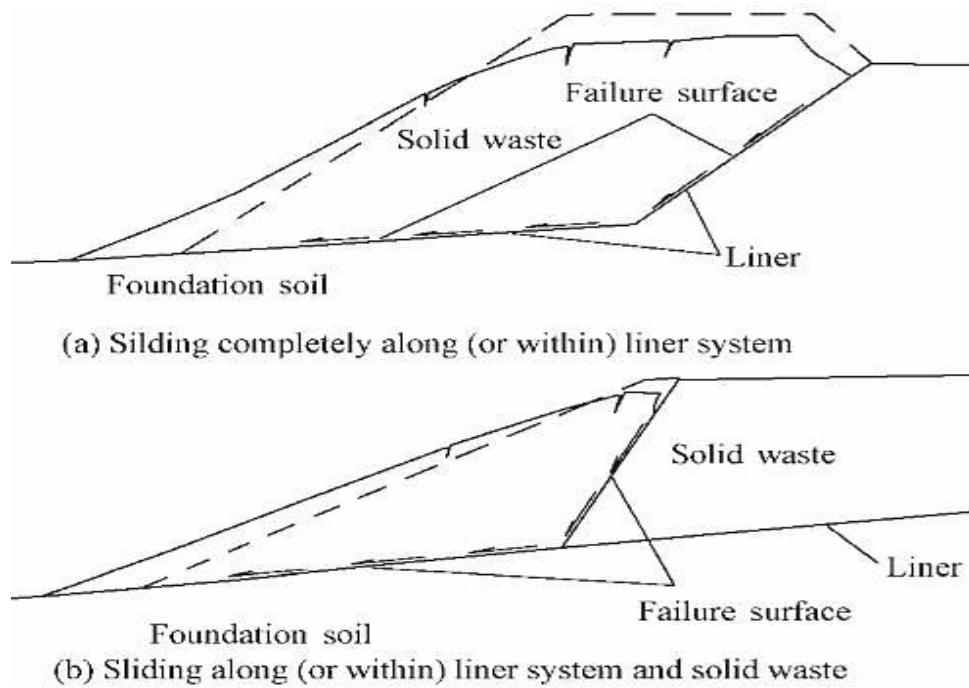
Fig. 2.1 Translational failure along (or within) the liner system (Qian et al., 2003)
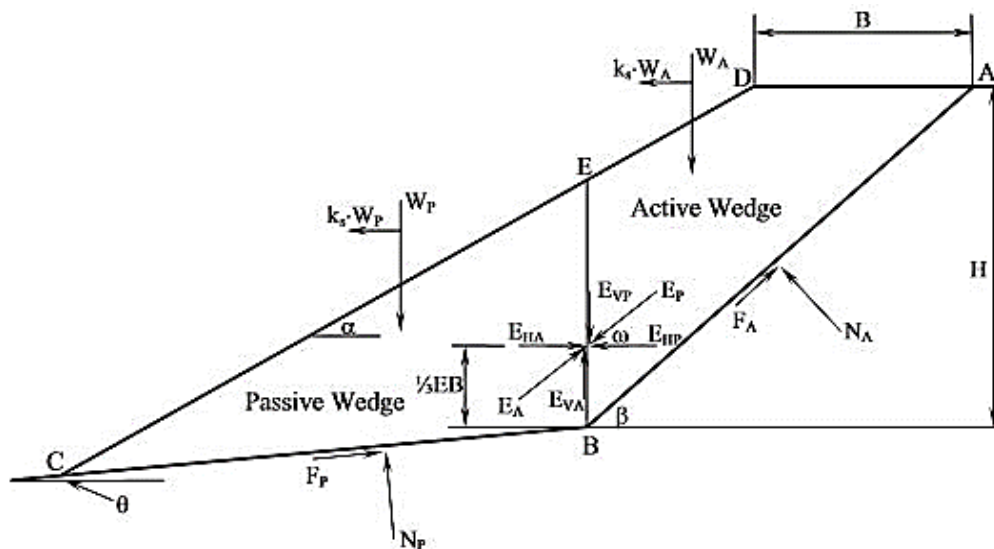
Fig. 2.2 Different forces acting on a waste mass in a landfill cell (Qian and Koerner., 2010)

Qian and Koerner (2010) used pseudo-static method for translational failure analysis of landfills by considering horizontal seismic force along with the other forces as shown in Fig 2.2. This method reviled the effect of seismic forces on the translational failure of landfills. Under seismic conditions, the critical interface within the liner system may be known by calculating the seismic yield coefficient (k_y) values for different interfaces located along the base and back slope. Sequence of waste filling may be simulated by maintaining a required

k_y–value during landfill operation. Parametric study reveals that the failure surface is changing from one interface to another by changing the dimensions (top width, depth, and front slope) of waste mass. The variation of critical interfaces with the changes in the top width is shown in Fig. 2.3.

Savoikar and Choudhury (2010) modified the equations of pseudo-static based translational failure analysis of landfills by considering seismic forces in both horizontal and vertical directions, also the cohesion of fill and the liner materials, and stated that neglecting cohesion component results in a lower *FS*, which is not an economic design. Feng and Li (2014) developed a 3-D pseudo-static method to have better reliable estimation of the seismic stability of landfills, and concluded that neglecting the size of the landfill in 2D model, leads to overestimation of *FS* than the actual, which is not safe.
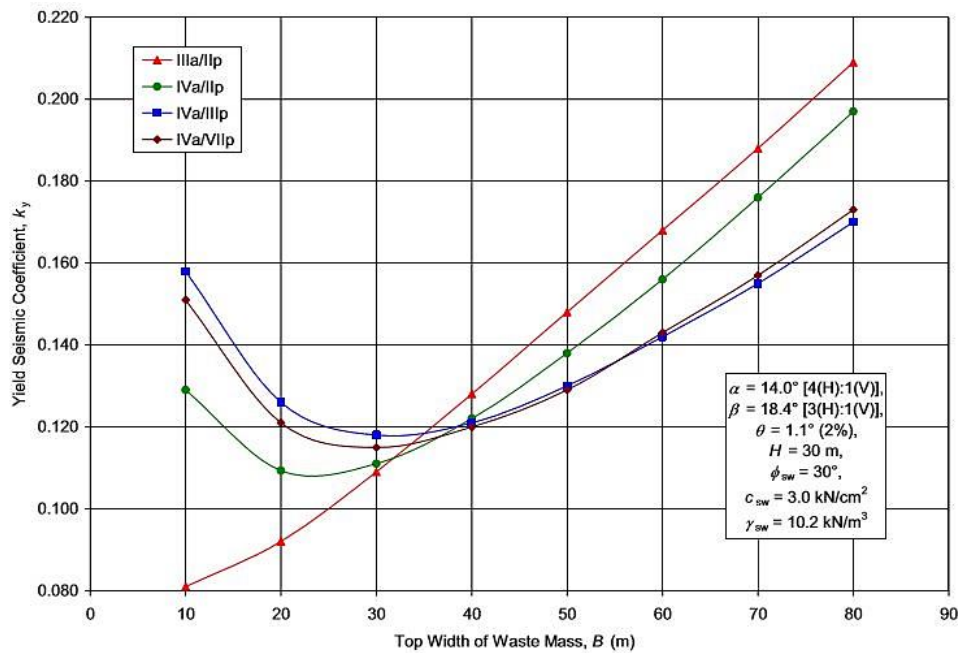
Fig. 2.3 Variation of k_y with top width of waste mass (Qian and Koerner., 2010)

Pseudo-static based approach is having some limitations such as, the method assumes that the MSW as a rigid body (V_s tends to infinity), which is not the case. Time dependent variation of earthquake forces was not considered in the analysis and the effects of shear and primary wave velocities were ignored.

Choudhury and Savoikar (2011) used pseudo-dynamic method for the first time in the seismic analysis of landfills that overcomes some of the limitations of pseudo-static method. This method ensures that only finite shear and compression wave velocities are considered, and

shear modulus is constant along the depth of the waste. The researchers had proposed equations for calculation of *FS* against sliding along the base and seismic yield accelerations for three different landfill configurations (hill type landfill, side hill type landfill, and canyon type landfill), by neglecting shear strength of the waste mass. The results are compared with the conventional pseudo-static method as shown in Fig 2.4.
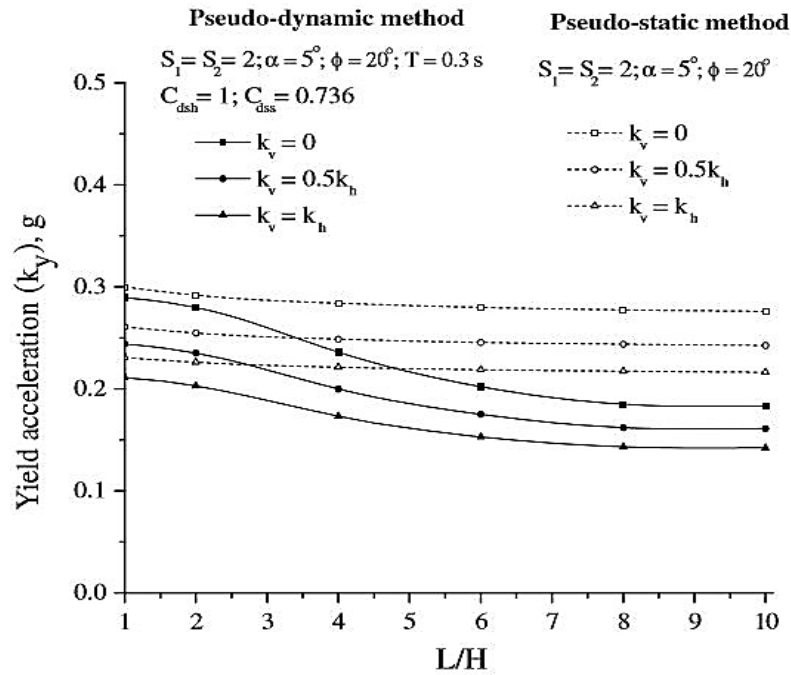
Fig. 2.4 Comparison of k_y, computed using pseudo-dynamic and pseudo-static methods (Choudhury and Savoikar, 2011)

Savoikar and Choudhury (2010), Savoikar and Choudhury (2012) studied a side hill type landfill considering the shear strength of waste mass and fill amplification using pseudo-dynamic method, and developed closed-form solutions for maximum, and minimum ranges of *FS* against translational failure and the seismic yield acceleration.

The pseudo-dynamic method also has some limitations; the seismic waves considered in this method are not satisfying the zero stress boundary condition at the MSW surface. The constructive interference of vertically upward propagating seismic wave and the reflected seismic waves from the free surface is not considered, and the variation of amplification along the depth of waste mass is considered as linear and it is an approximation. These issues may be smoothly handled using modified pseudo-dynamic method proposed by Bellezza (2014, 2015), Pain et al. (2015, 2016, 2017) and Rajesh and Choudhury (2016, 2017) applied

modified pseudo-dynamic approach to solve the earth pressure problems under seismic conditions for both dry and submerged soil conditions.

2.4 Translational Failure Analysis of Landfills with Retaining walls

The difficulties in the acquisition of land for constructing new landfills, forced the researchers/engineers to consider the expansion of existing landfills, without increasing the waste filling boundaries of the landfill with the objectives of, effective use of land, to increase waste capacity per unit area, economic design. The waste filling capacity of the existing landfills may be increased with reinforced earth walls or engineered berms, designed and constructed around the boundaries of the landfill. The available two-part wedge method is not suitable for the translational failure analysis of landfills with retaining walls.

Qian et al. (2009) developed a new three-part wedge method for the translational failure analysis of landfills with reinforced earth walls, to increase the waste filling capacity of landfills per unit area. Stability of retaining wall is very important for such expansions. Two translational failure conditions are possible using retaining walls to increase waste filling capacity. The failure plane may pass over the lined back slope of retaining wall (over-berm failure) or the failure plane may pass through base of the retaining wall (under-berm failure) as shown in the Fig. 2.5. The researchers had developed closed form solutions for the stability of retaining wall under the mentioned failure conditions (i.e., FS_{under} and FS_{over}), by applying limit equilibrium method. The study also highlights the effects of height, and back slope of retaining wall for the stability of retaining wall. The forces acting on the retaining wall may be determined using this method for the design of retaining wall and may check for the stability of retaining wall against overturning and bearing capacity failures.

This method doesn't consider the effect of seismic forces on the stability of translational failure of landfills with engineered berms.

Feng and Gao (2010) modified the three-part wedge method with triangular berm for the seismic stability against translational failure of landfills as shown in the Fig. 2.6, and developed analytical solution using conventional pseudo-static limit equilibrium method. This method considered the effect of horizontal seismic force and neglected vertical seismic force. Sun and Ruan, 2013 modified the equations considering the vertical seismic force, and stated that simply neglecting the vertical seismic force will leads to overestimation or underestimation of FS for seismic stability condition.
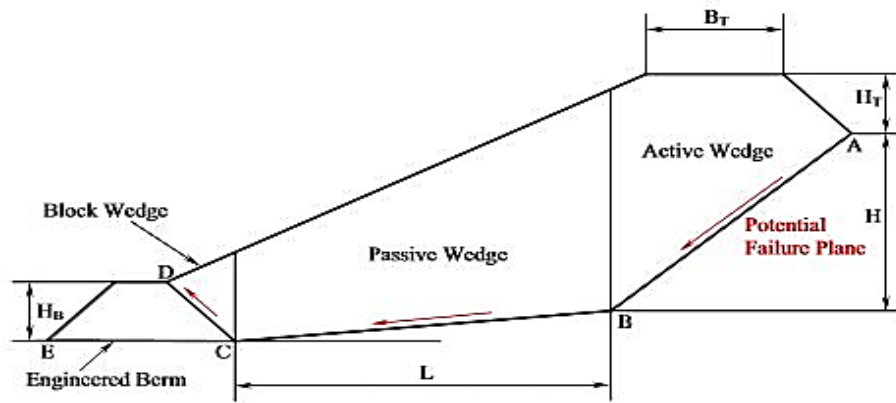
(a) Sliding over the back slope of the berm, i.e., over berm failure
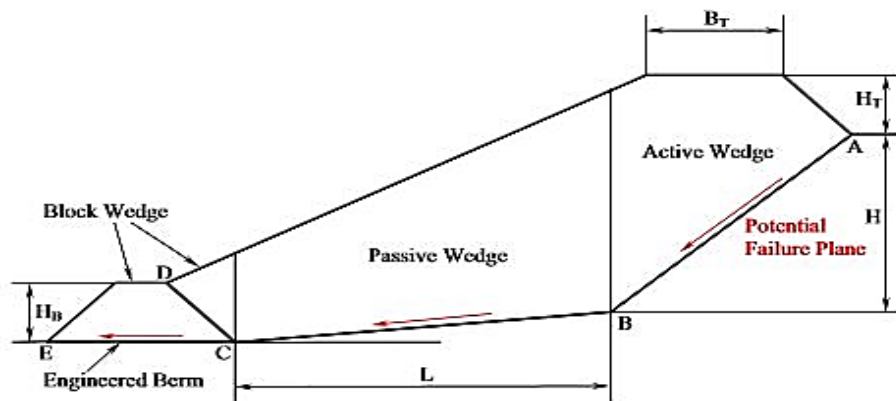
(b) Sliding under the bottom of the berm, i.e., under berm failure

Fig. 2.5 Two possible translational failure conditions, using retaining walls (Qian et al., 2009)

Ruan et al. (2013) proposed a pseudo-dynamic based limit equilibrium method for translational analysis of MSW landfill under seismic condition. Under berm failure condition was considered for a MSW landfill expanded with a trapezoidal berm. Using the developed equations, effects of amplification factor, seismic coefficient, variation in the geometry of berm, and depth of waste mass on the seismic stability of landfill were studied. Ruan and Lin (2015) extended it for over-berm failure condition, and formulated equation for average *FS*. A parametric study was done to know the effect of shear wave length on the average *FS*. For example, the variation of FS_{avg} with shear wave length (λ) for different values of Poisson's ratio is shown in Fig. 2.7
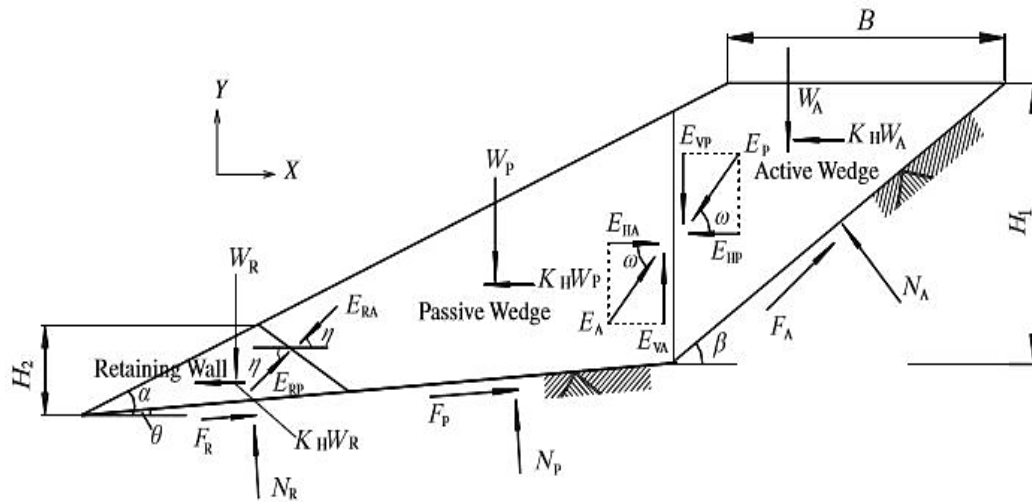
Fig. 2.6 Three-part wedge model with triangular berm (Feng and Gao, 2010)
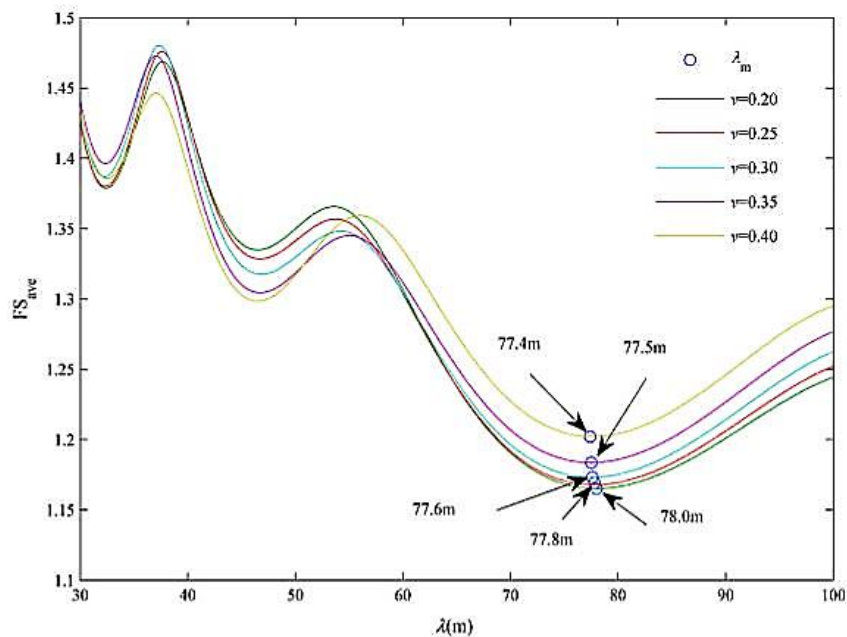
Fig. 2.7 Relation between shear wave length and Poisson's ratio (Ruan and Lin, 2015)

2.5 Site Response Analysis of MSW Landfills

The process of studying the variation in the seismic response of MSW landfills for a given input bedrock motion in the site of interest is termed as 'site response analysis of MSW landfills. Seismic acceleration may get amplified or de-amplified depending on the dynamic properties of foundation soil and MSW. Generally, bedrock motion in the site of interest is

26

predicted using seismic hazard analysis. The important dynamic properties that influence site response of MSW landfills are:

1) Shear wave velocity profile with depth
2) Modulus reduction curve
3) Damping ratio curve

The methods that are available for site response analysis may be broadly divided into following three categories:

1) Linear analysis
2) Equivalent-linear analysis
3) Non-linear analysis

Dynamic response of MSW landfills could be studied using software's such as SHAKE2000 (Ordonez, 2000), DEEPSOIL (Hashash et al., 2015), and QUAD4M (Hudson et al., 1994). The parameters that have influence on dynamic response include height, geometry, and unit weight of landfill, modulus reduction and damping of waste, characteristics of input ground motion etc. However, these analytical methods are not capable of estimating seismic stability conditions.

Bray et al. (1995) performed the 1-D equivalent-linear analysis using SHAKE91 for different landfill models founded on different foundation conditions with maximum input acceleration of 0.35g. Based on the results, he reported that, the maximum horizontal acceleration (MHA) is amplified throughout the depth of landfill and attains maximum near top of the landfill, MHA depends on dynamic properties of MSW, peak acceleration, and the predominant period of input bedrock motion.

Rathje and Bray (2001) studied the reliability of using 1D site response analysis to predict dynamic response of landfills. The study compared 1D site response analysis in SHAKE91 with 2D finite element simulation using QUAD4M. The results indicated 1D analysis could reasonably predict seismic loading and seismically induced permanent displacements for deep sliding surfaces (such as sliding along liners) conservatively.

The effects of local site conditions on the dynamic response of MSW landfill was studied by Psarropoulos et al. (2007) using 2D finite element program QUAD4M. The results indicated that dynamic response of landfills depends not only on the sub-surface conditions and input excitations but the geometrical and material properties of landfill also play a crucial role.

Choudhury and Savoikar (2009a) performed one dimensional equivalent-linear analysis using DEEPSOIL computer program for a model landfill with five different foundation conditions subjected to four different input motions with a MHA of 0.278g, 0.067g, 0.834g, and 0.2265g. The effects of different foundation conditions, height and stiffness of waste mass and input base accelerations on the seismic response on MSW landfill are determined in terms of surface accelerations, spectral amplification, and normalized stresses. Assuming a constant unit weight and shear wave velocity underestimates MHA, normalized stresses and spectral amplification values near the top of the landfill.

Anbazhagan et al. (2016) performed one dimensional non-linear analysis using DEEPSOIL computer program for Mavallipura landfill located in Bangalore, India and is subjected to ten different input ground motions, predicted based on the regional seismicity. The study observed that there is considerable amplification in the base acceleration values with the depth of landfill, increasing towards the top of the landfill as shown in Fig. 2.8. The low stiffness and high amplification of MSW is due to the poor compaction during waste filling.
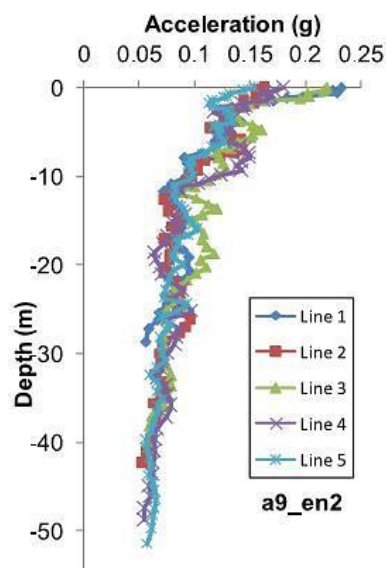
Fig. 2.8 Variation of base acceleration with depth of the landfill (Anbazhagan et al.,2016)

2.6 Critical Observations from Literature Review

The research gaps identified from extensive literature review, in the field of seismic design of landfills are:

❖ Pseudo-static method for seismic translational failure analysis of MSW landfills is having limitations as follows,

28

- This method assumes MSW as a rigid body (V_s tends to infinity), which is not the case.

- Time-dependent nature of seismic forces is not considered.
- Effect of frequency content of the input motion on the seismic stability of landfills is not considered.
- Effects of shear and primary wave velocities are not considered.

❖ Pseudo-dynamic method is also having some limitations as follows,
- The seismic waves considered in this method are not satisfying the zero stress boundary condition at the free surface of MSW landfill.
- The reflection of seismic waves at the free surface is not considered.
- The variation of amplification along the depth of waste mass is considered as linear and is a crude approximation.

❖ In both pseudo-static and pseudo-dynamic methods a constant values of MSW properties are used for entire depth of waste mass, but from the literature, it is found that these properties are changing significantly along the depth of the landfill.

❖ A significant amplification of base acceleration is observed form the literature on seismic site response studies of MSW landfills. No method is available to consider the effect amplification on the seismic stability of MSW landfills.

❖ Very limited study is available on the effect of local site condition on the seismic stability of MSW landfills.

❖ Very limited literature is available on dynamic properties of MSW and dynamic response of Indian landfills.

2.7 Scope of the Present Thesis

- Collection and compilation of the data reported on the dynamic properties of municipal solid waste from all over the world including India.
- Development of an analytical model for translational stability analysis of MSW landfill resting over a rigid stratum under seismic condition.
- Validation and comparison of the proposed model with the published literature. In addition, a detailed parametric study to evaluate the influence of dynamic properties of MSW on translational stability.
- Study the effect of inhomogeneity of MSW material on the translational stability of landfill under seismic condition.

❖ Study the effect of local site condition on the seismic translational stability of MSW landfills.

SEISMIC TRANSLATIONAL FAILURE ANALYSIS OF MSW LANDFILLS

3.1 General

In the present study, closed form solution is proposed to obtain factor of safety and yield acceleration coefficient for a typical side hill type landfill resting on rigid base using limit equilibrium method. The acceleration ratio obtained in present study is well compared with the same obtained using DEEPSOIL for a given set of input parameters. From parametric study it is observed that the landfill is vulnerable to seismic damage for low frequency input motions Obtained results are compared with available literature having same input parameters. The static factor of safety values obtained from the present method is also compared with a failure case history data of Kettleman Hills waste landfill (Seed et al., 1990).

3.2 Linear Analysis

3.2.1 Proposed Methodology

In the present study, modified pseudo-dynamic approach proposed by Bellezza (2014) and Pain et al. (2015) has been applied to get the stability condition of a MSW landfill against translational mode of failure under seismic conditions. Mathematical equations are proposed to obtain maximum and minimum ranges of the factor of safety (*FS*) and the yield acceleration coefficient (k_y) for a model landfill (side-hill type) resting on a horizontal rigid base. MSW is idealized as visco-elastic material that includes material damping, a significant parameter under earthquake conditions.

For mathematical representation of visco-elastic MSW Kelvin – Voigt (KV) solid model is used. The response of KV model is sum of elastic strain and viscous component. The viscous component is proportional to the rate of strain. Equation (3.1) gives the stress strain relationship of KV model.

$$\tau = \gamma_s G + \eta_{sw} \frac{\partial \gamma_s}{\partial t} \tag{3.1}$$

where, τ = shear stress; γ_s = shear strain; G = Shear Modulus and η_{sw} = viscosity of solid waste

Equation (3.1) may be made frequency independent with the relation $\eta_{sw} = \dfrac{2G\xi}{\omega}$, ω is the circular frequency of the harmonic excitation and ξ is damping ratio.

The governing differential equation of 1D vertically propagating plane shear wave in a KV medium is given in equation (3.2).

$$\rho_{sw} \frac{\partial^2 u_h}{\partial t^2} = G \frac{\partial^2 u_h}{\partial z^2} + \eta_{sw} \frac{\partial^3 u_h}{\partial z^2 \partial t} \tag{3.2}$$

where, u_h = horizontal displacement; ρ_{sw} = density of solid waste; τ = shear stress.

The general solution to this harmonic wave equation is of the form;

$$u_h(z,t) = C_1 e^{i(\omega t + k^* z)} + C_2 e^{i(\omega t - k^* z)} \tag{3.3}$$

where, C_1 & C_2 are the amplitudes of incident wave travelling in the upward ($-z$) direction and reflected wave travelling in the downward ($+z$) direction, respectively. These constants depends on the boundary conditions and $k^* = \omega \sqrt{\dfrac{\rho}{G^*}}$, is complex wave number

where, G^* is the complex shear modulus:

$$G^* = G + i\omega \eta_{sw} = G(1 + 2i\xi) \tag{3.4}$$

Equation (3.2) is solved by applying the boundary conditions for a harmonic horizontal shaking. Shear stress is zero at the free surface of landfill (i.e. $\tau = 0$ at $z = 0$). Assuming a base displacement $u_{hb} = u_{h0} \cos(\omega t)$, the horizontal displacement may be obtained as

$$u_h(z,t) = \frac{u_{h0}}{C^2 + S^2} \left[(CC_z + SS_z) \cos(\omega t) + (SC_z - CS_z) \sin(\omega t) \right] \tag{3.5}$$

where,

$$C_z = \cos\left(\frac{y_1 z}{H}\right) \cosh\left(\frac{y_2 z}{H}\right) \tag{3.6a}$$

$$S_z = -\sin\left(\frac{y_1 z}{H}\right) \sinh\left(\frac{y_2 z}{H}\right) \tag{3.6b}$$

$$C = \cos(y_1)\cosh(y_2) \tag{3.7a}$$

$$S = -\sin(y_1)\sinh(y_2) \tag{3.7b}$$

$$y_1 = \frac{\omega H}{V_s}\sqrt{\frac{\sqrt{1+4\xi^2}+1}{2(1+4\xi^2)}} \tag{3.8a}$$

$$y_2 = -\frac{\omega H}{V_s}\sqrt{\frac{\sqrt{1+4\xi^2}-1}{2(1+4\xi^2)}} \tag{3.8b}$$

Equation (3.9) is the expression for horizontal acceleration obtained by differentiating equation (3.5) twice w.r.t time:

$$a_h(z,t) = \frac{k_h g}{C^2 + S^2}\left[(CC_z + SS_z)\cos(\omega t) + (SC_z - CS_z)\sin(\omega t)\right] \tag{3.9}$$

where, $k_h g = -\omega^2 u_{h0}$; k_h = Horizontal seismic acceleration coefficient at the base

3.2.2 Model MSW Landfill

In the present study, a model landfill (side-hill type) as in shown in Fig. 3.1 is adopted and assumed that the landfill is resting on a horizontal rigid base. The height and top-width of landfill are represented as H and B respectively. The front and back slope angles are assumed as α and β respectively, with horizontal as shown in Fig. 3.1. The section of landfill similar to that of section C (viewing SW) of unit B-19 in Kattlemen Hills landfill is used in the present analysis (Chang, 2005, Mitchell et al., 1990).

A two-part wedge model (Qian et al., 2003) is used to calculate the *FS* of a MSW landfill against a predetermined translational failure under seismic conditions. In this model landfill mass is divided into two different wedges (active and passive wedges) as shown in Fig. 3.1. The one resting on back slope (that can be either liner system or existing laid waste) tends to cause failure, defined as active wedge. The one resting on previously laid waste fill or existing soil or base liner tends to resist failure, defined as passive wedge. The friction angle at the base interface of active and passive wedge is assumed as δ_a & δ_p respectively. The shear wave velocity (V_s) and unit weight (γ_{sw}) of MSW are kept constant for entire waste mass.

3.2.3 Seismic Forces in Landfill

Fig. 3.1 is showing different forces on both active and passive wedges of landfill. The direction of resultant inter-wedge force (Inter-wedge is an imaginary wall at the interface between active and passive wedges) acting at the interface between active and passive wedge (E_a or E_p) is assumed as ε with horizontal. The point of action is assumed at a height of $H/3$ from the base of interface (Qian et al., 2003). This resultant inter-wedge force is assumed to be resolved into two perpendicular components as shown in Fig. 3.1. This method assumes that, shear stress at the inter-wedge is always less than waste strength at this inter-wedge. In other words, FS at the inter-wedge (FS_V) should never be less than one. To keep whole waste mass in equilibrium, this method assumes that the FS at inter-wedge FS_V should be less than the FS of entire landfill. This assumption is similar to Qian et al. (2003). FS at all points on the failure plane is assumed to be same.

The explanations for the symbols used in following mathematical equations are given in ''Notations'' section.

To calculate the mass of each wedge, a small horizontal strip having 'dz' thickness is considered and is located at a distance of "z" from free surface. Integrate this horizontal strip vertically between the limits of respective wedge.

The mass of active wedge may be given as,

$$M_a = \int_0^{H_1} \frac{\gamma_{sw}}{g}\left(\frac{H-z}{\tan\beta} - \frac{H_1-z}{\tan\alpha}\right)dz + \int_{H_1}^{H} \frac{\gamma_{sw}}{g\tan\beta}(H-z)\cdot dz \qquad (3.10)$$

Similarly, mass of passive wedge may be given as,

$$M_p = \int_{H_1}^{H} \frac{\gamma_{sw}}{g\tan\alpha}(z-H_1)\cdot dz \qquad (3.11)$$

The seismic force in horizontal direction may be obtained by multiplying elemental mass with the elemental acceleration and integrating it over the limits of respective wedge.

The seismic force subjected by the active wedge may be obtained from,

$$Q_{Ha}(t) = \int_0^H m_a(z) \cdot a_h(z,t) \cdot dz$$

$$= \frac{\gamma_{sw}}{g \tan \beta} \int_0^H a_h(z,t) \cdot (H-z) \cdot dz - \frac{\gamma_{sw}}{g \tan \alpha} \int_0^{H_1} a_h(z,t) \cdot (H_1-z) \cdot dz$$

(3.12)
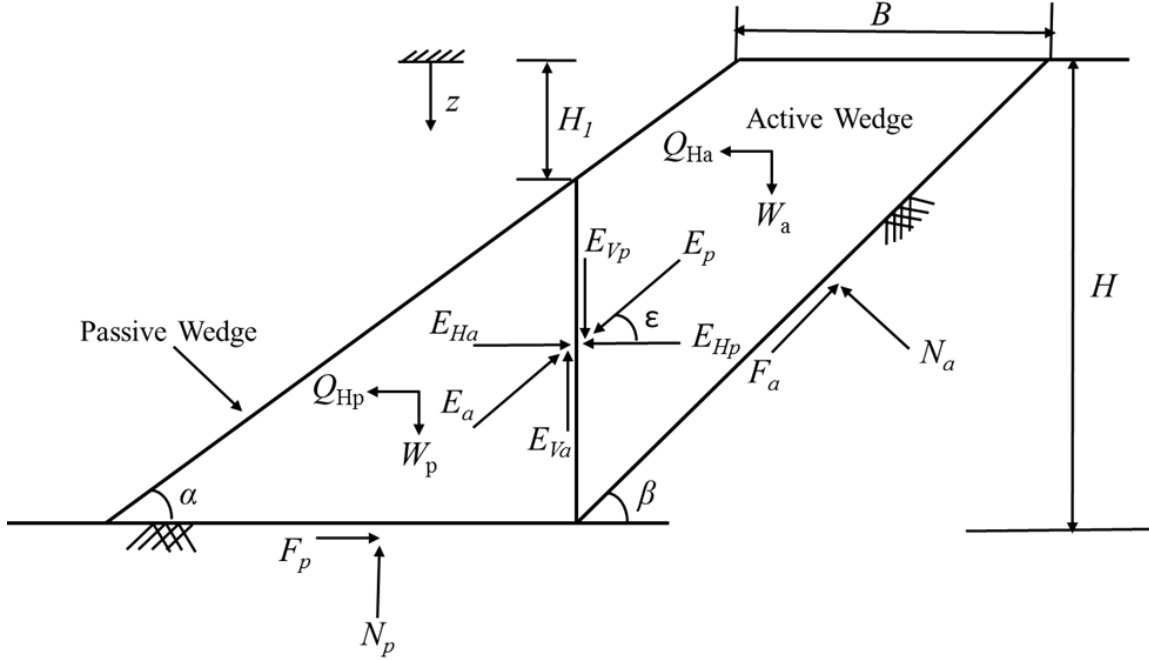
Fig. 3.1 Forces acting on two adjacent wedges of a typical MSW landfill cell under seismic condition

Hence, substituting equation (3.9) into equation (3.12), we get

$$Q_{Ha}(t) = \frac{k_h \gamma_{sw}}{\tan \beta} \left[\frac{CI_1 + SI_2}{C^2 + S^2} \cos(\omega t) + \frac{SI_1 - CI_2}{C^2 + S^2} \sin(\omega t) \right] - \frac{k_h \gamma_{sw}}{\tan \alpha} \left[\frac{CI_3 + SI_4}{C^2 + S^2} \cos(\omega t) + \frac{SI_3 - CI_4}{C^2 + S^2} \sin(\omega t) \right]$$

$$= k_h \cdot q_{Ha}$$

(3.13)

where,

$$I_1 = \int_0^H C_z (H-z) \cdot dz = \int_0^H \cos(k_1 z) \cosh(k_2 z)(H-z) \cdot dz$$

$$= \frac{H^2}{(y_1^2 + y_2^2)^2} \left\{ 2 y_1 y_2 \sin(y_1) \sinh(y_2) + (y_2^2 - y_1^2) \cos(y_1) \cosh(y_2) - (y_2^2 - y_1^2) \right\}$$

(3.14)

$$I_2 = \int_0^H S_z(H-z)\cdot dz = \int_0^H -\sin(k_1 z)\sinh(k_2 z)(H-z)\cdot dz$$

$$= \frac{H^2}{\left(y_1^2 + y_2^2\right)^2}\left\{2y_1 y_2 \cos(y_1)\cosh(y_2) + \left(y_1^2 - y_2^2\right)\sin(y_1)\sinh(y_2) - 2y_1 y_2\right\}$$

(3.15)

$$I_3 = \int_0^{H_1} C_z(H_1-z)\cdot dz = \int_0^{H_1} \cos(k_1 z)\cosh(k_2 z)(H_1-z)\cdot dz$$

$$= \frac{H^2}{\left(y_1^2 + y_2^2\right)^2}\left\{2y_1 y_2 \sin\left(\frac{y_1 H_1}{H}\right)\sinh\left(\frac{y_2 H_1}{H}\right) + \left(y_2^2 - y_1^2\right)\cos\left(\frac{y_1 H_1}{H}\right)\cosh\left(\frac{y_2 H_1}{H}\right) - \left(y_2^2 - y_1^2\right)\right\}$$

(3.16)

$$I_4 = \int_0^{H_1} S_z(H_1-z)\cdot dz = \int_0^{H_1} -\sin(k_1 z)\sinh(k_2 z)(H_1-z)\cdot dz$$

$$= \frac{H^2}{\left(y_1^2 + y_2^2\right)^2}\left\{2y_1 y_2 \cos\left(\frac{y_1 H_1}{H}\right)\cosh\left(\frac{y_2 H_1}{H}\right) + \left(y_1^2 - y_2^2\right)\sin\left(\frac{y_1 H_1}{H}\right)\sinh\left(\frac{y_2 H_1}{H}\right) - 2y_1 y_2\right\}$$

(3.17)

In the same way, the seismic force subjected by the passive wedge may be obtained from,

$$Q_{Hp}(t) = \int_{H_1}^H m_p(z)\cdot a_h(z,t)\cdot dz = \frac{\gamma_{sw}}{g\tan\alpha}\int_{H_1}^H a_h(z,t)(z-H_1)\cdot dz$$

(3.18)

Hence, substituting equation (3.9) into equation (3.18), we get

$$Q_{Hp}(t) = \frac{k_h \gamma_{sw}}{\tan\alpha}\left[\frac{CJ_1 + SJ_2}{C^2 + S^2}\cos(\omega t) + \frac{SJ_1 - CJ_2}{C^2 + S^2}\sin(\omega t)\right]$$

$$= k_h \cdot q_{Hp}$$

(3.19)

Where,

$$J_1 = \int_{H_1}^H C_z(z-H_1)\cdot dz = \int_{H_1}^H \cos(k_1 z)\cosh(k_2 z)(z-H_1)\cdot dz$$

$$= \frac{H^2}{\left(y_1^2 + y_2^2\right)^2}\left\{\begin{array}{l} \left(y_1^2 + y_2^2\right)\left(1 - \frac{H_1}{H}\right)\left[y_2\cos(y_1)\sinh(y_2) + y_1\sin(y_1)\cosh(y_2)\right] \\ -2y_1 y_2\left[\sin(y_1)\sinh(y_2) - \sin\left(\frac{y_1 H_1}{H}\right)\sinh\left(\frac{y_2 H_1}{H}\right)\right] \\ +\left(y_1^2 - y_2^2\right)\left[\cos(y_1)\cosh(y_2) - \cos\left(\frac{y_1 H_1}{H}\right)\cosh\left(\frac{y_2 H_2}{H}\right)\right] \end{array}\right\}$$

(3.20)

36

$$J_2 = \int_{H_1}^{H} S_z (z - H_1) \cdot dz = \int_{H_1}^{H} -\sin(k_1 z) \sinh(k_2 z)(z - H_1) \cdot dz$$

$$= \frac{H^2}{\left(y_1^2 + y_2^2\right)^2} \left\{ \begin{array}{l} \left(y_1^2 + y_2^2\right)\left(1 - \dfrac{H_1}{H}\right)\left[y_1 \cos(y_1) \sinh(y_2) - y_2 \sin(y_1) \cosh(y_2)\right] \\[2mm] -2 y_1 y_2 \left[\cos(y_1) \cosh(y_2) - \cos\left(\dfrac{y_1 H_1}{H}\right) \cosh\left(\dfrac{y_2 H_1}{H}\right)\right] \\[2mm] + \left(y_2^2 - y_1^2\right)\left[\sin(y_1) \sinh(y_2) - \sin\left(\dfrac{y_1 H_1}{H}\right) \sinh\left(\dfrac{y_2 H_2}{H}\right)\right] \end{array} \right\} \quad (3.21)$$

3.2.4 Force Equilibrium

First compute the seismic forces acting on waste mass with the help of equations derived in above section. Then the *FS* may be evaluated by considering force equilibrium of passive and active wedges of waste mass. Consider the free body diagram of passive wedge; By considering sum of all vertical forces acing on passive equals to zero gives,

$$N_p = E_{Vp} + W_p \tag{3.22}$$

$$E_{Vp} = E_{Hp} \cdot \tan\phi_{sw}/FS_V = E_{Hp} \cdot m_{sw} \tag{3.23}$$

where,

$$\tan\phi_{sw}/FS_V = m_{sw} \tag{3.24}$$

Put equation (3.23) into equation (3.22), we get

$$W_p + E_{Hp} \cdot m_{sw} = N_p \tag{3.25}$$

Similarly, by considering sum of all horizontal forces acting on passive wedge equals to zero gives,

$$F_p = E_{Hp} + Q_{Hp} \tag{3.26}$$

$$F_p = N_p \cdot \tan\delta_p/FS_p \tag{3.27}$$

Put equation (3.27) into equation (3.26), after simplification we get N_p as,

$$N_p = \frac{E_{Hp} + Q_{Hp}}{\tan\delta_p/FS_p} \tag{3.28}$$

Put equation (3.28) into equation (3.25), after simplification we get E_{Hp}

$$E_{Hp} = \frac{W_p \cdot \tan \delta_p / FS_p - Q_{Hp}}{1 - m_{sw} \cdot \tan \delta_p / FS_p} \qquad (3.29)$$

Now, consider the free body diagram of active wedge;

By considering the sum of all vertical forces acting on active wedge equals to zero gives,

$$W_a = N_a \cdot \cos \beta + F_a \cdot \sin \beta + E_{Va} \qquad (3.30)$$

$$F_a = N_a \cdot \tan \delta_a / FS_a \qquad (3.31)$$

$$E_{Va} = E_{Ha} \cdot \tan \phi_{sw} / FS_V = E_{Ha} \cdot m_{sw} \qquad (3.32)$$

Put equation (3.31) and (3.32) into equation (3.30), we get

$$W_a = N_a \left(\cos \beta + \sin \beta \cdot \tan \delta_a / FS_a \right) + E_{Ha} \cdot m_{sw} \qquad (3.33)$$

Similarly, by considering the sum of all horizontal forces acting on active wedge equals to zero gives,

$$F_a \cdot \cos \beta + E_{Ha} = Q_{Ha} + N_a \cdot \sin \beta \qquad (3.34)$$

Put, equation (3.31) into equation (3.34), after simplification we get N_a as,

$$N_a = \frac{E_{Ha} - Q_{Ha}}{\sin \beta - \cos \beta \cdot \tan \delta_a / FS_a} \qquad (3.35)$$

Now, Put equation (3.35) into equation (3.33), after simplification we get E_{Ha} as,

$$E_{Ha} = \frac{W_a \cdot \left(\sin \beta - \cos \beta \cdot \tan \delta_a / FS_a \right) + Q_{Ha} \cdot \left(\cos \beta + \sin \beta \cdot \tan \delta_a / FS_a \right)}{\cos \beta + \sin \beta \cdot \tan \delta_a / FS_a + m_{sw} \cdot \left(\sin \beta - \cos \beta \cdot \tan \delta_a / FS_a \right)} \qquad (3.36)$$

For the reason $E_{Ha} = E_{Hp}$ and $FS_a = FS_p = FS$, equation (3.29) is equals to equation (3.36) and the resultant equation may be rearranged into a quadratic equation $a \cdot FS^2 + b \cdot FS + c = 0$, the roots of this equation gives the solution of FS as given below,

$$FS = \frac{-b \pm \sqrt{b^2 - 4ac}}{2a} \qquad (3.37)$$

where,

$$a = Q_{Hp} \cdot \sin \beta \cdot m_{sw} + W_a \cdot \sin \beta + \left(Q_{Ha} + Q_{Hp} \right) \cdot \cos \beta;$$

$$b = - \begin{bmatrix} W_t \cdot \sin \beta \cdot \tan \delta_p \cdot m_{sw} + W_p \cdot \cos \beta \cdot \tan \delta_p + W_a \cdot \cos \beta \cdot \tan \delta_a + Q_{Hp} \cdot \cos \beta \cdot \tan \delta_a \cdot m_{sw} \\ + Q_{Ha} \cdot \cos \beta \cdot \tan \delta_p \cdot m_{sw} - \left(Q_{Ha} + Q_{Hp} \right) \cdot \sin \beta \cdot \tan \delta_a \end{bmatrix}; \quad (3.38)$$

$$c = W_t \cdot \cos \beta \cdot \tan \delta_a \cdot \tan \delta_p \cdot m_{sw} - W_p \cdot \sin \beta \cdot \tan \delta_a \cdot \tan \delta_p - Q_{Ha} \cdot \sin \beta \cdot \tan \delta_a \cdot \tan \delta_p \cdot m_{sw}$$

To compute active wedge weight (W_a) and passive wedge weight (W_p) following equations may be used,

For $B < H/\tan \beta$;

$$W_a = \frac{\gamma_{sw}}{2} \left[\frac{H^2}{\tan \beta} - \left(\frac{H}{\tan \beta} - B \right)^2 \cdot \tan \alpha \right]; \quad W_p = \frac{\gamma_{sw}}{2} \left(\frac{H}{\tan \alpha} - \frac{H}{\tan \beta} + B \right)^2 \cdot \tan \alpha;$$

$$(3.39)$$

For $B \geq H/\tan \beta$;

$$W_a = \frac{\gamma_{sw} \cdot H^2}{2 \tan \beta}; \quad W_p = \gamma_{sw} \cdot H \cdot \left(B - \frac{H}{\tan \beta} + \frac{H}{2 \tan \alpha} \right)$$

The sum of W_a and W_p gives the total weight of waste mass and is given by $W_t = W_a + W_p$.

The direction of inter-wedge force may be obtained as below,

$$\varepsilon = \tan^{-1} \left(E_{Vp}/E_{Hp} \right) = \tan^{-1} \left(m_{sw} \right) = \tan^{-1} \left(\phi_{sw}/FS_V \right) \quad (3.40)$$

If the value of $m_{sw} or \left(FS_V \right)$ is known precisely, then true factor of safety may be calculated using equation (3.37). To find m_{sw} we need the values of ϕ_{sw} and FS_V [refer equation (3.24)]. To maintain the equilibrium of entire landfill mass FS_V must be greater than FS. Therefore, FS_V ranges from FS to ∞. If $FS_{VS} = FS$, then m_{sw} will have a maximum value results in maximum factor of safety FS_{max}. If $FS_V = \infty$, then m_{sw} will have a least value of zero (i.e., neglecting the waste strength) results in minimum factor of safety FS_{min}. Thus the value of FS_{true} lies between FS_{min} and FS_{max}. The exact value of $m_{sw} or \left(FS_V \right)$ can't be determined because of assumptions made before. So, the average FS $\left(FS_{avg} \right)$ may be determined in this method using $FS_{avg} = \left(FS_{min} + FS_{max} \right)/2$ in place of FS_{true}. The absolute maximum difference between FS_{true} and FS_{avg} may also be predicted using, either difference between FS_{avg} and

39

$FS_{\min}$ or the difference between $FS_{\max}$ and FS_{avg}. Generally, this absolute maximum difference should be within 5% for most of the cases (Qian et al., 2003).

3.2.5 Computation of FS_{min} and FS_{max}

If $FS_V = \infty$, the value of $m_{sw} = 0$ in the equation (3.38) then the expression for $FS_{\min}$ is given by;

$$FS_{\min} = \frac{-b \pm \sqrt{b^2 - 4ac}}{2a} \qquad (3.41)$$

where,

$$a = W_a \cdot \sin \beta + \left(Q_{Ha} + Q_{Hp}\right) \cdot \cos \beta;$$
$$b = -\left[W_p \cdot \cos \beta \cdot \tan \delta_p + W_a \cdot \cos \beta \cdot \tan \delta_a - \left(Q_{Ha} + Q_{Hp}\right) \cdot \sin \beta \cdot \tan \delta_a\right];$$
$$c = -W_p \cdot \sin \beta \cdot \tan \delta_a \cdot \tan \delta_p$$

The *FS* obtained using equation (3.41) is more conservative and may be directly used in the design without having any risk.

Similarly, the value of $m_{sw} = \tan \phi_{sw} / FS$ when $FS_V = FS$. Then the equation (3.37) may be written as;

$$a_1 \cdot FS_{\max}^3 + b_1 \cdot FS_{\max}^2 + c_1 \cdot FS_{\max} + d_1 = 0 \qquad (3.42)$$

Where,

$$a_1 = W_a \cdot \sin \beta + \left(Q_{Ha} + Q_{Hp}\right) \cdot \cos \beta;$$
$$b_1 = -\left[W_p \cdot \tan \delta_p + W_a \cdot \tan \delta_a\right] \cdot \cos \beta + \left(Q_{Ha} + Q_{Hp}\right) \cdot \tan \delta_p \cdot \sin \beta + Q_{Hp} \cdot \sin \beta \cdot \tan \phi_{sw};$$
$$c_1 = -W_t \cdot \sin \beta \cdot \tan \phi_{sw} \cdot \tan \delta_p - \left(Q_{Ha} \cdot \tan \delta_p + Q_{Hp} \cdot \tan \delta_a\right) \cdot \cos \beta \cdot \tan \phi_{sw} - W_p \cdot \sin \beta \cdot \tan \delta_a \cdot \tan \delta_p;$$
$$d_1 = W_t \cdot \cos \beta \cdot \tan \delta_a \cdot \tan \delta_p \cdot \tan \phi_{sw} - Q_{Ha} \cdot \sin \beta \cdot \tan \delta_a \cdot \tan \delta_p \cdot \tan \phi_{sw}$$

The above equation is a cubical one, so obtain the values of a_1, b_1, c_1 and d_1 and substitute in equation (3.42). Then solve it for $FS_{\max}$ using synthetic division. After obtaining $FS_{\min}$ and $FS_{\max}$ using the equation (3.41) and (3.42), FS_{avg} may be obtained as explained above.

3.2.6 Expression for Yield Acceleration Coefficient (k_y)

When the value of *FS* is equals to unity (i.e., at the verge of failure) then the acceleration is known as yield acceleration, is very much helpful for the calculation of plastic deformations occurred in landfill during an earthquake. It may be calculated by substituting the values of *a*, *b*, and *c* into equation (3.37) and equate *FS* = 1. The expression for k_y is given below,

$$k_y = \left(\begin{array}{l} W_p \cdot \sin\beta \cdot \tan\delta_a \cdot \tan\delta_p \\ + \left(W_a \cdot \tan\delta_p + W_p \cdot \tan\delta_a \right) \cdot \cos\beta \\ + W_t \cdot \sin\beta \cdot \tan\delta_p \cdot m_{sw} - W_a \cdot \sin\beta \\ - W_t \cdot \cos\beta \cdot \tan\delta_a \cdot \tan\delta_p \cdot m_{sw} \end{array} \right) \bigg/ \left(\begin{array}{l} \left(q_{Ha} + q_{Hp} \right) \cdot \cos\beta + q_{Ha} \cdot \sin\beta \cdot m_{sw} \\ - \left(q_{Ha} \cdot \tan\delta_a + q_{Hp} \cdot \tan\delta_p \right) \cdot \cos\beta \cdot m_{sw} \\ + \left(q_{Ha} + q_{Hp} \right) \cdot \sin\beta \cdot \tan\gamma_a \\ - q_{Ha} \cdot \sin\beta \cdot \tan\delta_a \cdot \tan\delta_p \cdot m_{sw} \end{array} \right) \tag{3.43}$$

Here, $q_{Ha} \& q_{Hp}$ are from equation (3.13) and (3.19), respectively. The upper and lower bound solutions for yield acceleration (i.e., $k_{y,min}$ and $k_{y,max}$) may be calculated in the similar way of FS_{min} and FS_{max} are calculated.

3.2.7 Validation and Comparison of Results

To validate the distribution of acceleration in the landfill mass an acceleration ratio is computed. The acceleration ratio is the ratio of acceleration at the top of the landfill to the input acceleration at the base of the landfill. Present acceleration ratios are compared with the acceleration ratio obtained from linear analysis of model MSW using DEEPSOIL software. The assumptions and boundary conditions are kept identical in the DEEPSOIL analysis. A landfill of height 30 m, shear wave velocity 150 m/s, unit weight of MSW 10.5 kN/m^3, and damping ratio of 10% are used in the analysis. The results from the present study are in good agreement with the DEEPSOIL results as shown in Fig. 3.2. For an input frequency of 1.0 Hz ($\omega = 2\pi f = 6.28$ rad/s) the acceleration ratio from the present study is 3.103 and from DEEPSOIL it is 3.148. For an input frequency of 3.0 Hz ($\omega = 2\pi f = 18.85$ rad/s) the acceleration ratio from present study is 1.103 and from DEEPSOIL it is 1.113. The percentage difference between both the methods is even less than 1.5%.
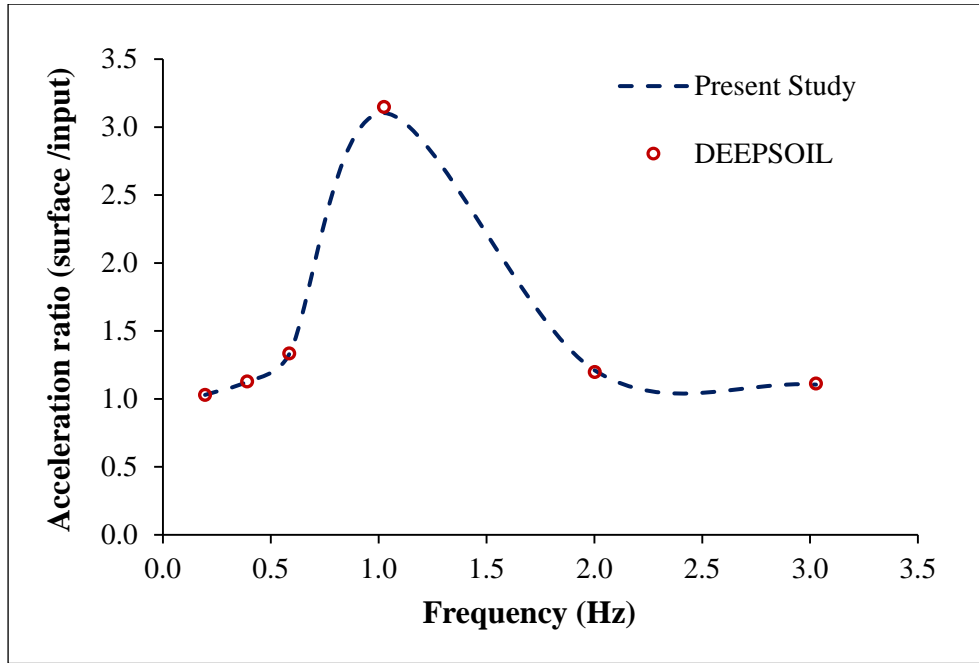
Fig. 3.2 Comparison of acceleration ratio values obtained by modified pseudo-dynamic method with the DEEPSOIL results for linear analysis

In the following section, results obtained using present method are compared with static analysis of Qian et al. (2003), pseudo-static analysis of Qian and Koerner (2010), and pseudo-dynamic analysis of Savoikar & Choudhury (2012) for similar landfill configurations and with same input parameters. By substituting the seismic forces equals to zero in the above equations results in similar equations of Qian et al. (2003). A comparison of results obtained in the present study with the Qian et al. (2003) for static conditions is presented in Table 3.1. As expected the results from present study matches exactly with the values of Qian et al. (2003) for the same input parameters. On comparing the results of present study with the existing methods shows the similar trends (Fig. 3.3 & Fig. 3.4). The present values lies between the results of static and pseudo-dynamic analysis. Qian et al. (2003) did not consider the seismic inertial forces and as a result the *FS* values is higher compared to all other methods. Method proposed by Qian and Koerner (2010) considered pseudo-static seismic force (constant inertial force as shown in Fig. 3.5) in their analysis, as a result *FS* values are 30-35% lower than values of static analysis. But, pseudo-static method ignored the time dependency nature of seismic forces. In case of pseudo-dynamic analysis of Savoikar and Choudhury (2012), researchers had considered the variation of seismic forces with time but the damping effect was ignored. And the solution proposed by Savoikar and Choudhury (2012) violates the boundary conditions. Pseudo-dynamic analysis addressed the phase change

42

of seismic inertia force but did not fully addressed, the effect of amplification on stability of landfill mass. For the mentioned set of input data, the seismic inertia force is not acting in same direction, whole waste mass is vibrating in third mode, as shown in Fig. 3.5. In which, the seismic force at bottom and top portions of landfill are acting in one direction and the seismic force at middle portions is acting in opposite direction. Because of that, net seismic inertia force acting on the waste mass is less compared to the one considered in pseudo-static analysis. This ultimately increases the *FS* values. The *FS* values calculated in the present study is 12 to 17% higher to pseudo-dynamic result [Fig. 3.4]. Also consideration of damping in the present analysis is reducing the seismic force; as a result *FS* values are increased.

Table 3.1: Comparison of factor of safety values obtained in the present study with Qian et al. (2003) for the static case

$H = 30$ m; $B = 40$ m; $\alpha = 14°$; $\delta_a = 15°$; $\delta_p = 20°$; $\gamma_{sw} = 10.2$ kN/m^2; $\phi_{sw} = 30°$			$H = 30$ m; $\beta = 18.4°$; $\alpha = 14°$; $\delta_a = 15°$; $\delta_p = 20°$; $\gamma_{sw} = 10.2$ kN/m^2; $\phi_{sw} = 30°$		
β (°)	Qian et al. (2003)	Present study ($k_h = 0$)	B/H	Qian et al. (2003)	Present study ($k_h = 0$)
12	1.36	1.36	0.25	1.26	1.26
14	1.40	1.40	0.50	1.31	1.31
18	1.53	1.53	0.75	1.37	1.37
22	1.65	1.65	1.00	1.44	1.44
26	1.77	1.77	1.25	1.51	1.51
30	1.89	1.89	1.50	1.60	1.60
34	2.02	2.02	2.00	1.80	1.80
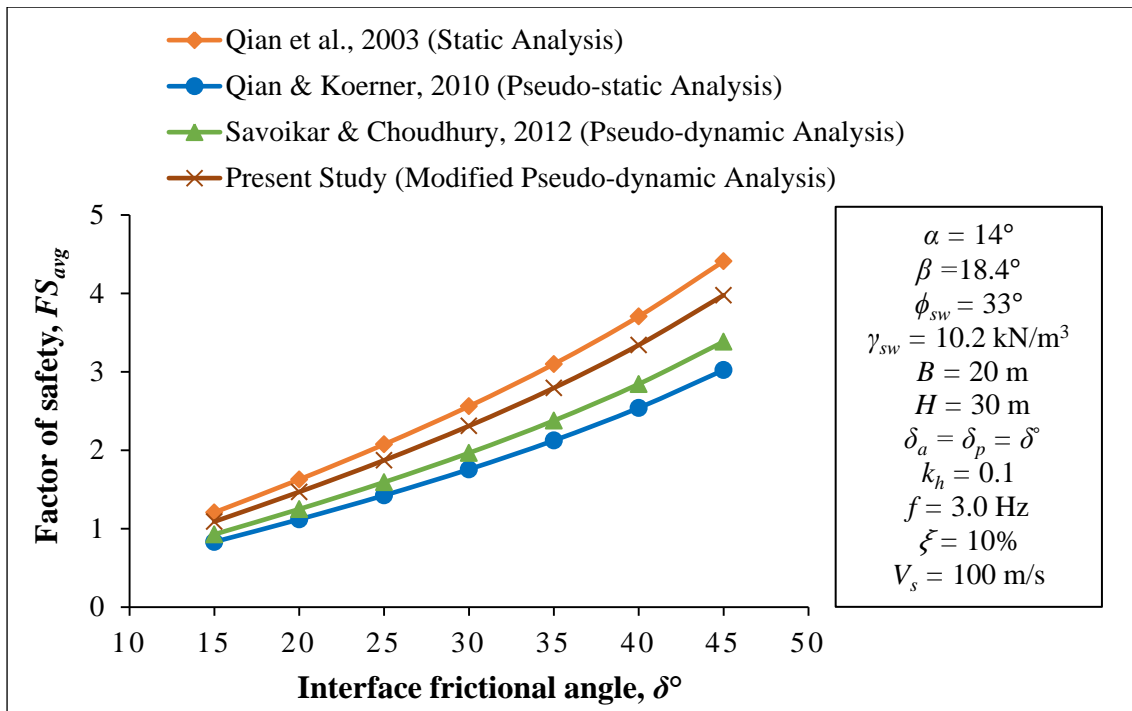
Fig. 3.3 Comparison of factor of safety values obtained in the present study with the similar existing literature for different values of δ°
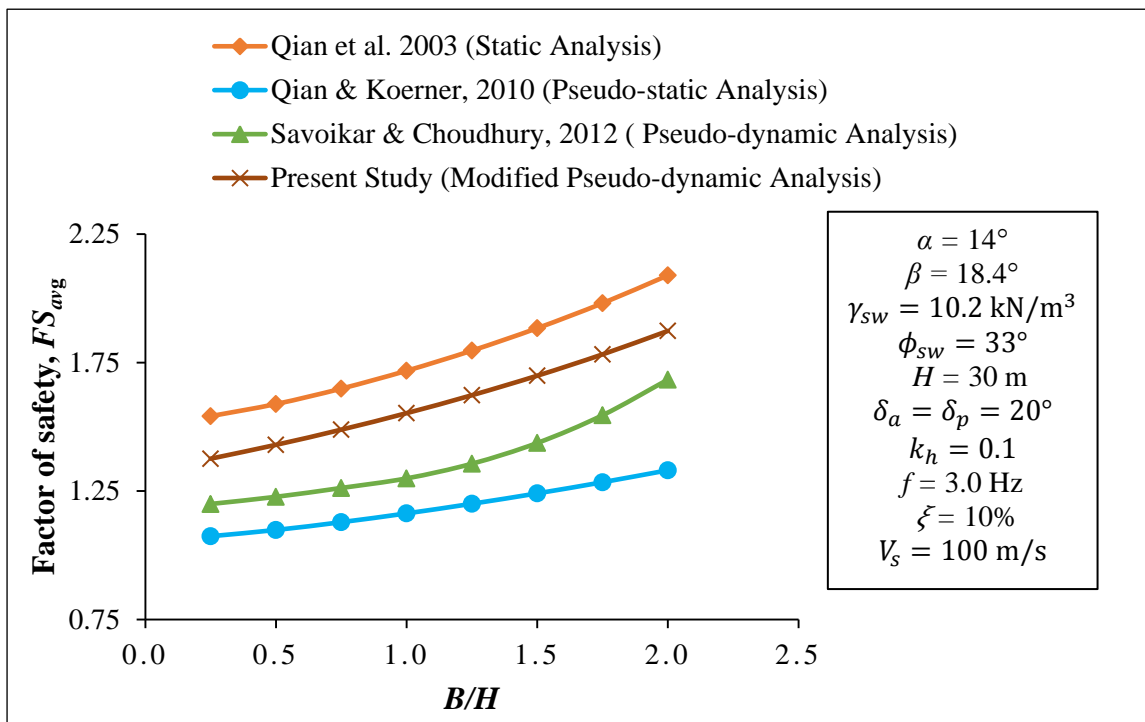
Fig. 3.4 Comparison of factor of safety values obtained in the present study with the similar existing literature for different *B/H* values

To show the importance of present study, the *FS* values for different front slope angles are computed at two different input frequencies ($f = 0.6$ Hz and $f = 3.0$ Hz) and compared in Table 3.2, with the existing pseudo-static and pseudo-dynamic methods keeping identical input parameters. For an input frequency of $f = 0.6$ Hz the FS values from pseudo-dynamic analysis are almost similar to the values of pseudo-static analysis. But from the present method the *FS* values are 16 – 20% lesser than the pseudo-static values. For another input frequency of $f = 3.0$ Hz the *FS* from pseudo-dynamic analysis are 11 – 16% higher than the values of pseudo-static analysis. But from the present method the *FS* values are 24 – 27% higher than the pseudo-static values. This can be attributed to the mode change behavior of landfill mass at different input frequencies. That means, for an input frequency of $f = 0.6$ Hz the landfill mass is in first mode of vibration where all the seismic inertial forces are acting in same direction. Because of increase in seismic forces, *FS* are decreased compared to pseudo-static results. But, for another input frequency of $f = 3$ Hz the landfill mass entered into third mode of vibration where some portion of the seismic force is acting in one direction and the remaining portion is acting in opposite direction. Because of this the net amount of seismic force acting on landfill mass is reduced, as a result higher *FS* is observed. Pseudo-dynamic method considered the phase change but violated boundary conditions and neglected mode change behavior. So, present method is suitable for the seismic translational stability analysis that gives safe and economical design.
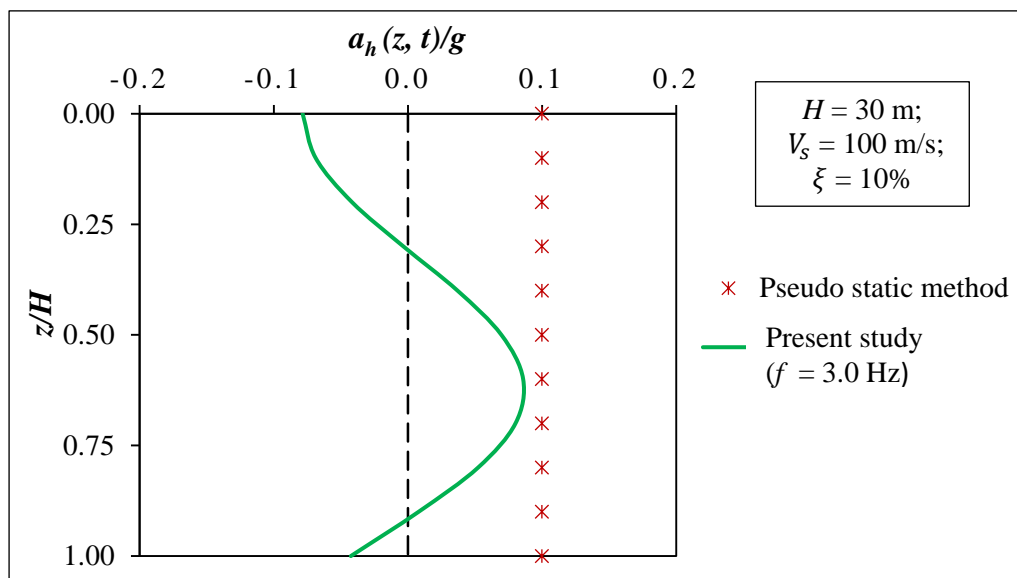
Fig. 3.5 Variation of acceleration profile with *z/H* for $H = 30$ m, $f = 3.0$ Hz, $V_s = 100$ m/s and $\xi = 10\%$

45

Present method is further validated against a well-documented failure case history under static condition. The static factor of safety values obtained from the present method is also compared with a failure case history data of Kettleman Hills waste landfill (Seed et al., 1990). The failure of Kettlemen Hills waste landfill was studied and reported well in literature. The geometric properties of Kettlemen Hills waste landfill at the location of was found from the literature as, the height of the landfill, H is 27.432 m, the average slope of fill slope, β is 18.43° (Seed et al., 1990). The interface residual strengths of liner after failure were found to be 8.5° for sloping sides and 8.0° for nearly level base (Seed et al., 1990). The average waste unit weight including the soil cover was found to be 17.62 kN/m³. The estimated FS at the time of failure was reported as 0.85 (Seed et al., 1990). Considering the above properties of Kettlemen Hills waste landfill as the input parameters and for $B = 40$ m; $\alpha = 14°$; $\phi_{sw} = 0°$ the static FS from the present method is 0.73. Difference in the FS values may be attributed to the difference in the calculation procedures and uncertainties in some of the geometric properties of landfill. So, present method is suitable for the seismic translational stability analysis that gives safe and economical design.

Table 3.2: Comparison of factor of safety values obtained in the present study with Qian and Koerner (2010) and Savoikar and Choudhury (2012) at two different input frequencies, for different values of front slope angle

$H = 30$ m; $B = 20$ m; $k_h = 0.1$; $\beta = 18.4°$; $\delta_a = 20°$; $\delta_p = 20°$; $\gamma_{sw} = 10.2$ kN/m²; $\phi_{sw} = 33°$; $V_s = 100$ m/s; $\xi = 10\%$					
α (°)	Qian and Koerner (2010)	$f = 0.6$ Hz		$f = 3.0$ Hz	
		Savoikar and Choudhury (2012)	Present study	Savoikar and Choudhury (2012)	Present study
10	1.40	1.41	1.13	1.63	1.92
12.5	1.21	1.22	0.99	1.36	1.61
15	1.06	1.07	0.88	1.20	1.39
17.5	0.95	0.96	0.79	1.13	1.23
20	0.86	0.88	0.71	1.10	1.13
22.5	0.82	0.83	0.65	0.99	1.09

3.2.8 Parametric Study

Using modified pseudo-dynamic method expressions upper and lower bound solutions of factor of safety are obtained. Minimum and maximum factor of safety is computed for different values of back slope angle β, front slope angle α, internal frictional angle of MSW ϕ_{sw}, minimum interface friction angles of liner components at the base of active and passive wedges δ_a and δ_p respectively and ratio of top width-to-height B/H. In addition, effect of angular frequency ω of input motion (or $f = 2\pi/\omega$) and damping of MSW on the values of factor of safeties and yield acceleration is also reported.

In the present parametric study, the following variation of parameters is used: $H = 30$ m, $B/H = 0.25$ to 2, $\alpha = 10$ to $25°$, $\beta = 12$ to $45°$, $\phi_{sw} = 15$ to $45°$, $\delta_a = \delta_p = 15$ to $45°$, $\gamma_{sw} = 10.5$ kN/m^3, $k_h = 0.1$, $V_s = 100$ and 150 m/s, $\omega H/V_s = 0$ to $3\pi/2$, $t/T = 0$ to 1, $z/H = 0$ to 1, and $\xi = 5$ to 15 %. The proposed method is coded using MATLAB program which compute the FS value at each time step for a given set of input parameters. For a given set of input parameters, the code first compute the acceleration profiles along the depth at each time step and these acceleration profiles are used to compute seismic inertial forces at each time step. FS values are computed at all the time steps using the proposed equations. In the present study, a non-dimensional time interval is used in the form of t/T. t/T is varied at an interval of 0.01 between 0 and 1. The value of FS is minimized with respect to t/T. In the similar way, minimum value of yield acceleration is calculated using same techniques that are employed for FS.

Fig. 3.6 shows the variation of factor of safety (i.e. FS_{min}, FS_{max} and FS_{avg}) for different values of internal friction angle of MSW$\left(\phi_{sw}\right)$. From Fig. 3.6, it is observe that FS_{max} goes on increasing with an increment in the value of $\left(\phi_{sw}\right)$ (i.e., stability increases with increase in ϕ_{sw}), while the lower bound value$\left(FS_{min}\right)$ remains constant. The strength of waste mass is ignored in the calculation of $FS_{min}\left[FS_V \rightarrow \infty\right]$. The absolute maximum difference between FS_{true} and FS_{avg} is less than 2.96% when ϕ_{sw} is changed from 15 to $50°$. FS_{max} is 1.25 % higher than FS_{min} for $\phi_{sw} = 15°$. The difference between these is increased to 5% for $\phi_{sw} = 50°$.

Fig. 3.7 shows the variation of FS for different values of front slope angle$\left(\alpha\right)$. From, it is observe that the FS is significantly decreased with the increase of α. This is because an

increase in front slope angle is decreasing the weight of passive wedge, which is one of the major resisting forces. As a result FS is decreasing. The absolute maximum difference between FS_{true} and FS_{avg} is less than 1.6% when α is varied from 10 to $25°$. FS_{max} is 3.2% higher than FS_{min} for $\alpha = 10°$. It should be noted that FS_{max} and FS_{min} are same for $\alpha = 22.5°$.
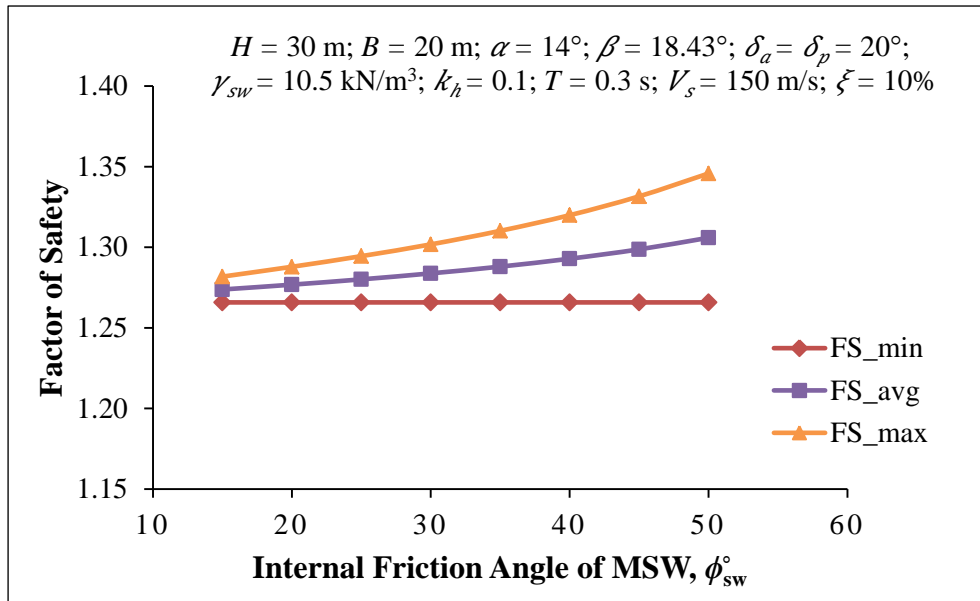
Fig. 3.6 Variation of factor of safety with ϕ_{sw}°
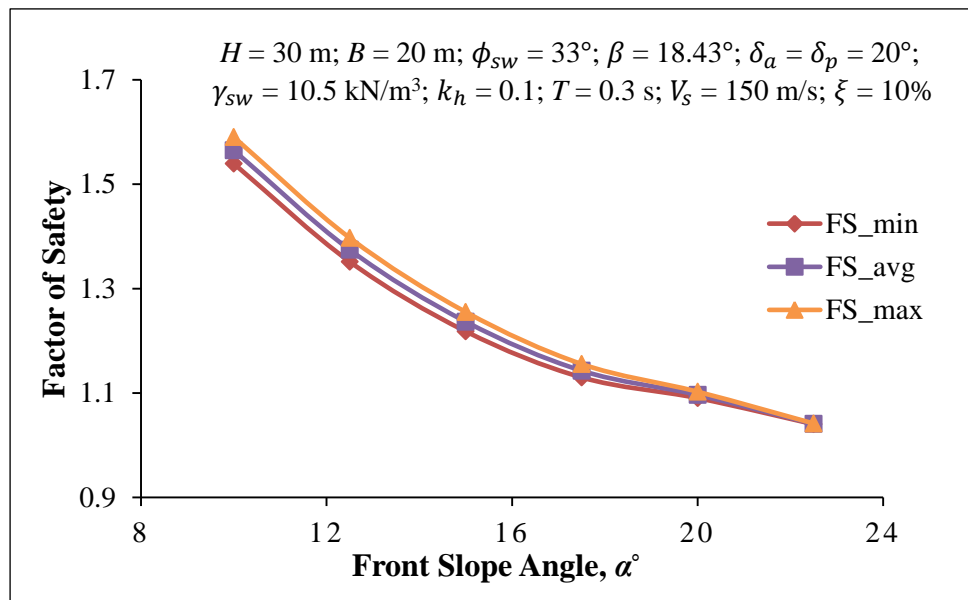
Fig. 3.7 Variation of factor of safety with α°

Fig. 3.8 shows the variation of FS for different values of base slope angle (β). It is observed that the FS is first decreasing when β is increasing from 12 to $18.4°$ and then FS is increasing

when β is increased up to 45°. This is because when black slope angle is increasing the driving force acting on the active wedge is also increasing; as a result FS is decreasing when β is between 12 to 18.4°. At the same time, with an increase in β the weight of passive wedge is also increasing. When $\beta > 18.4°$, the increase in weight of passive wedge is capable of resisting the increased driving force acting on active wedge which increases the FS. FS_{max} and FS_{min} are same for $\beta = 12°$. FS_{max} is 13.8% higher than FS_{min} for $\beta = 46°$. The upper bound difference between FS_{true} and FS_{avg} is more than 5% when β is $> 34°$, but still less than 10% for $\beta = 40°$. Form conservative consideration, FS_{min} may be used when β is $> 34°$.
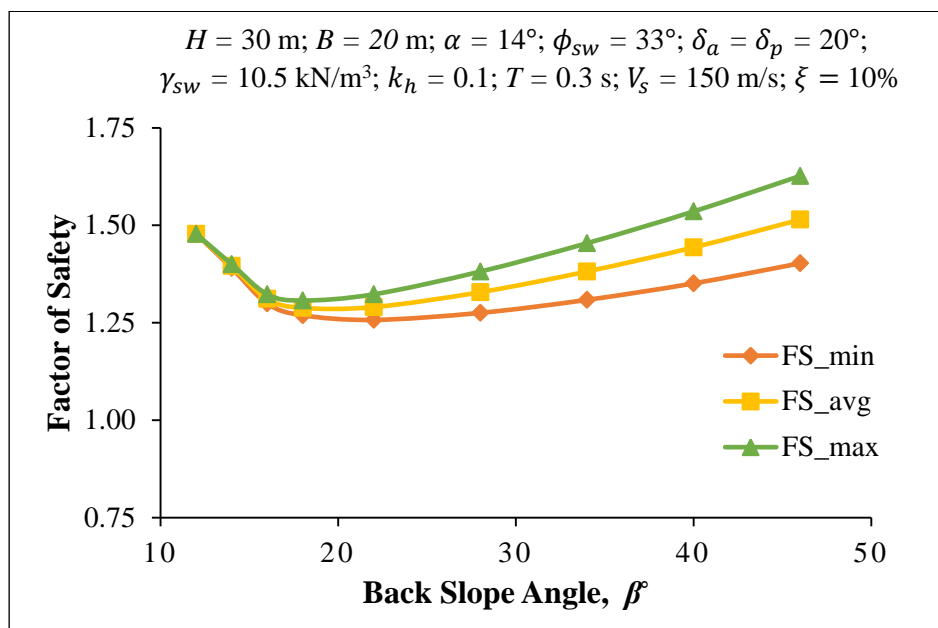
Fig. 3.8 Variation of factor of safety with $\beta°$

The effect of minimum interface friction angle of liner components at the base of active wedge δ_a on the FS is shown in Fig. 3.9. As expected, increase in δ_a results a higher FS value. The absolute maximum difference between FS_{true} and FS_{avg} is approximately 3.2% when δ_a is changed from 15 to 45°. For lower value of δ_a FS_{max} is 6.49% higher than FS_{min}. FS_{max} and FS_{min} values are same for higher values of δ_a. The effect of minimum interface friction angle of liner components at the base of passive wedge δ_p on the FS is shown in Fig. 3.10. It should also be noted that, increase in δ_p results a higher FS value. The absolute maximum difference between FS_{true} and FS_{avg} is approximately 4% when δ_p is changed

49

from 15 to 45°. For lower value of δ_p FS_{max} is 1.7% higher than FS_{min}. But for higher values of δ_p FS_{max} is 8% higher than FS_{min}.

$H = 30$ m; $B = 20$ m; $\alpha = 14°$; $\phi_{sw} = 33°$; $\beta = 18.43°$; $\delta_p = 20°$; $\gamma_{sw} = 10.5$ kN/m³; $k_h = 0.1$; $T = 0.3$ s; $V_s = 150$ m/s; $\xi = 10\%$

Fig. 3.9 Variation of factor of safety with δ_a°

$H = 30$ m; $B = 20$ m; $\alpha = 14°$; $\phi_{sw} = 33°$; $\beta = 18.43°$; $\delta_a = 20°$; $\gamma_{sw} = 10.5$ kN/m³; $k_h = 0.1$; $T = 0.3$ s; $V_s = 150$ m/s; $\xi = 10\%$
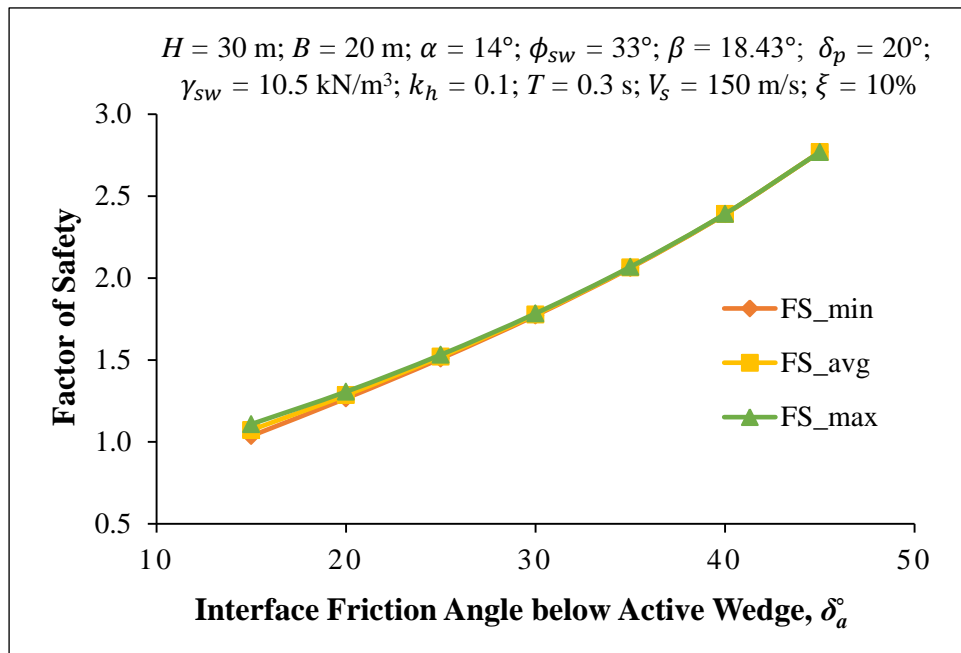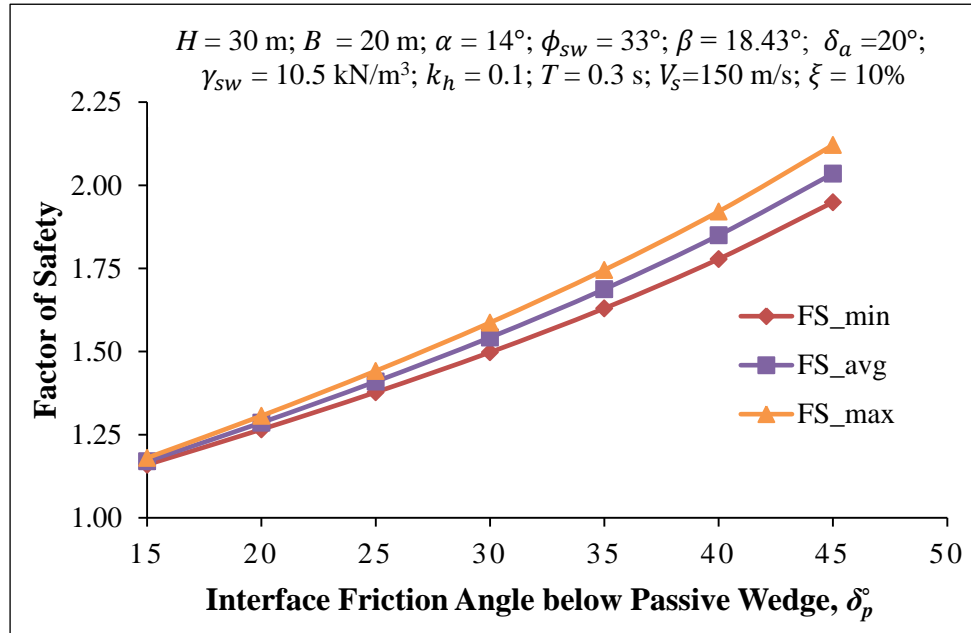
Fig. 3.10 Variation of factor of safety with δ_p°

Fig. 3.11 shows the variation of *FS* for different values of *B/H*. *FS* values are increasing when *B/H* is increased from 0.25 to 2.0. The upper bound difference between FS_{true} and FS_{avg} is

less than 1.7% when *B/H* is varied between 0.25 and 2.0. FS_{max} is 3.4% higher than FS_{min} for *B/H* = 0.25 and this difference is decreasing slightly with increase of *B/H*.
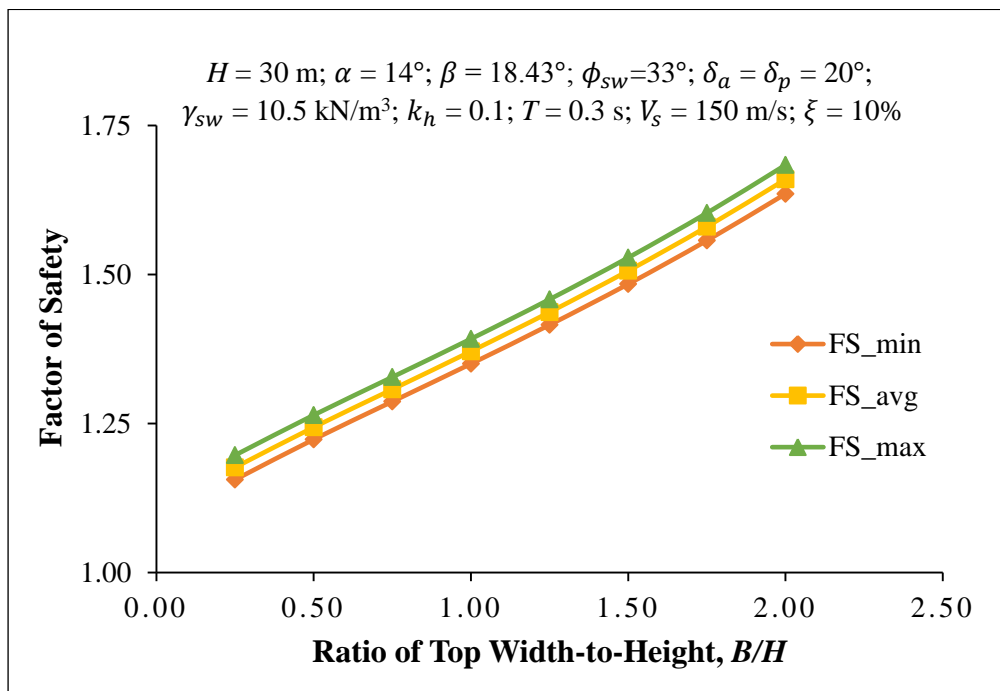
Fig. 3.11 Variation of factor of safety with *B/H*

Fig. 3.12 shows the variation of k_y for different values of *B/H*. k_y is increasing with the increase of *B/H* between 0.25 and 2.0. Also effect of input frequency of harmonic excitation (*f*) on k_y is shown in Fig. 3.12. When *f* is 3.33 Hz (*T* = 0.3 s) the k_y values are higher. This is because, if we see the acceleration profile when *f* = 3.33 Hz in Fig. 3.13, it is very clear that the landfill is in second mode of vibration. One portion of the waste mass is moving in one direction and the rest of the portion of the waste mass is moving in the opposite direction. As a result low inertial force is acting on the waste mass. Hence, input motion with higher amplitude is required to cause failure. When *f* = 1 Hz (*T* =1 s) the k_y values are the lowest. From Fig. 3.13 it may be seen that the base acceleration coefficient for *f* = 1 Hz is highly amplified. As a result very high inertial forces are generating and which is reducing the k_y – values to a greater extent. When *f* = 0.2 Hz (*T* = 5 s) the k_y values are in intermediate range because of no amplification of input acceleration. That means, it is similar to acceleration profile in pseudo- static case as shown in Fig. 3.13. Present method not only considers the amplification of input acceleration and higher mode of vibration is also considered.
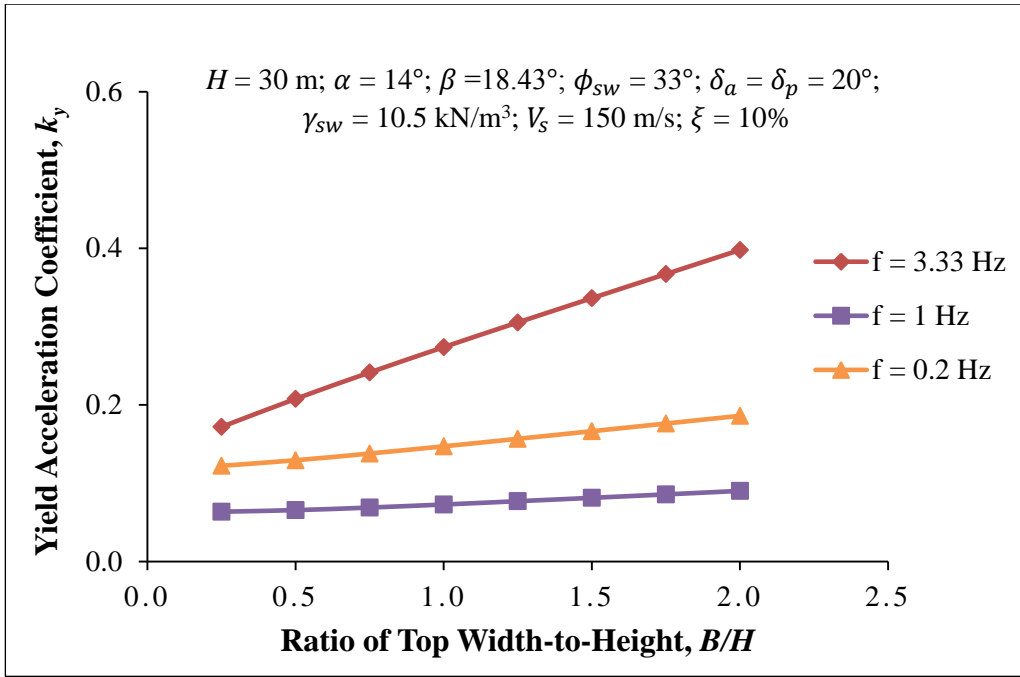
Fig. 3.12 Variation of yield acceleration coefficient with *B/H* and *f*
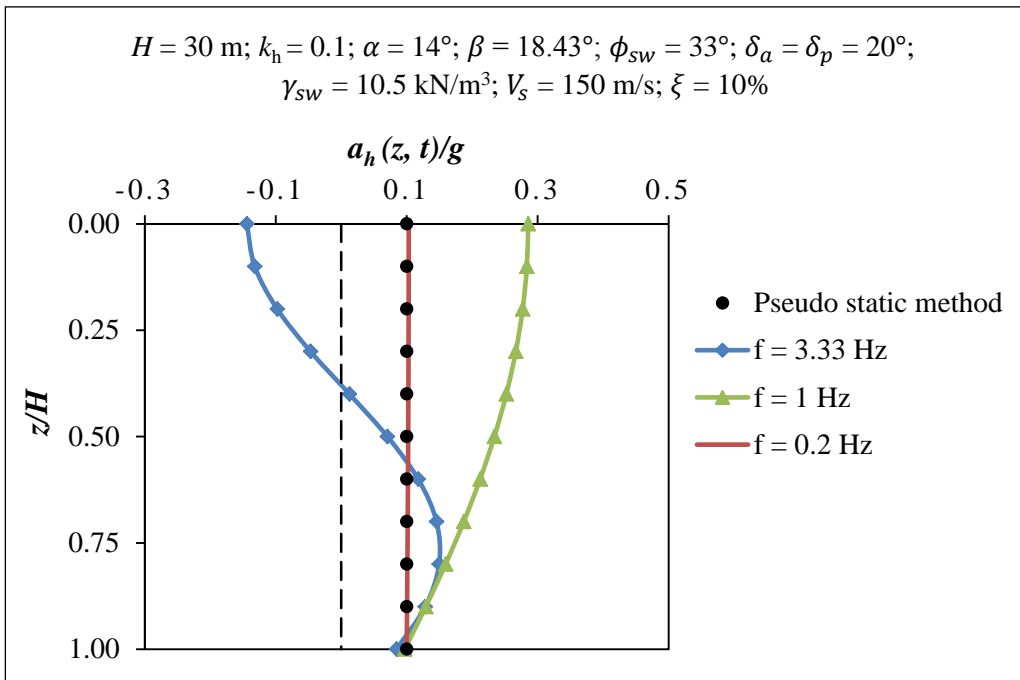
Fig. 3.13 Variation of acceleration profile with *z/H* for different input frequencies of 0.2, 1.0, and 3.33 Hz

The variation of amplification ratio with a non-dimensional parameter *kH* is shown in Fig. 3.14. Amplification ratio depends on input frequency f, shear wave velocity V_s of the waste

mass, and the thickness of waste mass H. When kH is equals to 1.5 (for frequency $f = 0.8$ Hz), input frequency is very close to fundamental frequency $f = V_s/4H = 0.833$ Hz ($kH = 1.57$), the amplification factor is 7.11 for 10% damping. When $kH = 4.5$ (for frequency $f = 2.39$ Hz), that means for a input frequency approaching to second fundamental frequency $f = 2.49$ Hz, the amplification factor is 2.35 for 10% damping. So, it is clear that as kH approaches to $\pi/2 + n\pi$ resonance is occurring. At the fundamental frequency the landfill acceleration is in phase at all depths. But for frequencies higher than fundamental frequency it enters into higher modes of vibration where some part of landfill mass moves in one direction and the remaining moves in opposite direction. As a result the effect of net seismic forces acting on landfill will reduce as already discussed earlier. This may be understood in better way with the help of acceleration profiles in Fig. 3.15 and the variation of yield acceleration coefficient and FS values for different frequencies in Table 3.3. The acceleration at all depths are in phase and the acceleration ratio is increasing with increase in frequency up to 0.8 Hz as shown in Fig. 3.15 for the mentioned set of input parameters, as a result yield acceleration coefficient and FS values are decreasing as shown in Table 3.3. The amplification ratio for the frequencies 0.2 Hz, 0.4 Hz and 0.6 Hz are 1.07, 1.35, and 2.24 respectively. When frequency is increased to 1 Hz (amplification ratio is 4.17) the landfill enters into second mode, as a result yield acceleration and FS value is increased as shown in Table 3.3. To have an economical design of landfills this phenomenon should be consider while calculating seismic inertial forces acting on landfill which are used in stability analysis. This parametric analysis highlights that landfills with the configuration same as mentioned in Table 3.3 are highly susceptible to earthquakes with corner frequency < 1Hz. The effect of damping is also shown in Fig. 3.14, with increasing damping the peak amplification ratio is significantly decreasing. When kH is 1.5 the amplification factor is 12.1 for 5% damping and is reduced to 7.11 for 10 % damping, nearly $30 - 40\%$ decrement of forces is observed with 5% increase in damping. The effect of damping is more at higher frequencies than at lower frequencies.
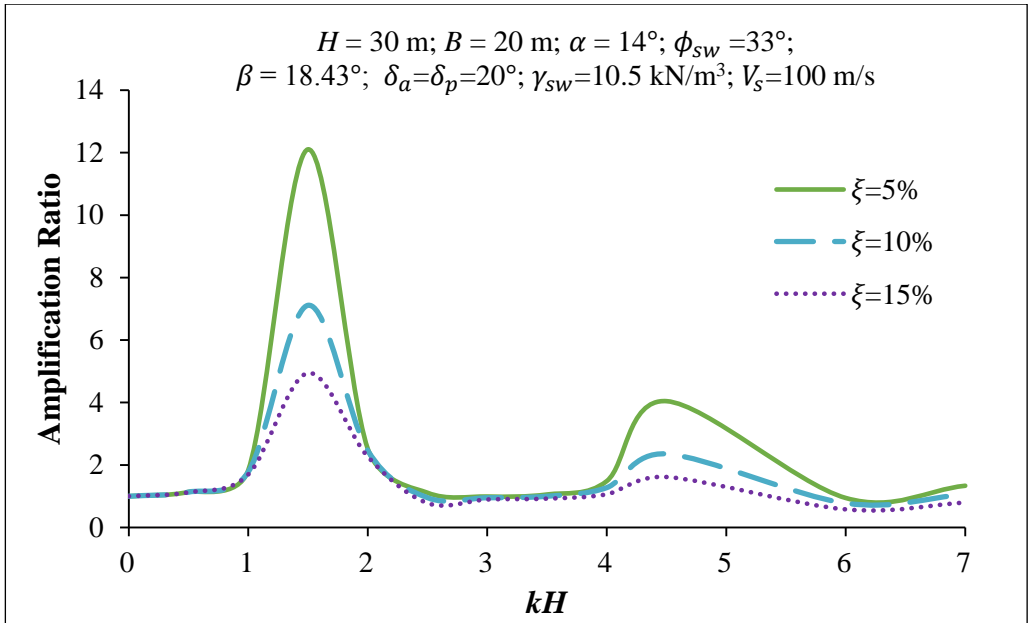
Fig. 3.14 Variation of amplification ratio with *kH* and damping ratio
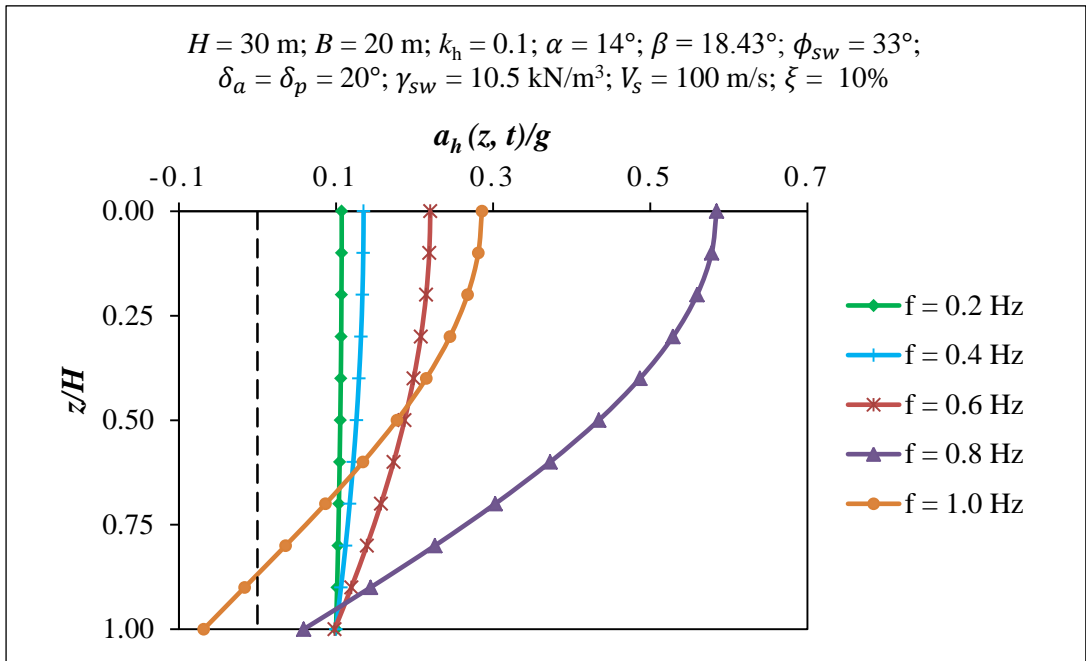
Fig. 3.15 Variation of acceleration profile with *z/H* for different input frequencies between

0 to 1 Hz

54

Table 3.3: Yield acceleration coefficient and factor of safety values for different values of frequency

$H = 30$ m; $B = 20$ m; $k_h = 0.05$; $\alpha = 14°$; $\phi_{sw} = 33°$; $\beta = 18.43°$; $\delta_a = \delta p = 20°$; $\gamma_{sw} = 10.5$ kN/m³; $V_s = 100$ m/s; $\xi = 10\%$		
Frequency, f (Hz)	Yield acceleration coefficient, k_y	Factor of safety, FS_{avg}
0.2	0.132	1.318
0.4	0.114	1.280
0.6	0.082	1.179
0.8	0.039	0.903
1.0	0.113	1.272

3.3 Equivalent Linear Analysis

3.3.1 Proposed Methodology

In the above linear analysis, low-strain shear modulus and constant damping ratio of MSW are used. But in reality, the shear strain generated during a seismic event is significantly large. So, in the present equivalent linear analysis strain-dependent shear modulus and damping ratio have been used to compute acceleration profiles, *FS* and yield acceleration coefficient of a MSW landfill.

The partial derivative of equation (3.5) with respect to 'z' gives the expression for shear strain, γ_s as a function of depth (z) and time (t), and the expression is as follows;

$$\gamma_s(z,t) = \frac{\partial u(z,t)}{\partial z} = \frac{u_{ho}}{C^2 + S^2}\left[A_h \cos(\omega t) + B_h \sin(\omega t)\right] \tag{3.44}$$

Where,

$$A_h = y_2 C_{c_z} C_c - y_1 S_{s_z} C_c + y_1 C_{c_z} S_s + y_2 S_{s_z} S_s \tag{3.45a}$$

$$B_h = y_1 S_{s_z} S_s - y_2 C_{c_z} S_s + y_1 C_{c_z} C_c + y_2 S_{s_z} C_c \tag{3.45b}$$

Where,

$$C_{c_z} = \frac{1}{H}\left[\cos\left(\frac{y_1 z}{H}\right)\sinh\left(\frac{y_2 z}{H}\right)\right] \tag{3.46a}$$

$$S_{s_z} = \frac{1}{H}\left[\sin\left(\frac{y_1 z}{H}\right)\cosh\left(\frac{y_2 z}{H}\right)\right] \tag{3.46b}$$

$$C_c = \cos\left(y_1\right)\cosh\left(y_2\right) \tag{3.46c}$$

$$S_s = \sin\left(y_1\right)\sinh\left(y_2\right) \tag{3.46d}$$

It is worth mentioning that modulus reduction and damping ratio curves are required in the present solution. These two curves are developed by conducting cyclic triaxial tests on MSW from a specific landfill. Zekkos et al. (2008) proposed the shear modulus and damping curves of MSW from a landfill in the San Francisco, USA. Similarly, Ramaiah et al. (2016a, 2017) proposed the shear modulus and damping curves of MSW from two waste dumps in Delhi, India. In the absence of specific landfill data, curves available in the literature may be used. Choudhury and Savoikar (2009b) proposed the modulus reduction and damping curves of MSW by using world wide data available in the literature, with the help of best curve fitting techniques. In the present study, the curves proposed by Choudhury and Savoikar (2009b) are used. The mathematical expressions for these curves are as follows;

Expression for modulus reduction curve is;

$$\frac{G_{sec}}{G_{max}} = \frac{1}{1 + 7.85\gamma_u^{0.95}} \tag{3.47a}$$

Expression for damping ratio curve is;

$$\xi = 30\left(1 - e^{-1.4\,\gamma_u^{0.36}}\right) \tag{3.47b}$$

where, γ_u is the percentage shear strain; G_{sec} is the secant shear modulus; and $G_{max} = V_s^2\rho_{sw}$ is the low strain shear modulus.

The equations given in section 3.2.4 are modified by considering the minimum interface cohesion of liner materials.

Inter-wedge forces acting at the interface between active and passive wedges may be given as;

56

$$E_{Vp} = E_{Hp} \cdot \tan\phi_{sw}/FS_V + C_{sw}/FS_V$$

$$= E_{Hp} \cdot m_{sw} + n_{sw} \qquad \left(\begin{array}{c} \text{say, } \tan\phi_{sw}/FS_V = m_{sw} \\ C_{sw}/FS_V = n_{sw} \end{array} \right) \qquad \text{(3.48a)}$$

$$E_{Va} = E_{Ha} \cdot \tan\phi_{sw}/FS_V + C_{sw}/FS_V$$

$$= E_{Ha} \cdot m_{sw} + n_{sw} \qquad \qquad \text{(3.48b)}$$

Frictional forces acting along the liners of active and passive wedges may be given as;

$$F_p = N_p \cdot \tan\delta_p/FS_p + C_p/FS_p \qquad \qquad \text{(3.48c)}$$

$$F_a = N_a \cdot \tan\delta_a/FS_a + C_a/FS_a \qquad \qquad \text{(3.48d)}$$

where, $\phi_{sw} \& C_{sw}$ are the internal shear strength parameters of solid waste; $\delta_a \& C_a$ are the interface shear strength parameters below active wedge; $\delta_p \& C_p$ are the interface shear strength parameters below passive wedge; $FS_a, FS_p \& FS_V$ are the factor of safeties for an active wedge, passive wedge and at the interface between the wedges respectively.

Applying the equations of equilibrium for both active and passive wedges by considering all the forces acting on it, including the weights of active (W_a) and passive (W_p) wedges. After simplifying the equations, the normal forces acting at the interface of active and passive wedges (i.e., $E_{Ha} \& E_{Hp}$ respectively) may be represented as;

$$E_{Ha} = \frac{(W_a + n_{sw}) \cdot (\sin\beta - \cos\beta \cdot \tan\delta_a/FS_a) + Q_{Ha} \cdot (\cos\beta + \sin\beta \cdot \tan\delta_a/FS_a) - C_a/FS_a}{\cos\beta + \sin\beta \cdot \tan\delta_a/FS_a + m_{sw} \cdot (\sin\beta - \cos\beta \cdot \tan\delta_a/FS_a)} \quad \text{(3.49a)}$$

$$E_{Hp} = \frac{(W_p + n_{sw}) \cdot \tan\delta_p/FS_p - Q_{Hp} + C_p/FS_p}{1 - m_{sw} \cdot \tan\delta_p/FS_p} \qquad \qquad \text{(3.49b)}$$

For the equilibrium of entire waste mass, requres $E_{Ha} = E_{Hp}$. Consider $FS_a = FS_p = FS$ (factor of safety of entire waste mass). After rearranging the terms, the final FS equation may be of the form;

$$a \cdot FS^2 + b \cdot FS + c = 0 \qquad \qquad \text{(3.50)}$$

Where

$$a = Q_{Hp} \cdot \sin \beta \cdot m_{sw} + W_a \cdot \sin \beta + \left(Q_{Ha} + Q_{Hp}\right) \cdot \cos \beta - n_{sw} \cdot \sin \beta;$$

$$b = -\begin{bmatrix} W_t \cdot \sin \beta \cdot \tan \delta_p \cdot m_{sw} + W_p \cdot \cos \beta \cdot \tan \delta_p + W_a \cdot \cos \beta \cdot \tan \delta_a + Q_{Hp} \cdot \cos \beta \cdot \tan \delta_a \cdot m_{sw} \\ + Q_{Ha} \cdot \cos \beta \cdot \tan \delta_p \cdot m_{sw} - \left(Q_{Ha} + Q_{Hp}\right) \cdot \sin \beta \cdot \tan \delta_a + n_{sw} \cdot \cos \beta \left(\tan \delta_p - \tan \delta_a\right) \\ + C_p \cdot \sin \beta \cdot m_{sw} + C_a + C_p \cdot \cos \beta \end{bmatrix};$$

$$c = W_t \cdot \cos \beta \cdot \tan \delta_a \cdot \tan \delta_p \cdot m_{sw} - W_p \cdot \sin \beta \cdot \tan \delta_a \cdot \tan \delta_p - Q_{Ha} \cdot \sin \beta \cdot \tan \delta_a \cdot \tan \delta_p \cdot m_{sw} -$$
$$n_{sw} . \tan \delta_a \cdot \tan \delta_p \cdot \sin \beta - C_p \cdot \sin \beta . \tan \delta_a + m_{sw} \left(C_p \cdot \cos \beta . \tan \delta_a + C_a \cdot \tan \delta_p\right)$$

The expressions for the factor of safety of FS_{min}, FS_{max} and FS_{avg} could be derived in the similar way explained in section 3.2.5. The procedure for the calculation of FS is coded using MATLAB program.

The following are the programming steps:

1. Develop modulus reduction and damping curves of MSW from laboratory tests performed on an MSW of the specific landfill. In the absence of those, curves available in the published literature may be used.

2. Assign low strain values of shear modulus (G) and damping ratio (ξ).

3. At a particular time step use shear modulus (G) and damping ratio (ξ) to compute the maximum shear strain along the depth of the landfill using equation (3.44).

4. Compute the effective shear strain from maximum shear strain using,

$$\gamma_{eff}^i = R_\gamma * \gamma_{max}^i$$

where the superscript (i) indicates the iteration number and R_γ is the ratio of effective shear strain and maximum shear strain. In the present study R_γ is treated as one.

5. Use the effective shear strain to compute a new set of values ($G^{(i+1)}$ and $\xi^{(i+1)}$) using the modulus reduction and damping ratio curves for the next iteration.

6. Repeat the steps 3 to 5 until the difference between the computed shear modulus and damping ratio in two successive iterations is less than 5%.

7. The shear modulus and damping ratio corresponding to the last iteration are the equivalent linear values. Use the equivalent linear values to compute the acceleration profiles along the depth at that particular time step.

8. Use the acceleration profiles to compute seismic inertial forces at the same time step.

9. Use the seismic inertial forces to compute the FS values for the same time step using the proposed equations.

10. Repeat the steps 2 to 9 for the next time step.

The minimum acceleration coefficient required for the yielding of waste mass along the failure plane may be termed as yield acceleration coefficient, k_y. Yielding of waste mass just starts when the *FS* is unity. Similar to the *FS*, the expression for the average yield acceleration coefficient could be derived in the similar way explained in section 3.2.6.

3.3.2 Linear and equivalent linear ground response analysis using DEEPSOIL

Site-specific ground response analysis is a very handy tool to access the acceleration distribution in an MSW landfill body when it is subjected to base shaking. The ground response analysis may be categorized into three type's linear, equivalent linear and non-linear. Many researchers had employed an equivalent linear approach to quantify the amplification or de-amplification of the input seismic ground motion in the MSW landfill (Bray et al., 1995, Choudhury and Savoikar, 2009a, Anbazhagan et al., 2016). In the present study, DEEPSOIL is used to carry out 1-D ground response analysis using linear and equivalent linear approach. The height of the MSW column is kept equal to the total height of the landfill. In the linear analysis, small strain value of shear wave velocity is used and a fixed damping ratio value is assigned to MSW material. The input parameters for the linear analysis are H = 30m, V_s = 150 m/s, γ_{sw} = 10.5 kN/m^3 and ξ = 10%. The boundary condition in DEEPSOIL is kept exactly same as in the proposed method i.e. the MSW column is resting on rigid bedrock. The MSW column is subjected to a harmonic shaking $k_h g^* cos(\omega t)$. And the duration of shaking is kept equal to the time period of the input motion, T $(2\pi/\omega)$. The seismic acceleration at the surface is obtained using the linear analysis in DEEPSOIL. Acceleration ratio is computed, which is nothing but the ratio of the acceleration at the top of the MSW column to the input acceleration.

In reality, the shear strain generated during a seismic event is significantly large. And it is well established in geotechnical earthquake engineering that the shear modulus decreases significantly with the increase in the shear strain and at the same time damping ratio value increases. The equivalent linear approach of ground response analysis uses two curves namely modulus reduction curve and damping ratio curve to arrive at a strain dependent shear modulus and damping ratio value. It is an iterative process. In the present study, the modulus reduction curve and damping ratio curve proposed by Choudhury and Savoikar (2009b) is used in the DEEPSOIL equivalent linear analysis. Unit weight of the MSW, boundary condition and input motion are kept same as the linear analysis. Acceleration ratio is also computed for the equivalent linear approach.

3.3.3 Comparison of acceleration ratio from present analytical method with the results of 1D site response analysis, DEEPSOIL

Distribution of acceleration along the depth of waste mass is very important for the evaluation of seismic inertial forces over the landfill. The acceleration profiles obtained from the present study linear and equivalent linear analysis are validated using DEEPSOIL linear and equivalent linear results. A non-dimensional parameter named as acceleration ratio is computed. The ratio of surface acceleration to that of input acceleration is known as acceleration ratio or, sometimes called as amplification ratio. The acceleration ratios obtained from the present analytical method are in good agreement with the DEEPSOIL results as shown in Fig. 3.16. It also shows the comparison of results from linear and equivalent linear analysis using the present method as well as DEEPSOIL.

In the case of linear analysis, a constant low strain shear modulus and damping properties are used. In the present analysis low strain $G_{max} = 24.082$ MPa ($V_s = 150$ m/s), $\gamma_{sw} = 10.5$ kN/m^3 and $\xi = 10\%$ are used as input parameters. For an input frequency of $f = 0.4$ Hz ($\omega = 2\pi f = 2.513$ rad/s), the acceleration ratio from the present linear analysis is 1.127 and from the DEEPSOIL linear analysis is 1.129. Similarly, for another input frequency of $f = 1$ Hz ($\omega = 2\pi f = 6.283$ rad/s), the acceleration ratio from present linear analysis is 3.104 and from DEEPSOIL linear analysis is 3.148. The percentage error in linear analysis is very less, infect it is less than 1.5%.

In the case of equivalent linear analysis, the properties such as modulus reduction and damping increase with an increase in cyclic shear strain are considered. The strain-dependent dynamic properties obtained from the present equivalent linear analysis is given in Table 3.4. For an input frequency of $f = 0.65$ Hz ($\omega = 2\pi f = 4.084$ rad/s), the acceleration ratio from present equivalent linear analysis is 2.61 and from DEEPSOIL equivalent linear analysis is 2.79. Similarly, for another input frequency of $f = 3$ Hz ($\omega = 2\pi f = 18.849$ rad/s), the acceleration ratio from present equivalent linear analysis is 1.502 and from DEEPSOIL equivalent linear analysis is 1.58. The percentage error in equivalent linear analysis is about 5 − 10%. The equivalent linear analysis graphs are shifted towards left side of linear analysis graphs [Fig. 3.16]. This might be attributed to the use of strain dependent dynamic properties instead of using low strain dynamic properties.
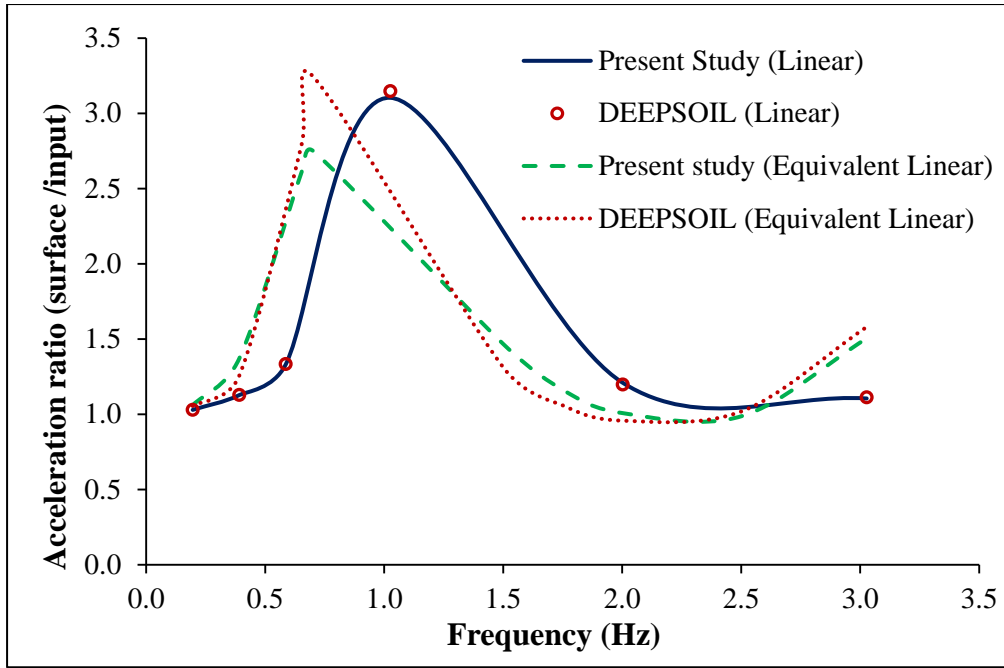
Fig. 3.16 Comparison of acceleration ratio obtained from the proposed linear and equivalent linear based approach with DEEPSOIL

Table 3.4: Strain dependent equivalent linear properties of MSW used in present study

S.no.	Frequency (Hz)	Shear wave velocity (m/s)	Damping ratio (%)
1	0.5	54.706	21.86
2	1.0	93.508	15.99
3	1.5	120.112	12.07
4	2.0	132.549	9.81
5	2.5	136.199	9.00
6	3.0	132.809	9.76

3.3.4 Convergence of the proposed iterative scheme

As explained in the above sections, computation of equivalent linear properties is an iterative procedure. To check the convergence of the proposed method, shear strain at different frequencies is plotted [Fig. 3.17]. In the present analysis, $H = 30$ m, $\gamma_{sw} = 10.5$ kN/m^3 and the low strain dynamic properties $V_s = 150$ m/s and $\xi = 10\%$ are used as input parameters. Fig. 3.17 clearly indicates that the results are converging after a maximum of 15 iterations. The number of iterations required for the convergence of results is changing with input frequency.

And also a change in the input frequency results in the change of maximum shear strain value and its point of occurrence along the depth of the landfill. For an input frequency of $f = 0.2$ Hz ($\omega = 2\pi f = 1.256$ rad/s), the maximum shear strain obtained is 0.14 % and it is occurred in the bottom portion of landfill as shown in Fig. 3.17(a). For an input frequency of $f = 0.5$ Hz ($\omega = 2\pi f = 3.142$ rad/s), the maximum shear strain obtained is 0.81 % and it occurred just above the base of the landfill [Fig. 3.17(b)]. Further increase in input frequency the maximum shear strain value is highly decreased as the landfill is entered into higher modes. And point of occurrence of maximum shear strain is shifted towards the top of landfill as in Fig. 3.17(c) and Fig. 3.17(d).
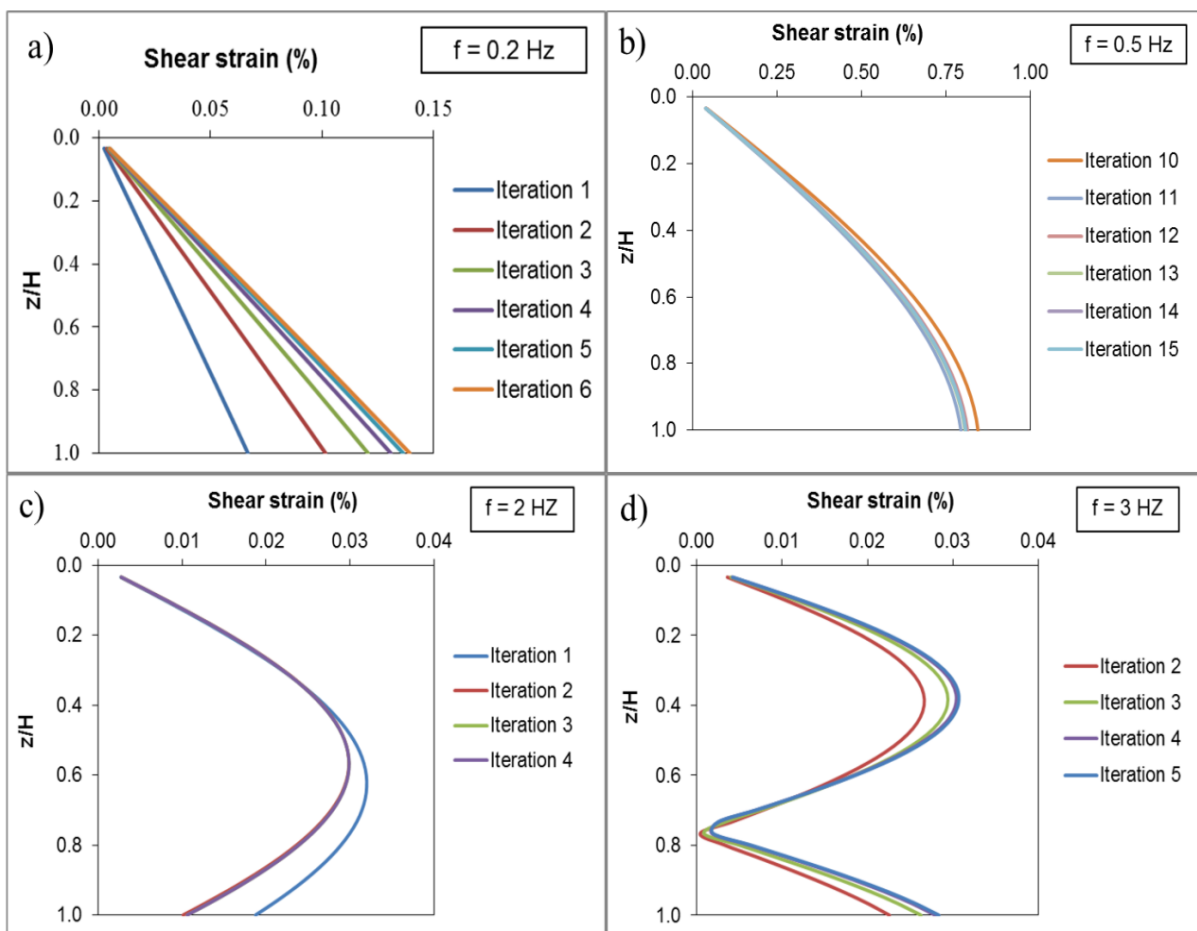
Fig. 3.17 Variation of shear strain along the depth of landfill for different input frequencies

3.3.5 Comparison of factor of safety and yield acceleration coefficient

To access the seismic stability of landfills, a *FS* values are computed and also compared with the existing pseudo-static and pseudo-dynamic methods. In the present study, a non-dimensional time interval is used in the form of *t/T (t* is time and *T* is period of lateral

shaking). The *FS* is minimized by varying *t/T* at an interval of 0.01 between 0 and 1 in the developed MATLAB program. The input parameters used in the present analysis are $H = 30$ m, $B = 20$ m, $\alpha = 14°$, $\beta = 18.43°$, $\gamma_{sw} = 10.5$ kN/m³, $\delta_a = \delta_p = 10 - 40°$, $C_a = C_p = 5 - 40$ kN/m², $\phi_{sw} = 30°$, $C_{sw} = 0 - 3$ kN/m², $V_s = 150$ m/s, $f = 0 - 3$ Hz and $\xi = 10\%$.

Effect of interface cohesion of liner materials is shown in Fig. 3.18 and the comparison of the present study with the pseudo-static and pseudo-dynamic methods is also shown. It may be clearly seen that an increase in interface cohesion increases the *FS*. The increase in interface cohesion increases the total resistive force as a result factor safety is increasing. Results from the present study follow the similar trend as that of pseudo-static and pseudo-dynamic methods. But, the values are about 11% higher than the pseudo-static method in case of present study linear analysis in which low strain dynamic properties are used. And about 7% higher in the case of present study equivalent linear analysis in which equivalent linear dynamic properties are used. For the present set of data, landfill entered into the second mode of vibration which reduces the net seismic force acting on the landfill. As a result, the *FS* values is getting higher than the conventional pseudo-static method.

Effect of interface friction angle of liner materials is shown in Fig. 3.19. The same figure also shows the effect of frequency content. It may be clearly seen that increase in interface friction increases the *FS*. The increase in interface friction increases the total resisting force as a result *FS* is increased. The *FS* values are about 25 % higher as compare to pseudo-static method for an input frequency of 2 Hz. But, at the same time *FS* values are about 4 % lesser than the pseudo-static results for an input frequency of 0.2 Hz as shown in Fig. 3.19. The reason for the change in the *FS* values by changing input frequency may be drawn with the help of acceleration profiles at same input frequencies [Fig. 3.20]. When the frequency equals to 0.2 Hz, surface acceleration is amplified by 1.8 times the base input acceleration which increases the magnitude of the seismic inertial force. As a result, a *FS* values is obtained lesser in comparison of pseudo-static method. Similarly, when the frequency equals to 2 Hz, landfill mass vibrating in the second mode (i.e., some part of the landfill is moving in one direction and the remaining part is moving in opposite direction as shown in Fig. 3.20) which reduces the net seismic force acting on the landfill. As a result, a *FS* values obtained using the proposed method is higher in comparison to pseudo-static based method. The *FS* values is obtained using present study linear and equivalent linear approach for different interface friction angle values and presented in Table 3.5. The results are compared with the

conventional pseudo-static results. The *FS* values from the present study are higher than the pseudo-static values and the reason for this stands same as already explained above.
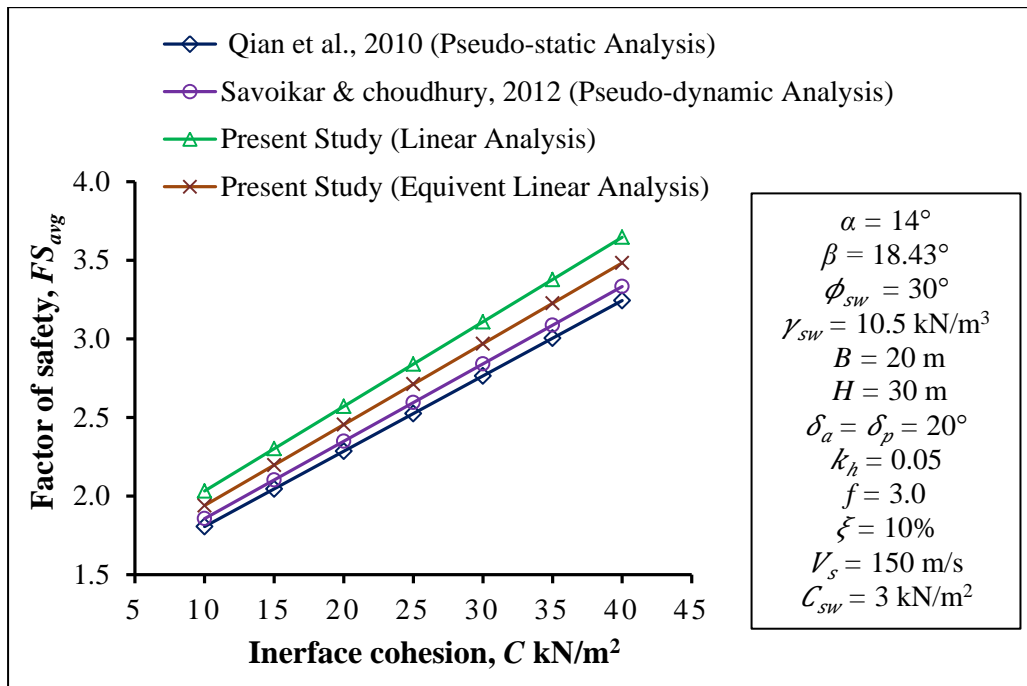
Fig. 3.18 Comparison of average factor of safety values from present study with pseudo-static and pseudo-dynamic methods for different interface cohesion values

The yield acceleration coefficients for different combinations of interface shear strength parameters of liner material are computed and presented in Table 3.6. The interface friction angle is varied from $9 - 21°$ and the interface cohesion is varied from $0 - 13$ kN/m^2 and the remaining parameters are kept constant.
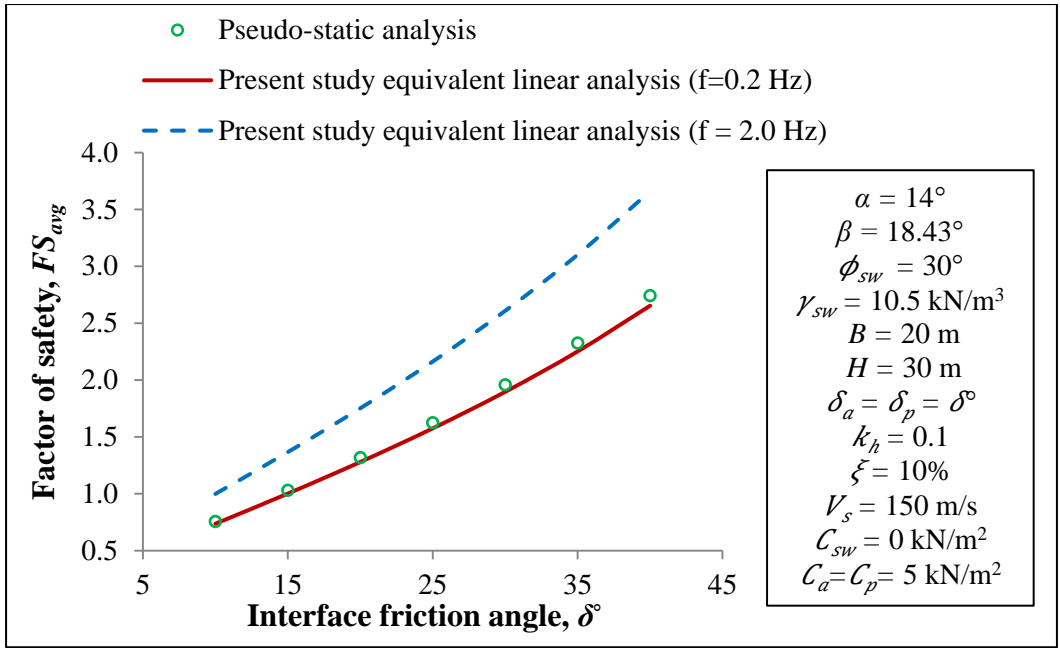
Fig. 3.19 Effect of input frequency on factor of safety values computed using the proposed equivalent linear based method
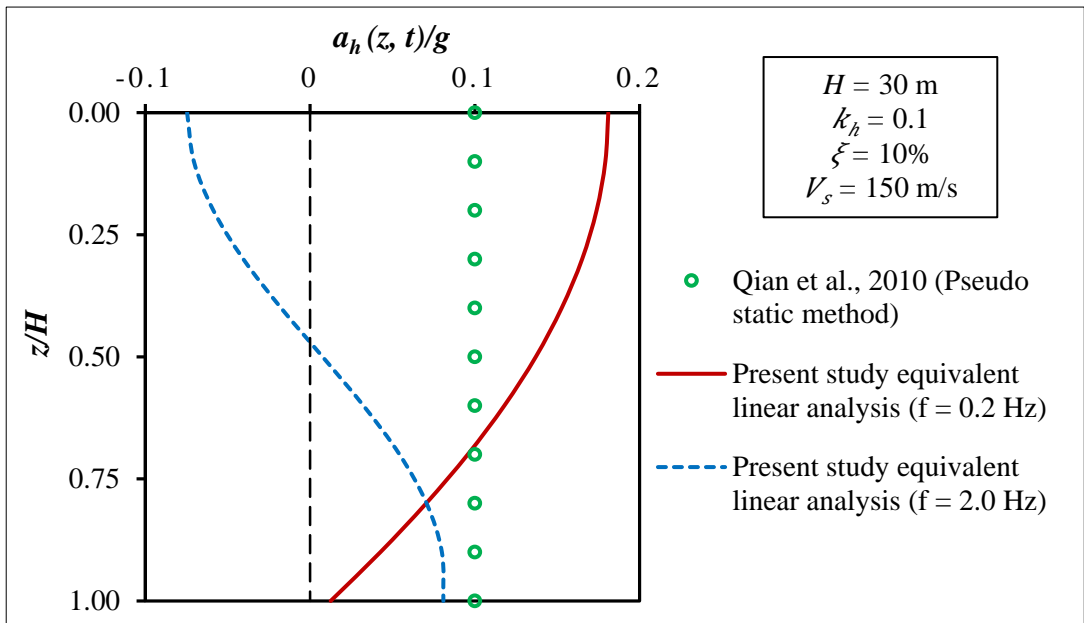
Fig. 3.20 Acceleration profiles at an input frequencies of 0.2 Hz and 2.0 Hz

Table 3.5: Comparison of factor of safety values from the proposed linear and equivalent linear based approach with the conventional pseudo-static analysis

$H = 30$ m; $B = 20$ m; $k_h = 0.05$; $\alpha = 14°$; $\phi_{sw} = 30°$; $\beta = 18.43°$; $\xi = 10\%$; $\delta_a = \delta_p = \delta$; $\gamma_{sw} = 10.5$ kN/m^3; $C_a = C_p = 10$ kN/m^2; $C_{sw} = 3$ kN/m^2; $f = 3$ Hz; $V_s = 150$ m/s			
Interface friction angle, $\delta°$	Savoikar and Choudhury, 2010 (Pseudo-static analysis)	Present study (Linear analysis)	Present study (Equivalent linear analysis)
15	1.46	1.64	1.57
20	1.80	2.03	1.94
25	2.17	2.44	2.33
30	2.56	2.89	2.76
35	3.00	3.38	3.23
40	3.50	3.94	3.76

Table 3.6: Average yield acceleration (k_{yavg}) values for different combinations of friction angle (δ) and cohesion (C) of liner materials

$H = 30$ m; $B = 20$ m; $k_h = 0.1$; $\alpha = 14°$; $\phi_{sw} = 30°$; $\beta = 18.43°$; $\delta_a = \delta_p = \delta°$; $\gamma_{sw} = 10.5$ kN/m^3; $C_a = C_p = C$ kN/m^2; $C_{sw} = 3$ kN/m^2; $f = 1$ Hz		
Interface friction angle, $\delta°$	Interface Cohesion, C (kN/m^2)	Present study (Equivalent linear analysis)
21	0.0	0.354
18	2.5	0.300
15	5.0	0.251
13	7.0	0.229
11	10	0.238
9.0	13	0.248
18.5	0.0	0.249

3.4 Summary

The acceleration ratios and *FS* values for the model MSW landfill resting on a rigid base are computed using present method linear and equivalent linear analysis. The acceleration ratios are validated using DEEPSOIL linear and equivalent linear analysis. The *FS* values are compared with the similar existing literature. And detailed parametric study is also carried out.

EFFECT OF INHOMOGENEITY OF MSW MATERIAL ON THE TRANSLATIONAL STABILITY OF LINED LANDFILL UNDER SEISMIC CONDITION

4.1 General

In the previous chapters, expressions for computation of acceleration profiles and factor of safety (*FS*) are developed. The landfill body is treated as a homogenous medium and an average value of unit weight and shear wave velocity of the MSW material is considered. Geophysical and geotechnical investigation on landfill has shown that the landfill mass is not homogeneous and the value of unit weight and shear wave velocity increases along the depth of the landfill. In the present study, previously developed equations are modified considering the interface cohesion of liner materials. And the acceleration profiles and *FS* values are obtained from the developed equations using the unit weight and shear wave velocity profiles that are available in the literature. For the same input parameters, the results from the present study are compared with the results of conventional pseudo-static limit equilibrium analysis highlighting the effect of inhomogeneity of MSW material on the *FS* value. A detailed parametric study is also reported.

4.2 Proposed Methodology

Most of the seismic stability methods used for MSW landfills assume constant unit weight and shear wave velocity values for the entire depth of the landfill. But, it is found from the literature that these properties may significantly vary along the depth of the landfill. The present method uses the unit weight profile and the shear wave velocity profile to compute the acceleration profiles and *FS* of MSW landfills under seismic condition.

In the present study, unit weight profiles proposed by Zekkos et al. (2006) for three different compaction effort and amount of soil cover are used. The following are the mathematical expressions for unit weight profiles;

The expression of unit weight profile for low compaction effort and soil cover is;

$$\gamma_{low} = 5 + \frac{z}{2 + 0.1z} \tag{4.1}$$

The expression of unit weight profile for medium compaction effort and soil cover is;

$$\gamma_{medium} = 10 + \frac{z}{3 + 0.2z} \tag{4.2}$$

The expression of unit weight profile for high compaction effort and soil cover is;

$$\gamma_{high} = 15.5 + \frac{z}{6 + 0.9z} \tag{4.3}$$

where, z is the depth at which unit weight is required.

The shear wave velocity profile proposed by Ramaiah et al. (2016b) based on the worldwide data set is used in the present study.

The mathematical expression for the shear wave velocity used in the present study is;

$$V_{sz} = 108 + 4.08z \tag{4.4}$$

The expression for horizontal acceleration of a plane SH-wave travelling through an inhomogeneous KV medium and having a layer thickness of H is given by;

$$a_h(z,t) = \frac{k_h g}{\left(C(z)\right)^2 + \left(S(z)\right)^2} \left[\left(C(z)C_z + S(z)S_z\right)\cos(\omega t) + \left(S(z)C_z - C(z)S_z\right)\sin(\omega t) \right] \tag{4.5}$$

Where,

$$C(z) = \cos\left(y_{1z}\right)\cosh\left(y_{2z}\right) \tag{4.6a}$$

$$S(z) = -\sin\left(y_{1z}\right)\sinh\left(y_{2z}\right) \tag{4.6b}$$

$$C_z = \cos\left(\frac{y_{1z}z}{H}\right)\cosh\left(\frac{y_{2z}z}{H}\right) \tag{4.6c}$$

$$S_z = -\sin\left(\frac{y_{1z}z}{H}\right)\sinh\left(\frac{y_{2z}z}{H}\right) \tag{4.6d}$$

$$y_{1z} = \frac{\omega H}{V_{sz}} \sqrt{\frac{\sqrt{1+4\xi^2}+1}{2(1+4\xi^2)}}$$ (4.7a)

$$y_{2z} = -\frac{\omega H}{V_{sz}} \sqrt{\frac{\sqrt{1+4\xi^2}-1}{2(1+4\xi^2)}}$$ (4.7b)

The same *FS* expressions given in section 3.3.1 of chapter 3 are used to calculate the average *FS* values. The procedure for the calculation of *FS* is coded using MATLAB program.

The following are the programing steps:

1. Develop characteristic profiles for unit weight and shear wave velocity of a specific MSW landfill from field and laboratory tests. In the absence of those, generalized profiles available in the published literature may be used.
2. For a particular time, the code first computes acceleration profile using the velocity profile along the depth.
3. For the same time step, compute the seismic inertial force over the landfill body using acceleration and the unit weight profiles along the depth.
4. Compute the seismic *FS* using the seismic inertial force with the help of developed equations.
5. Repeat the steps from 2 to 4 for the next time step.

4.3 Comparison of Results

In the following section, results obtained using present method is compared with the conventional pseudo-static analysis of Savoikar and Choudhury (2010) for similar landfill configuration and with same input parameters except the unit weight and shear wave velocity. Constant unit weight and shear wave velocities are used in pseudo-static analysis. The unit weight profile for medium compaction effort and soil cover has been used for comparison. On comparing the results of present study with the existing pseudo-static method shows the similar trends.

Fig. 4.1 shows the comparison of *FS* values from the present study with the conventional pseudo-static analysis for different values of minimum interface friction angle of liner materials, δ From Fig. 4.1 it is noted that increase in interface friction angle result in higher *FS*. For the given input parameters the *FS* values from the present method are nearly 15 to 18

70

% higher than the pseudo-static values. Fig. 4.2 shows the comparison of *FS* values from the present study with the conventional pseudo-static analysis for different values of front slope angle, α. From Fig. 4.2 it is noted that increase in front slope angle result in lower *FS*. For the given input parameters the *FS* values from the present method are nearly 10 to 20% higher than the pseudo-static values. This could be attributed to the mode change behavior of landfill. Referring to Fig. 4.3, the landfill is vibrating in second mode for the mentioned input frequency where some part of seismic acceleration is acting in one direction and the remaining part is moving in the opposite direction. As a result the net amount of seismic inertial force acting on the landfill mass gets reduces which ultimately increase the *FS*.

Fig. 4.1 Comparison of factor of safety values from present study with the pseudo-static values for different values of interface friction angle

The *FS* values for different top width-to-height ratio of the landfill are computed and compared with the pseudo-static analysis (Table 4.1). It is observed from Table 4.1, increase in top width-to-height ratio of the landfill result in increased *FS*. For the given input parameters the *FS* values from the present method are nearly 18 to 20% higher than the pseudo-static values. Table 4.1 also gives the comparison of *FS* values from the present study with the pseudo-static values for different values of black slope angle. It is observed that increase in β from 12 to 18° result in lower *FS* and further increase in β from 18 to 34° result

in higher *FS*. For the given input parameters the *FS* values from the present method are nearly 12 to 20% higher than the pseudo-static values.

Table 4.1: Comparison of factor of safety values from present study with the pseudo-static analysis for different values of top width-to-height ratio of landfill, *B/H* and back slope angle, $\beta°$

$H = 30$ m; $k_h = 0.1$; $\alpha = 14°$; $\phi_{sw} = 30°$; $\delta_a = \delta_p = 20°$; $\beta = 18.4°$; $D = 10\%$; $f = 2$ Hz; $\gamma_{constant} = 10.2$ kN/m³; $C_a = C_p = 0$ kN/m²; $C_{sw} = 0$ kN/m²; $V_{constant} = 100$ m/s			$H = 30$ m; $k_h = 0.1$; $\alpha = 14°$; $\phi_{sw} = 30°$; $\delta_a = \delta_p = 20°$; $B = 40$ m; $D = 10\%$; $f = 2$ Hz; $\gamma_{constant} = 10.2$ kN/m³; $C_a = C_p = 5$ kN/m²; $C_{sw} = 5$ kN/m²; $V_{constant} = 100$ m/s		
Top width-to-height ratio, *B/H*	Savoikar and Choudhury, 2010 (Pseudo-static analysis)	Present study	Back slope angle, $\beta°$	Savoikar and Choudhury, 2010 (Pseudo-static analysis)	Present study
0.50	1.09	1.33	12	1.49	1.68
0.75	1.12	1.37	14	1.40	1.64
1.00	1.15	1.42	16	1.37	1.64
1.25	1.19	1.47	18	1.37	1.65
1.50	1.23	1.53	22	1.39	1.71
1.75	1.28	1.59	26	1.43	1.77
2.00	1.32	1.66	34	1.53	1.93

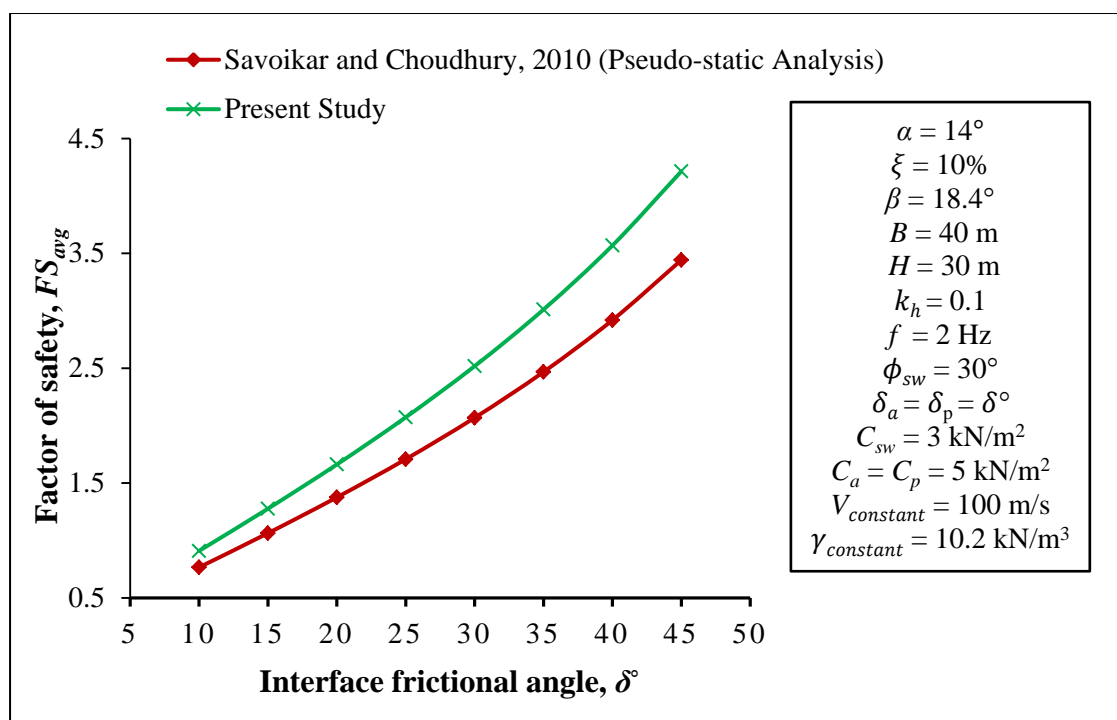**Fig. 4.2** Comparison of factor of safety values from present study with the pseudo-static values for different values of front slope angle

Fig. 4.3 Variation of acceleration along the depth of the landfill obtained from the present method for an input frequency of 2.0 Hz

4.4 Parametric Study

In the present parametric study, the following parameters are used: H = 30 m, B = 20 m, α = 14°, β = 18.4°, ϕ_{sw} = 15 to 45°, δ_a = δ_p = 10 to 45°, C_a = C_p = 5 kN/m², $\gamma_{constant}$ = 10.2 kN/m3, k_h= 0.1, $V_{constant}$ = 150 m/s, f = 0.5 Hz and 2 Hz, t/T = 0 to 1, D = 10%. The *FS* values are computed using the present method for three different compaction efforts namely low, medium and high. *FS* values are also computed for keeping the constant values of unit weight and shear wave velocity using the present method.

Fig. 4.4 shows the variation of *FS* for different values of internal friction angle of solid waste, ϕ_{sw}. From Fig. 4.4, it is noted that the increase in internal friction angle result in slightly higher *FS*. Fig. 4.4 also shows the variation in the *FS* using actual profiles of unit weight for three different compaction efforts and shear wave velocity. Increase in the compaction effort may reduce the *FS*. The *FS* values computed using unit weight profile for low compaction effort and shear wave velocity profile are nearly 6.5% higher than the values using constant unit weight and shear wave velocity. The *FS* values computed using unit weight profile for medium compaction effort and shear wave velocity profile are nearly 1.5% lower than the values computed using constant unit weight and shear wave velocity. The *FS* values computed using unit weight profile for medium compaction effort and shear wave velocity profile are nearly 5 to 6% lower than the values using constant unit weight and shear wave velocity.

Fig. 4.5 shows the variation of *FS* for different values of minimum interface cohesion of liner materials, *C*. From Fig. 4.5, it is noted that increase in interface cohesion value result in higher *FS*. Fig. 4.5 also shows the variation in the *FS* computed using actual profiles of unit weight for three different compaction efforts and shear wave velocity. It is observed from Fig. 4.5, increase in the unit weight may reduce the *FS*. The *FS* values computed using unit weight profile for low compaction effort and shear wave velocity profile are nearly 8 to 10% higher than the values using constant unit weight and shear wave velocity. The *FS* values computed using unit weight profile for medium compaction effort and shear wave velocity profile are nearly 4 to 10% lower than the values computed using constant unit weight and shear wave velocity. The *FS* values computed using unit weight profile for medium compaction effort and shear wave velocity profile are nearly 12 to 24% lower than the values using constant unit weight and shear wave velocity.
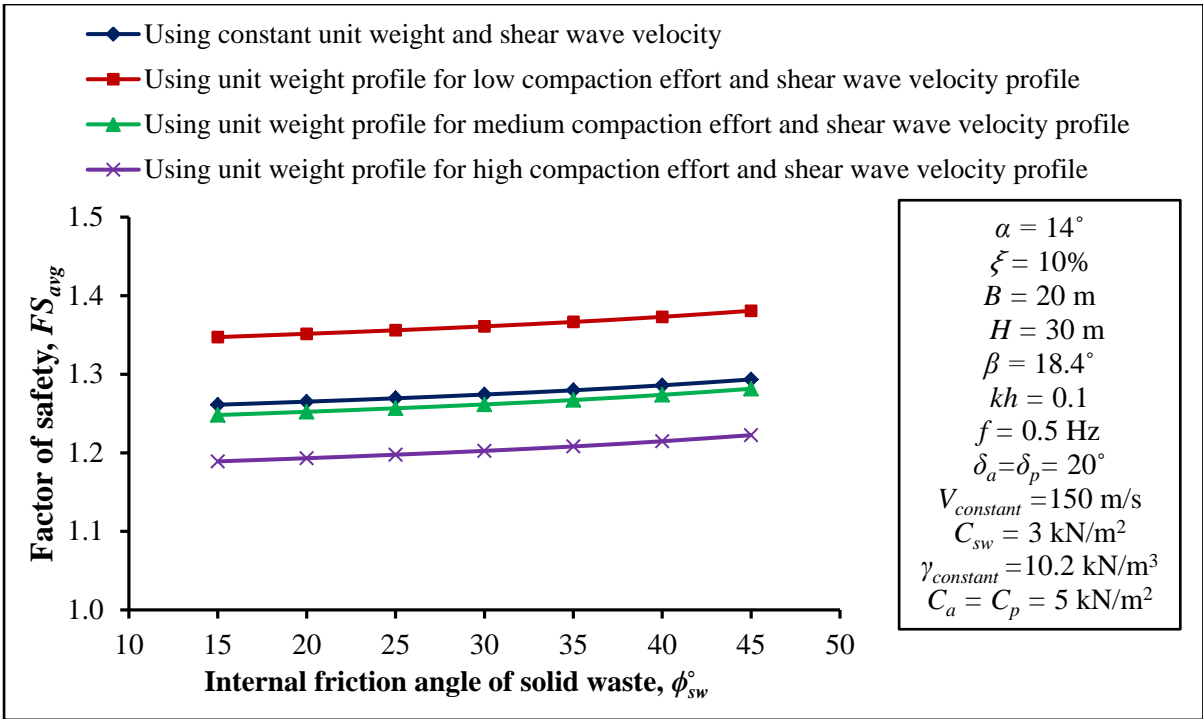
Fig. 4.4 Effect of the use of unit weight and shear wave velocity profiles on the factor of safety for different internal friction angle values
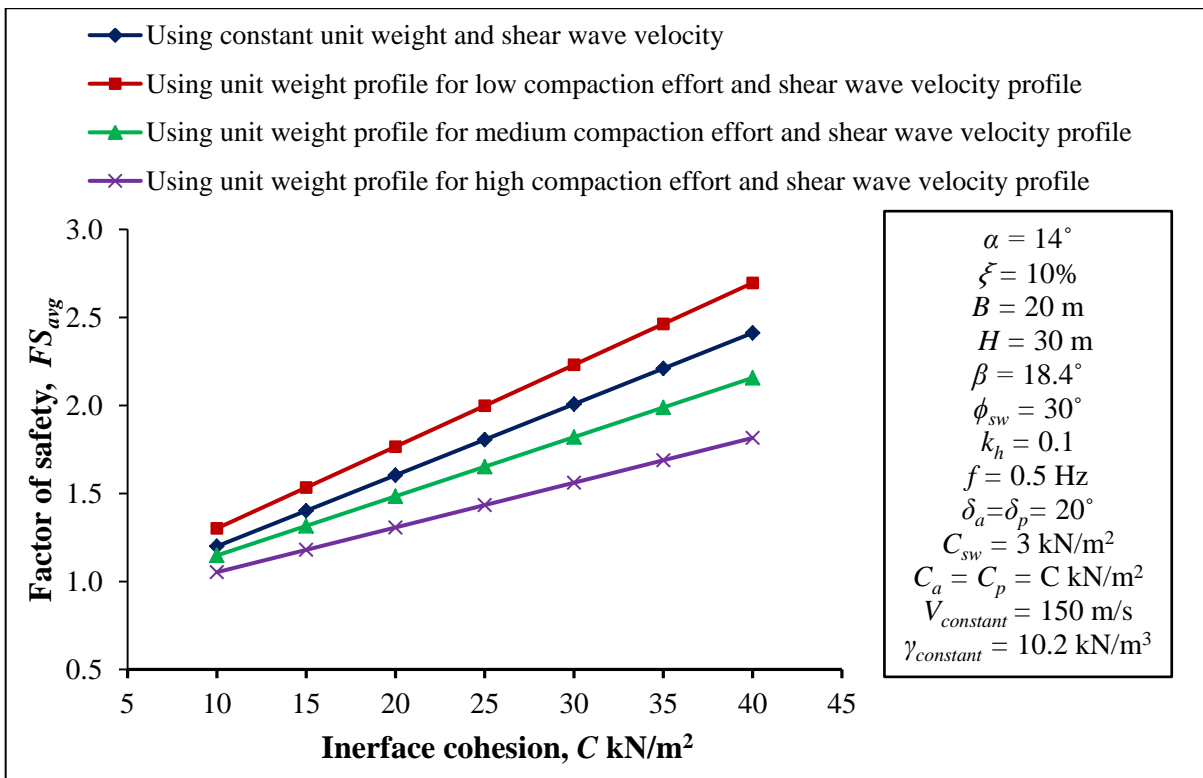
Fig. 4.5 Effect of the use of unit weight and shear wave velocity profiles on the factor of safety for different interface cohesion values

Fig. 4.6 shows the variation of *FS* for different values of minimum interface friction angle of liner materials, δ. Form Fig. 4.6, it is noted that increase in interface friction angle result in higher *FS*. Fig. 4.6 also shows the variation in the *FS* computed using actual profiles of unit weight for three different compaction efforts and shear wave velocity. It is observed from Fig. 4.6, increase in the unit weight may reduce the *FS*. Fig. 4.6 also shows the effect of frequency content on the *FS*. It is noted that the *FS* values for an input frequency of 0.5 Hz are nearly 19 to 20% higher when compared for an input frequency of 2.0 Hz. This could be explained with the help of Fig. 4.7. For an input frequency of 0.5 Hz the landfill is vibrating in first mode and for an input frequency of 2.0 Hz the landfill is vibrating in second mode as shown in Fig. 4.7, is the reason for the higher *FS* when the input frequency is equal to 2.0 Hz.
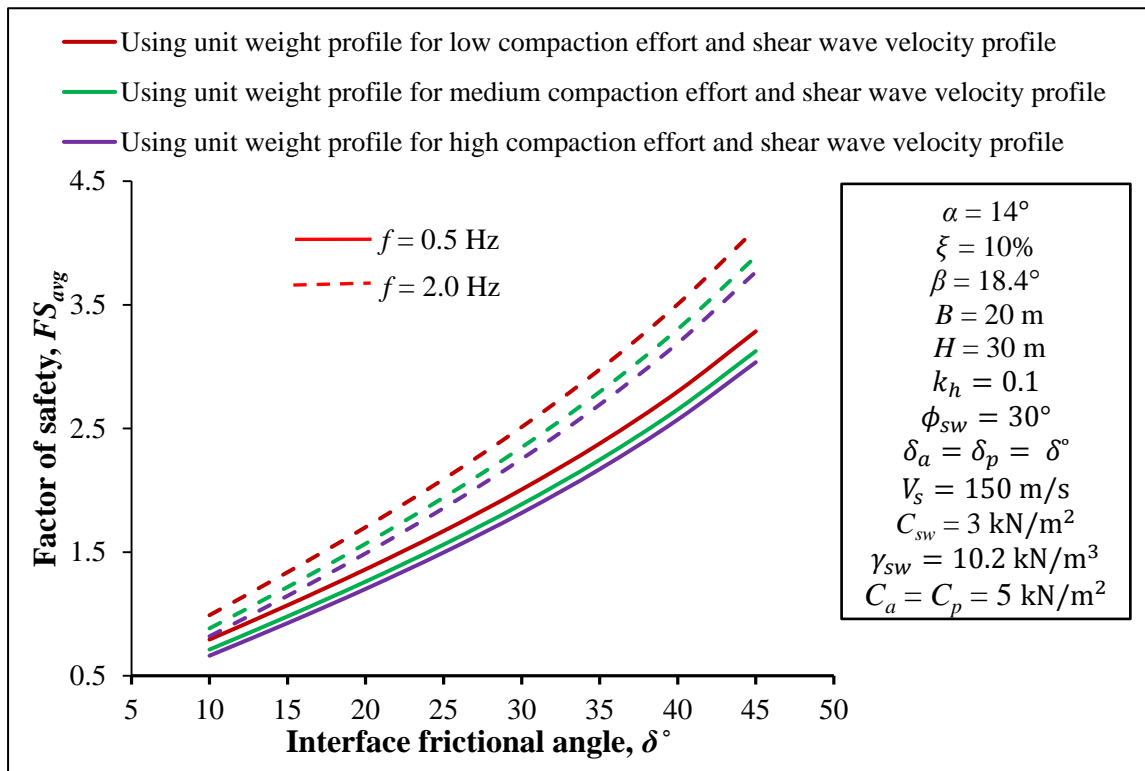
Fig. 4.6 Effect of the use of unit weight and shear wave velocity profiles on the factor of safety for different interface friction angle values when f = 0.5 Hz and 2.0 Hz
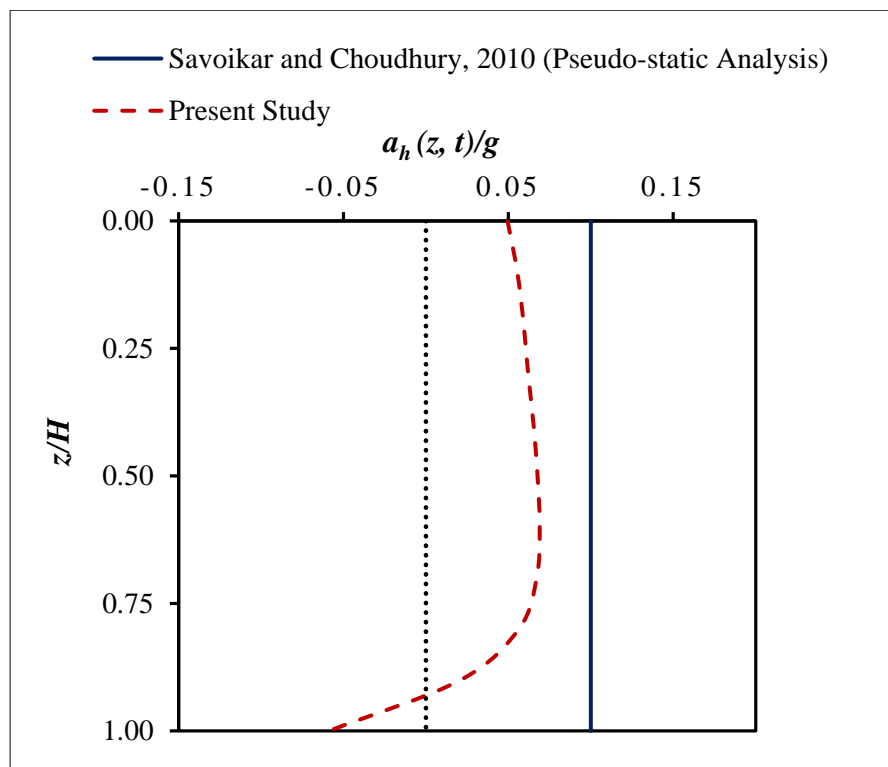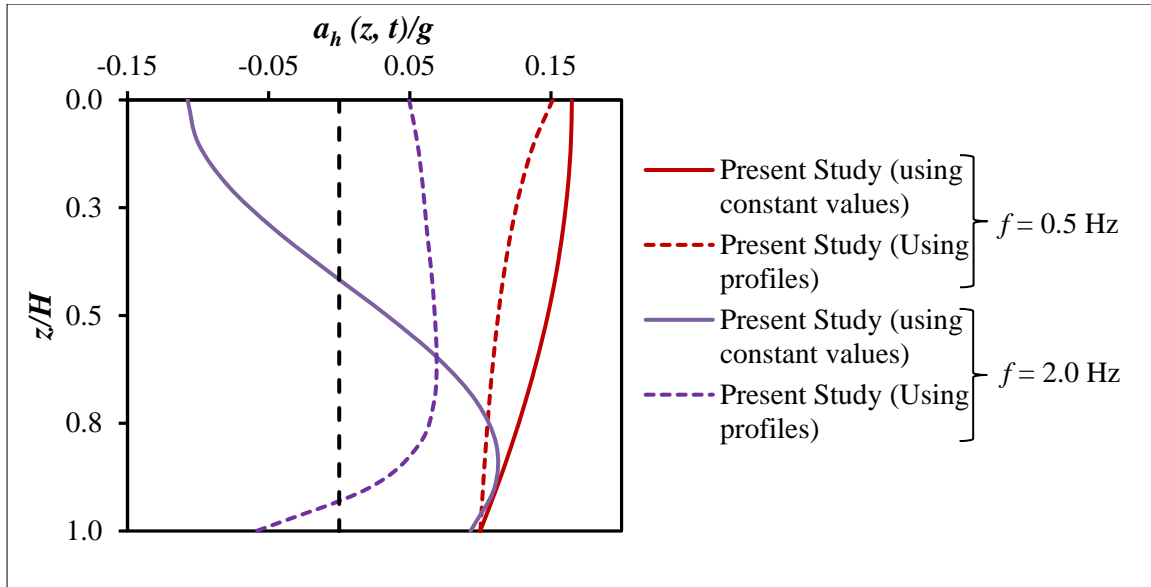
Fig. 4.7 Variation of acceleration along the depth of the landfill obtained from the present method for an input frequency of 0.5 Hz and 2.0 Hz

4.5 Summary

The acceleration profiles and *FS* values for the model MSW landfill resting on a rigid base are obtained in the present study. The unit weight and shear wave velocity profiles are used in place of constant values to compute the acceleration profiles and *FS*. And it is found that use of the characteristic profiles for unit weight and shear wave velocity has significant effect on the results. The results obtained from the present study are compared with the similar existing literature.

EFFECT OF LOCAL SITE CONDITION ON THE SEISMIC STABILITY OF MSW LANDFILLS

5.1 General

The dynamic properties of foundation soil significantly affect the stability of MSW landfills under seismic conditions. Closed form solutions have been developed to compute acceleration ratio (surface/input), factor of safety (*FS*) of an MSW landfill. Five different foundation types have been studied in the linear analysis and four different foundation types have been studied in the equivalent linear analysis. Two-part wedge method together with limit equilibrium method has been adopted. The acceleration ratios obtained in the present study are compared and found to be in good agreement with the DEEPSOIL results. The present results are compared with the similar existing literature. In addition, an extensive parametric has been done to know the effect of all the parameters on the seismic stability of MSW landfill resting on a respective foundation type.

5.2 Linear Analysis

5.2.1 Proposed Methodology

Let us consider the MSW landfill resting on foundation soil. The subscripts '*sw*' and '*fs*' refer to solid waste and foundation soil respectively, the displacements due to vertically travelling SH-waves in each medium may be written as,

$$u_{sw}\left(z_{sw},t\right) = A_{sw}e^{i\left(\omega t+k_{sw}^{*}z_{sw}\right)} + B_{sw}e^{i\left(\omega t-k_{sw}^{*}z_{sw}\right)} \tag{5.1}$$

$$u_{fs}\left(z_{fs},t\right) = A_{fs}e^{i\left(\omega t+k_{fs}^{*}z_{fs}\right)} + B_{fs}e^{i\left(\omega t-k_{fs}^{*}z_{fs}\right)} \tag{5.2}$$

where A_{sw}, A_{fs} are the amplitudes of incident waves travelling in the upward (–z) direction and B_{sw}, B_{fs} are the amplitudes of reflected waves travelling in the downward (+z) direction (Fig. 5.1). These four constants may be solved using the four boundary conditions.

For a stress free surface ($\tau_{sw} = 0$ at $z_{sw} = 0$), requires $A_{sw} = B_{sw}$,

$$u_{sw}(z_{sw}, t) = 2A_{sw} e^{i\omega t} \cos\left(k_{sw}^* z_{sw}\right) \tag{5.3}$$

The displacement compatibility and stress continuity at the soil-MSW interface requires,

$$u_{sw}(z_{sw} = H_{sw}) = u_{fs}(z_{fs} = 0) \tag{5.4}$$

$$\tau_{sw}(z_{sw} = H_{sw}) = \tau_{fs}(z_{fs} = 0) \tag{5.5}$$

From the equations (5.4), (5.5) and the definition of shear stress,

$$A_{fs} = A_{sw}\left(\cos\left(k_{sw}^* H_{sw}\right) + i\alpha^* \sin\left(k_{sw}^* H_{sw}\right)\right) \tag{5.6}$$

$$B_{fs} = A_{sw}\left(\cos\left(k_{sw}^* H_{sw}\right) - i\alpha^* \sin\left(k_{sw}^* H_{sw}\right)\right) \tag{5.7}$$

α^* is the complex impedance ratio at the soil-MSW interface,

$$\alpha^* = \frac{G_{sw} k_{sw}^*}{G_{fs} k_{fs}^*} = \frac{\rho_{sw} v_{sw}^*}{\rho_{fs} v_{fs}^*} = \frac{\rho_{sw} v_{sw}(1 + iD_{sw})}{\rho_{fs} v_{fs}(1 + iD_{fs})} = (D_{c1} - iD_{c2})\chi \tag{5.8}$$

where,

$$D_{c1} = 1 + D_{sw} D_{fs} \tag{5.9a}$$

$$D_{c2} = D_{fs} - D_{sw} \tag{5.9b}$$

$$\chi = \frac{\lambda}{1 + D_{fs}^2} \tag{5.10}$$

where,

$$\lambda = \frac{\rho_{sw} v_{sw}}{\rho_{fs} v_{fs}} \tag{5.11}$$

By substituting equation (5.6) and (5.7) into equation (5.2) gives,

79

$$u_{fs} = A_{sw} e^{i\left(\omega t + k_{fs}^* z_{fs}\right)} \left(\cos\left(k_{sw}^* H_{sw}\right) + i\alpha^* \sin\left(k_{sw}^* H_{sw}\right)\right)$$
$$+ A_{sw} e^{i\left(\omega t - k_{fs}^* z_{fs}\right)} \left(\cos\left(k_{sw}^* H_{sw}\right) - i\alpha^* \sin\left(k_{sw}^* H_{sw}\right)\right) \tag{5.10}$$

Using the last boundary condition $u_{fs}\left(z_{fs} = H_{fs}\right) = u_{ho} e^{i\omega t}$ gives,

$$A_{sw} = \frac{u_{ho}}{\cos\left(k_{sw}^* H_{sw}\right)\left(e^{ik_{fs}^* H_{fs}} + e^{-ik_{fs}^* H_{fs}}\right) + i\alpha^* \sin\left(k_{sw}^* H_{sw}\right)\left(e^{ik_{fs}^* H_{fs}} - e^{-ik_{fs}^* H_{fs}}\right)} \tag{5.11}$$

where, $k_{sw}^* = k_{sw_1} + ik_{sw_2}$ and $k_{fs}^* = k_{fs_1} + ik_{fs_2}$. Substitute equation (5.11) into equation (5.3) and (5.10). After rearranging, the expressions for horizontal displacement of both the layers may be obtained as,

$$u_{sw}\left(z_{sw}, t\right) = \frac{u_{ho}}{M^2 + N^2}\left[\left(M_{z_{sw}} M + N_{z_{sw}} N\right)\cos\left(\omega t\right) + \left(N_{z_{sw}} M - M_{z_{sw}} N\right)\sin\left(\omega t\right)\right] \tag{5.12}$$

$$u_{fs}\left(z_{fs}, t\right) = \frac{u_{ho}}{M^2 + N^2}\left[\left(M_{z_{fs}} M + N_{z_{fs}} N\right)\cos\left(\omega t\right) + \left(N_{z_{fs}} M - M_{z_{fs}} N\right)\sin\left(\omega t\right)\right] \tag{5.13}$$

Where,

$$M_{z_{sw}} = \cos\left(y_{sw_1} z_{sw}/H_{sw}\right)\cosh\left(y_{sw_2} z_{sw}/H_{sw}\right) \tag{5.14a}$$

$$N_{z_{sw}} = \sin\left(y_{sw_1} z_{sw}/H_{sw}\right)\sinh\left(y_{sw_2} z_{sw}/H_{sw}\right) \tag{5.14b}$$

$$M_{z_{fs}} = C_{1_{z_{fs}}} - C_{3_{z_{fs}}} D_{c1}\chi - C_{4_{z_{fs}}} D_{c2}\chi \tag{5.15a}$$

$$N_{z_{fs}} = C_{2_{z_{fs}}} + C_{4_{z_{fs}}} D_{c1}\chi - C_{3_{z_{fs}}} D_{c2}\chi \tag{5.15b}$$

$$M = C_1 - C_3 D_{c1}\chi - C_4 D_{c2}\chi \tag{5.16a}$$

$$N = C_2 + C_4 D_{c1}\chi - C_3 D_{c2}\chi \tag{5.16b}$$

Where,

$$C_{1_{z_{fs}}} = \cos\left(y_{sw_1}\right)\cosh\left(y_{sw_2}\right)\cos\left(y_{fs_1} z_{fs}/H_{fs}\right)\cosh\left(y_{fs_2} z_{fs}/H_{fs}\right)$$
$$- \sin\left(y_{sw_1}\right)\sinh\left(y_{sw_2}\right)\sin\left(y_{fs_1} z_{fs}/H_{fs}\right)\sinh\left(y_{fs_2} z_{fs}/H_{fs}\right)$$
(5.17a)

$$C_{2_{z_{fs}}} = \cos\left(y_{sw_1}\right)\cosh\left(y_{sw_2}\right)\sin\left(y_{fs_1} z_{fs}/H_{fs}\right)\sinh\left(y_{fs_2} z_{fs}/H_{fs}\right)$$
$$+ \sin\left(y_{sw_1}\right)\sinh\left(y_{sw_2}\right)\cos\left(y_{fs_1} z_{fs}/H_{fs}\right)\cosh\left(y_{fs_2} z_{fs}/H_{fs}\right)$$
(5.17b)

$$C_{3_{z_{fs}}} = \sin\left(y_{sw_1}\right)\cosh\left(y_{sw_2}\right)\sin\left(y_{fs_1} z_{fs}/H_{fs}\right)\cosh\left(y_{fs_2} z_{fs}/H_{fs}\right)$$
$$- \cos\left(y_{sw_1}\right)\sinh\left(y_{sw_2}\right)\cos\left(y_{fs_1} z_{fs}/H_{fs}\right)\sinh\left(y_{fs_2} z_{fs}/H_{fs}\right)$$
(5.17c)

$$C_{4_{z_{fs}}} = \sin\left(y_{sw_1}\right)\cosh\left(y_{sw_2}\right)\cos\left(y_{fs_1} z_{fs}/H_{fs}\right)\sinh\left(y_{fs_2} z_{fs}/H_{fs}\right)$$
$$+ \cos\left(y_{sw_1}\right)\sinh\left(y_{sw_2}\right)\sin\left(y_{fs_1} z_{fs}/H_{fs}\right)\cosh\left(y_{fs_2} z_{fs}/H_{fs}\right)$$
(5.17d)

$$C_1 = \cos\left(y_{sw_1}\right)\cosh\left(y_{sw_2}\right)\cos\left(y_{fs_1}\right)\cosh\left(y_{fs_2}\right)$$
$$- \sin\left(y_{sw_1}\right)\sinh\left(y_{sw_2}\right)\sin\left(y_{fs_1}\right)\sinh\left(y_{fs_2}\right)$$
(5.18a)

$$C_2 = \cos\left(y_{sw_1}\right)\cosh\left(y_{sw_2}\right)\sin\left(y_{fs_1}\right)\sinh\left(y_{fs_2}\right)$$
$$+ \sin\left(y_{sw_1}\right)\sinh\left(y_{sw_2}\right)\cos\left(y_{fs_1}\right)\cosh\left(y_{fs_2}\right)$$
(5.18b)

$$C_3 = \sin\left(y_{sw_1}\right)\cosh\left(y_{sw_2}\right)\sin\left(y_{fs_1}\right)\cosh\left(y_{fs_2}\right)$$
$$- \cos\left(y_{sw_1}\right)\sinh\left(y_{sw_2}\right)\cos\left(y_{fs_1}\right)\sinh\left(y_{fs_2}\right)$$
(5.18c)

$$C_4 = \sin\left(y_{sw_1}\right)\cosh\left(y_{sw_2}\right)\cos\left(y_{fs_1}\right)\sinh\left(y_{fs_2}\right)$$
$$+ \cos\left(y_{sw_1}\right)\sinh\left(y_{sw_2}\right)\sin\left(y_{fs_1}\right)\cosh\left(y_{fs_2}\right)$$
(5.18d)

Where,

$$y_{sw_1} = \frac{\omega H_{sw}}{V_{sw}}\sqrt{\frac{\sqrt{1+4D_{sw}^2}+1}{2\left(1+4D_{sw}^2\right)}}$$
(5.19a)

$$y_{sw_2} = -\frac{\omega H_{sw}}{V_{sw}}\sqrt{\frac{\sqrt{1+4D_{sw}^2}-1}{2\left(1+4D_{sw}^2\right)}}$$
(5.19b)

$$y_{fs_1} = \frac{\omega H_{fs}}{V_{fs}} \sqrt{\frac{\sqrt{1+4D_{fs}^2}+1}{2\left(1+4D_{fs}^2\right)}}$$ (5.20a)

$$y_{fs_2} = -\frac{\omega H_{fs}}{V_{fs}} \sqrt{\frac{\sqrt{1+4D_{fs}^2}-1}{2\left(1+4D_{fs}^2\right)}}$$ (5.20b)

The expressions for horizontal acceleration of both the layers could be obtained by differentiating equation (5.12) and (5.13) twice with respect to time,

$$a_{sw}\left(z_{sw},t\right) = \frac{k_h g}{M^2+N^2}\left[\left(M_{z_{sw}}M+N_{z_{sw}}N\right)\cos\left(\omega t\right)+\left(N_{z_{sw}}M-M_{z_{sw}}N\right)\sin\left(\omega t\right)\right]$$ (5.21)

$$a_{fs}\left(z_{fs},t\right) = \frac{k_h g}{M^2+N^2}\left[\left(M_{z_{fs}}M+N_{z_{fs}}N\right)\cos\left(\omega t\right)+\left(N_{z_{fs}}M-M_{z_{fs}}N\right)\sin\left(\omega t\right)\right]$$ (5.22)

where, $k_h g = -\omega^2 u_{h0}$; k_h = Base horizontal seismic acceleration coefficient.
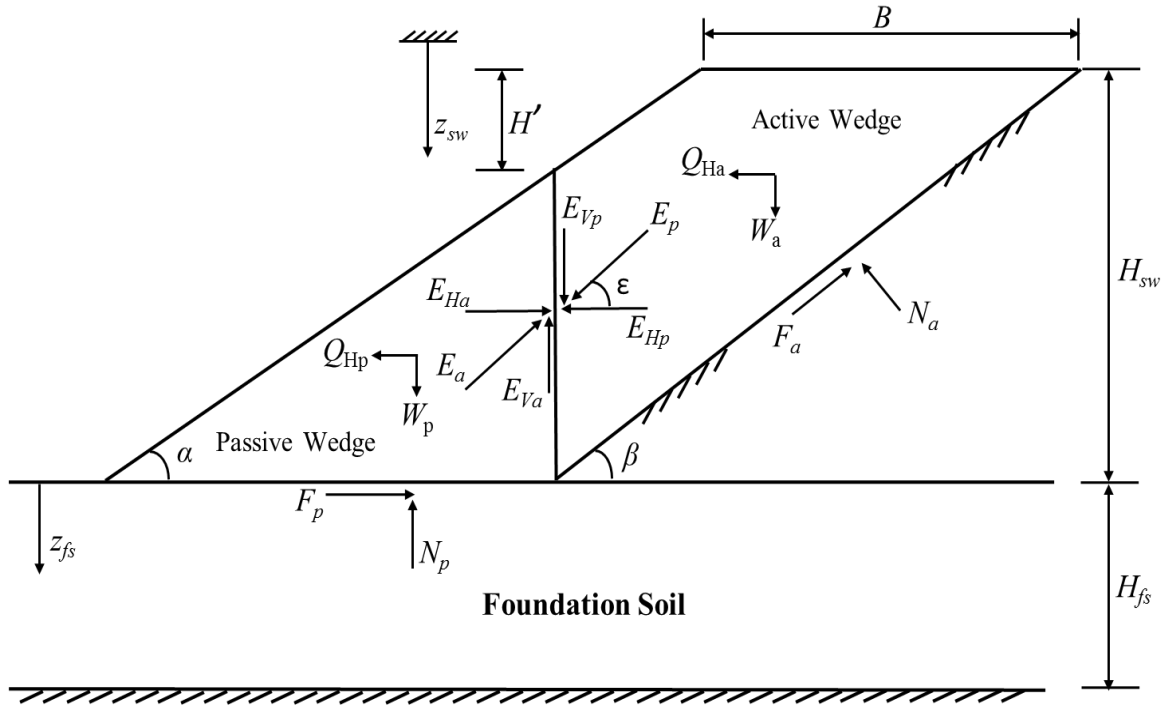
Fig. 5.1 Used model MSW landfill resting on a foundation soil

Fig. 5.1 shows the details of model landfill used in the present study. In the model, geometric features of the landfill such top width, height, front and back slope angles are represented as B, H_{sw}, α, and β respectively. The entire waste mass is divided into two wedges namely active

82

wedge and passive wedge resting on back slope liner and base liner respectively. These two wedges are separated by an imaginary wall for the mathematical treatment.
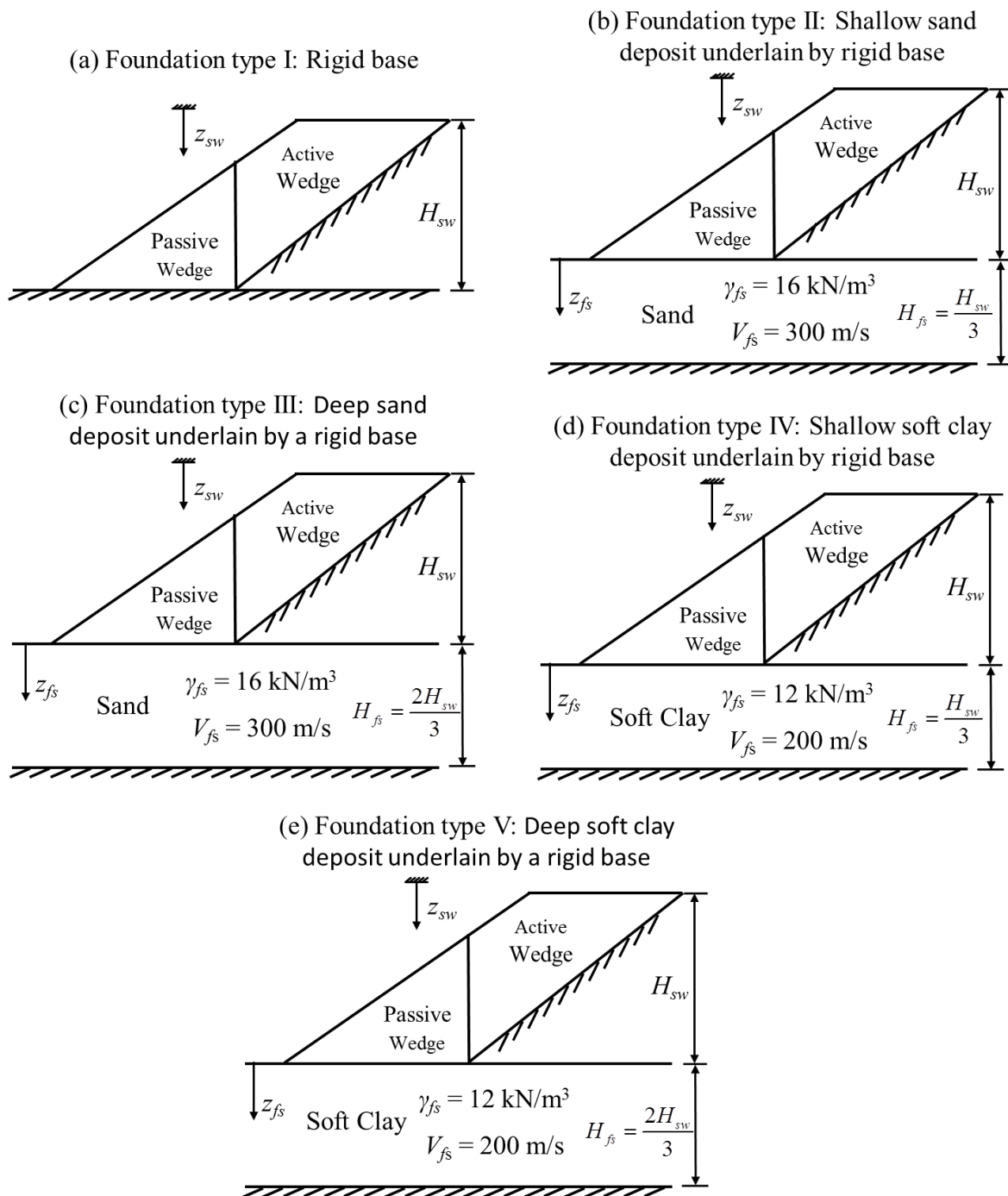
Fig. 5.2 Different types of foundations for MSW landfills used in the present study

In the present study, side-hill type landfill resting on the five different foundation soil has been studied. Fig. 5.2 gives the details of foundation type and its properties used in the present study.

Foundation type I: Rigid base

Foundation type II: Shallow sand deposit underlain by a rigid base

Foundation type III: Deep sand deposit underlain by a rigid base

Foundation type IV: Shallow clay deposit underlain by a rigid base

Foundation type V: Deep clay deposit underlain by a rigid base

The same *FS* expressions given in section 3.3.1 of chapter 3 are used to calculate the average *FS* values.

5.2.2 Validation of Acceleration Profiles from Linear Analysis using DEEPSOIL

In the present study, DEEPSOIL is used to carry out 1-D ground response analysis using linear approach for a MSW landfill resting on five different types of foundations shown in Fig. 5.2. Height of the MSW column is kept equal to the total height of the landfill. In the linear analysis, small strain value of shear wave velocity is used and a fixed damping ratio value is assigned to MSW material. The input parameters of MSW are H_{sw} = 30 m, V_{sw} = 100 m/s, γ_{sw} = 10.5 kN/m^3 and D_{sw} = 10%. The input parameters of sand are V_{fs} = 300 m/s, γ_{sw} = 16 kN/m^3 and D_{fs} = 5%. For shallow sand deposit the depth is considered as one-third of height of the landfill and for deep sand deposit the depth is considered as two-third of height of the landfill as shown in Fig. 5.2. The input parameters of clay are V_{fs} = 200 m/s, γ_{sw} = 12 kN/m^3 and D_{fs} = 5%. For shallow clay deposit the depth is considered as one-third of the height of landfill and for deep clay deposit the depth is considered as two-third of the height of landfill as shown in Fig. 5.2. The boundary conditions in DEEPSOIL are kept exactly same as in the proposed method i.e. the MSW column is resting on respective foundation type. The MSW column is subjected to a harmonic shaking k_hg*cos(ωt). And the duration of shaking is kept equal to the time period of the input motion, *T* (2π/ω). The seismic acceleration at the surface is obtained using the linear analysis in DEEPSOIL.

Distribution of acceleration along the depth of waste mass is very important for the evaluation of seismic inertial forces over the landfill. The acceleration profiles obtained from the present study are validated using DEEPSOIL linear analysis results. A non-dimensional parameter named as acceleration ratio is computed. The ratio of surface acceleration to that of input

acceleration is defined as acceleration ratio or, sometimes called as amplification ratio. The acceleration ratios obtained from the present analytical method are found to be in good agreement with the DEEPSOIL results.

Fig. 5.3 shows the validation of acceleration ratios computed for foundation type I with the results of DEEPSOIL. For an input frequency of $f = 0.40$ Hz ($\omega = 2\pi f = 2.513$ rad/s), the acceleration ratio from the present linear analysis is 1.330 and from the DEEPSOIL linear analysis is 1.334, the percentage difference is 0.29%. Similarly, for another input frequency of $f = 1.17$ Hz ($\omega = 2\pi f = 9.80$ rad/s), the acceleration ratio from present linear analysis is 1.640 and from DEEPSOIL linear analysis is 1.616, the percentage difference is 1.47%. The percentage error is very less, infect it is less than 1.5%.

Fig. 5.3 Validation graph of acceleration ratio for foundation type I using present linear analysis and DEEPSOIL linear analysis

Fig. 5.4 shows the validation of acceleration ratios computed for foundation type II and III with the results of DEEPSOIL linear analysis. For an input frequency of $f = 0.58$ Hz ($\omega = 2\pi f = 3.644$ rad/s), the acceleration ratio from the present method for foundation type II is 2.218 and from the DEEPSOIL is 2.224, the percentage difference is 0.23%. At the same input frequency the acceleration ratio from the present method for foundation type III is 2.391 and from the DEEPSOIL is 2.402, the percentage difference is 0.44%. At this input frequency the acceleration ratio for foundation type III is nearly 7.5% higher to the value of foundation type II. Similarly, for another input frequency of $f = 1.75$ Hz ($\omega = 2\pi f = 10.995$ rad/s), the

acceleration ratio from present method for foundation type II is 1.030 and from DEEPSOIL is 1.033, the percentage difference is 0.29%. At the same input frequency the acceleration ratio from the present method for foundation type III is 1.301 and from the DEEPSOIL is 1.311, the percentage difference is 0.74%. At this input frequency the acceleration ratio for foundation type III is nearly 21% higher to the value of foundation type II. It is also observed from Fig. 5.4 the peak amplification in foundation type III is nearly 12.5% higher than in foundation type II.
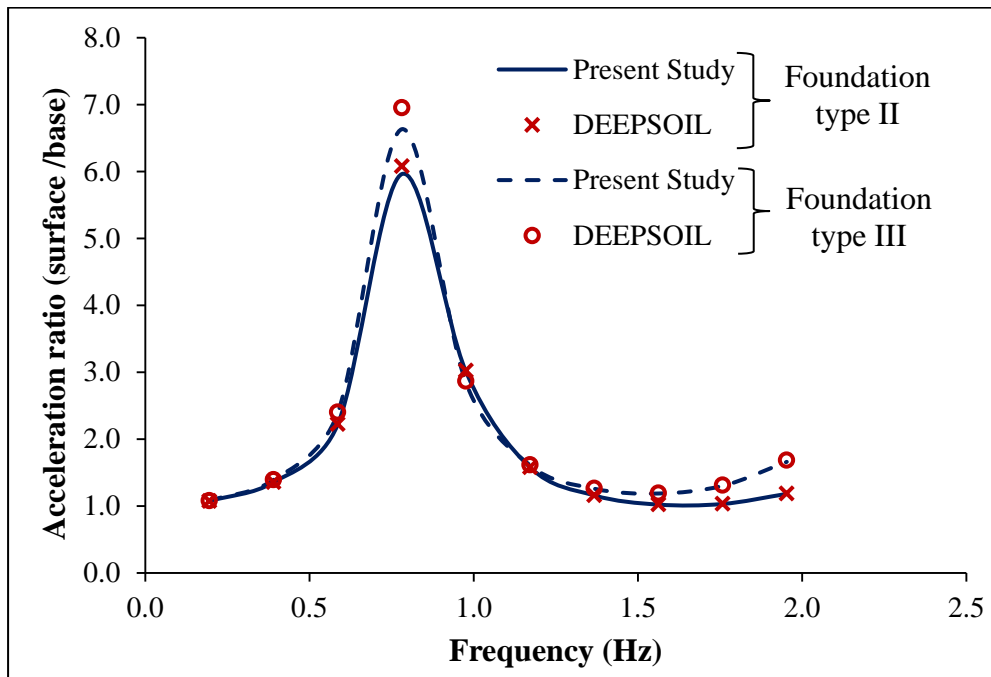
Fig. 5.4 Validation graph of acceleration ratio for foundation type II and III using present linear analysis and DEEPSOIL linear analysis

Fig. 5.5 shows the validation of acceleration ratios computed for foundation type IV and V with the results of DEEPSOIL. For an input frequency of $f = 0.4$ Hz ($\omega = 2\pi f = 0.4$ rad/s), the acceleration ratio from the present method for foundation type IV is 1.405 and from the DEEPSOIL is 1.407, the percentage difference is 0.13%. At the same input frequency of 0.4 Hz the acceleration ratio from the present method for foundation type V is 1.513 and from the DEEPSOIL is 1.518, the percentage difference is 0.33%. At this input frequency the acceleration ratio for foundation type V is nearly 7.0% higher to the value of foundation type IV. Similarly, for another input frequency of $f = 1.56$ Hz ($\omega = 2\pi f = 9.801$ rad/s), the acceleration ratio from present method for foundation type IV is 1.051 and from DEEPSOIL is 1.058, the percentage difference is 0.58%. At the same input frequency of 1.56 Hz the acceleration ratio from the present method for foundation type IV is 1.483 and from the

DEEPSOIL is 1.503, the percentage difference is 1.32%. At this input frequency the acceleration ratio for foundation type V is nearly 29% higher to the value of foundation type IV. It is also observed from Fig. 5.5 the peak amplification in foundation type V is nearly 17% lower than in foundation type IV.
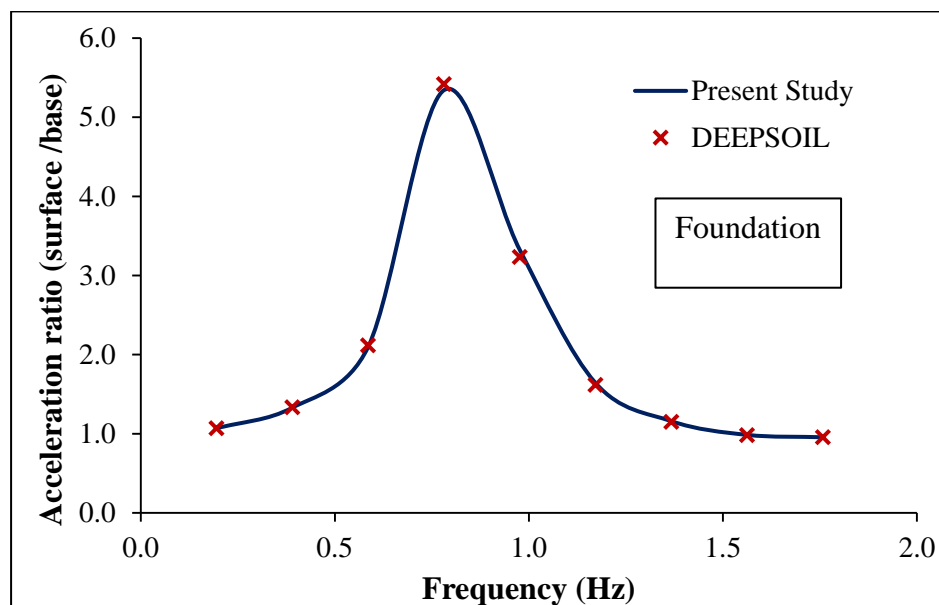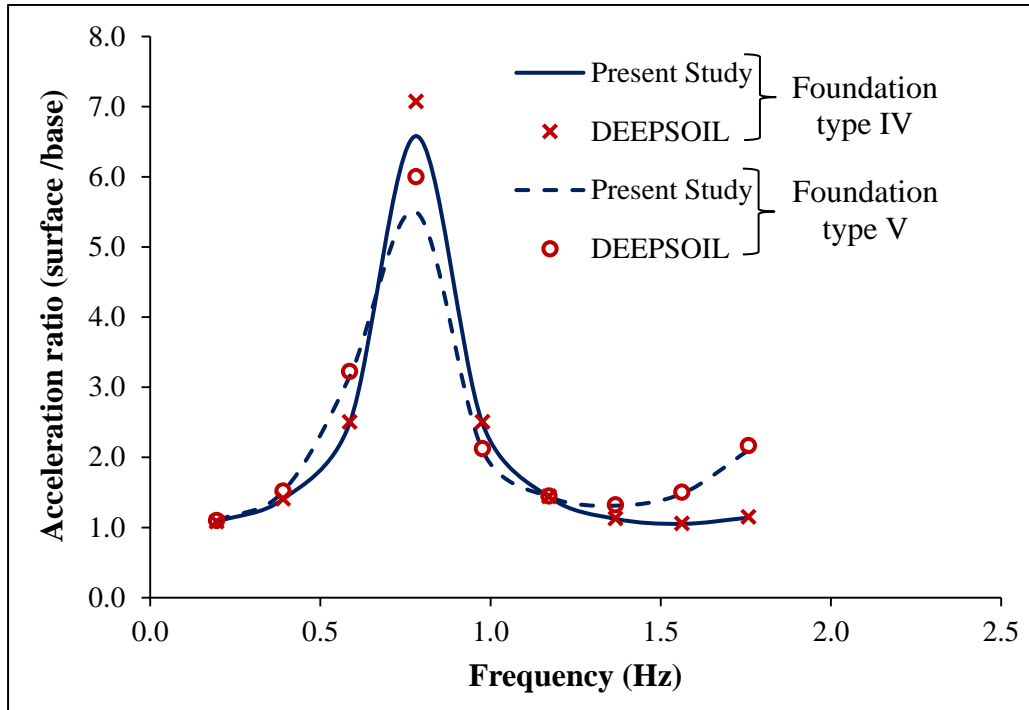

Fig. 5.5 Validation graph of acceleration ratio for foundation type IV and V using present linear analysis and DEEPSOIL linear analysis

5.2.3 Parametric Study

In the present parametric study, the following variation of parameters is used: $H_{sw} = 30$ m, $B/H_{sw} = 0.25$ to 2, $\alpha = 14°$, $\beta = 18.4°$, $\phi_{sw} = 15$ to $45°$, $\delta_a = \delta_p = 15$ to $45°$, $C_a = C_p = 5$ to 40 kN/m², $\gamma_{sw} = 10.5$ kN/m³, $k_h = 0.0$ to 0.2, $V_{sw} = 100$ and 150 m/s, $\omega H_{sw}/V_{sw} = 0$ to $6, f = 3$ Hz; $t/T = 0$ to 1, $z/H = 0$ to 1, $D_{sw} = 10\%$ and $D_{fs} = 5\%$. The proposed method is coded using MATLAB program which compute the *FS* value at each time step for a given set of input parameters. For a given set of input parameters, the code first compute the acceleration profiles along the depth at each time step and these acceleration profiles are used to compute seismic inertial forces at each time step. *FS* values are computed at all the time steps using the proposed equations. In the present study, a non-dimensional time interval is used in the form of *t/T*. *t/T* is varied at an interval of 0.01 between 0 and 1. The value of *FS* is minimized with

respect to *t/T*. In the similar way, yield acceleration coefficient is minimized using a same technique that is employed for *FS*.

Fig. 5.6 shows the variation of *FS* for different values interface friction angle, δ. From Fig. 5.6, it is noted that increase in interface friction angle results a higher *FS*. Fig. 5.6 also shows the variation of *FS* with the given foundation type. For the given input parameters, foundation type III is having the least and foundation type I is having the highest *FS* in comparison to other foundation types. This can be attributed to the net amount of seismic inertial force acting on the landfill mass is maximum for foundation type III and is minimum for foundation type I [Fig.5.9]. The *FS* values for foundation type II and V are having negligible difference and are nearly 5.5% lower compared to foundation type I. The *FS* values for foundation type III are nearly 30% lower compared to foundation type I. The *FS* values for foundation type IV are nearly 15% lower compared to foundation type I.

Fig. 5.7 shows the variation of *FS* for different values of internal friction angle of waste mass, ϕ_{sw}. From Fig. 5.7, it is noted that increase in internal friction angle results a slightly higher *FS*. Fig. 5.7 also shows the variation of *FS* with the given foundation type. For the given input parameters, foundation type III is having the least and foundation type I is having the highest *FS* in comparison to other foundation types. This can be attributed to the net amount of seismic inertial force acting on the landfill mass is maximum for foundation type III and is minimum for foundation type I [refer Fig.5.9]. The *FS* values for foundation type II and V are having negligible difference and are nearly 5% lower compared to foundation type I. The *FS* values for foundation type III are nearly 30% lower compared to foundation type I. The *FS* values for foundation type IV are nearly 15-16% lower compared to foundation type I.

Fig. 5.8 shows the variation of *FS* for different values of top width-to-height ratio, B/H_{sw}. From Fig. 5.8, it is noted that increase B/H_{sw} results a higher *FS*. Fig. 5.8 also shows the variation of *FS* with the given foundation type. For the given input parameters, foundation type III is having the least and foundation type I is having the highest *FS* in comparison to other foundation types. This can be attributed to the net amount of seismic inertial force acting on the landfill mass is maximum for foundation type III and is minimum for foundation type I [Fig.5.9]. The *FS* values for foundation type II and V are having negligible difference and are nearly 5-6% lower compared to foundation type I. The *FS* values for foundation type III are nearly 28-33% lower compared to foundation type I. The *FS* values for foundation type IV are nearly 16-18% lower compared to foundation type I.
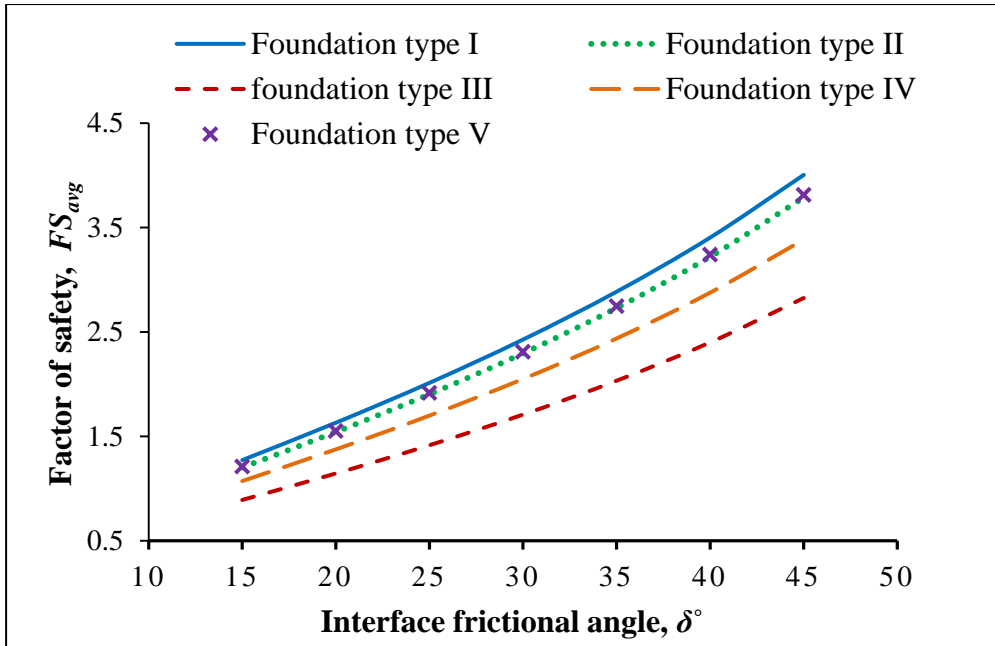
Fig. 5.6 Variation of factor of safety with the minimum interface friction angle of liner materials for five different foundation types, using present linear analysis
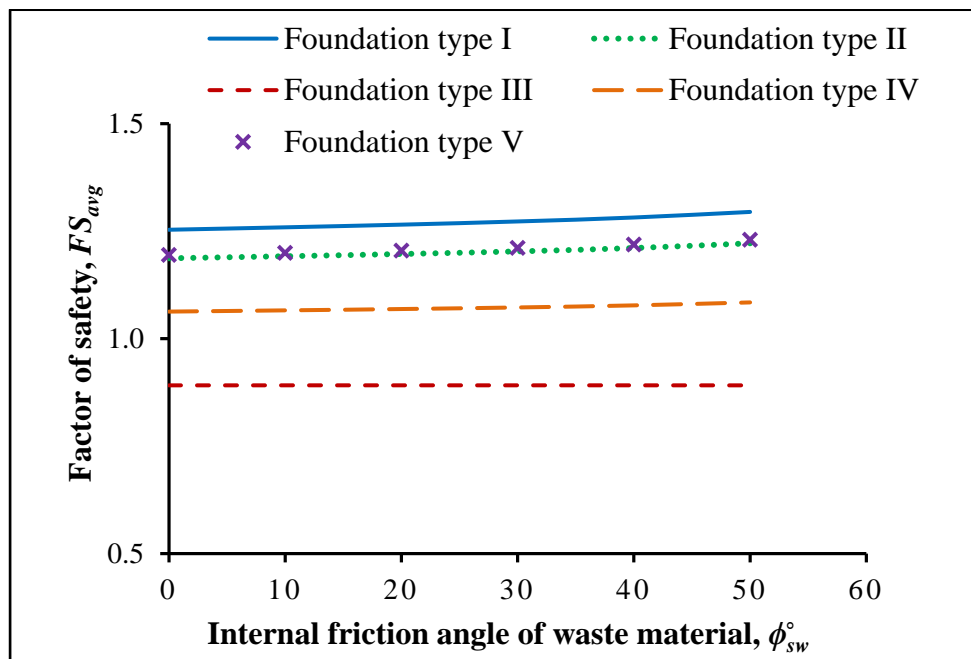
Fig. 5.7 Variation of factor of safety with the internal friction angle of waste mass for five different foundation types, using present linear analysis
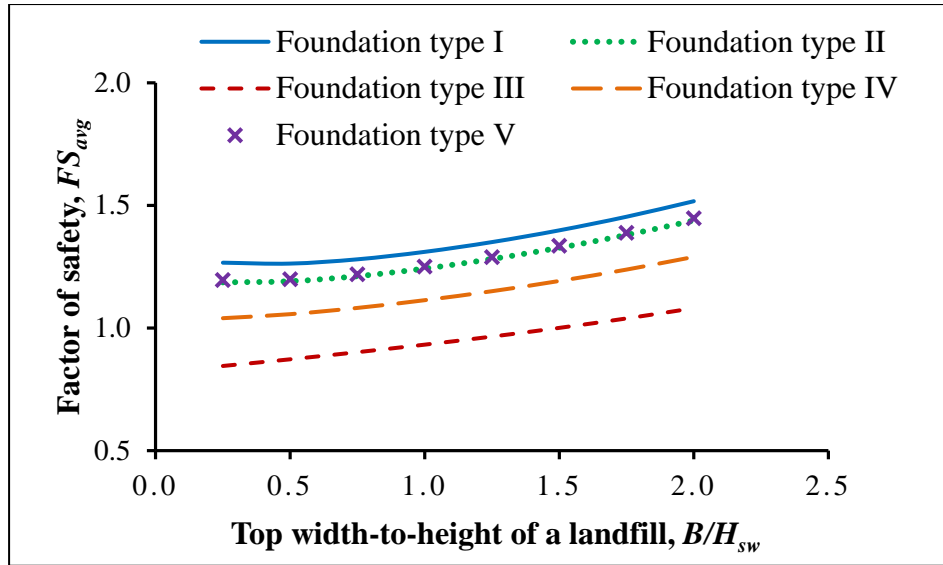
Fig. 5.8 variation of factor of safety with the top width-to-height ratio of a landfill for five different foundation types, using present linear analysis
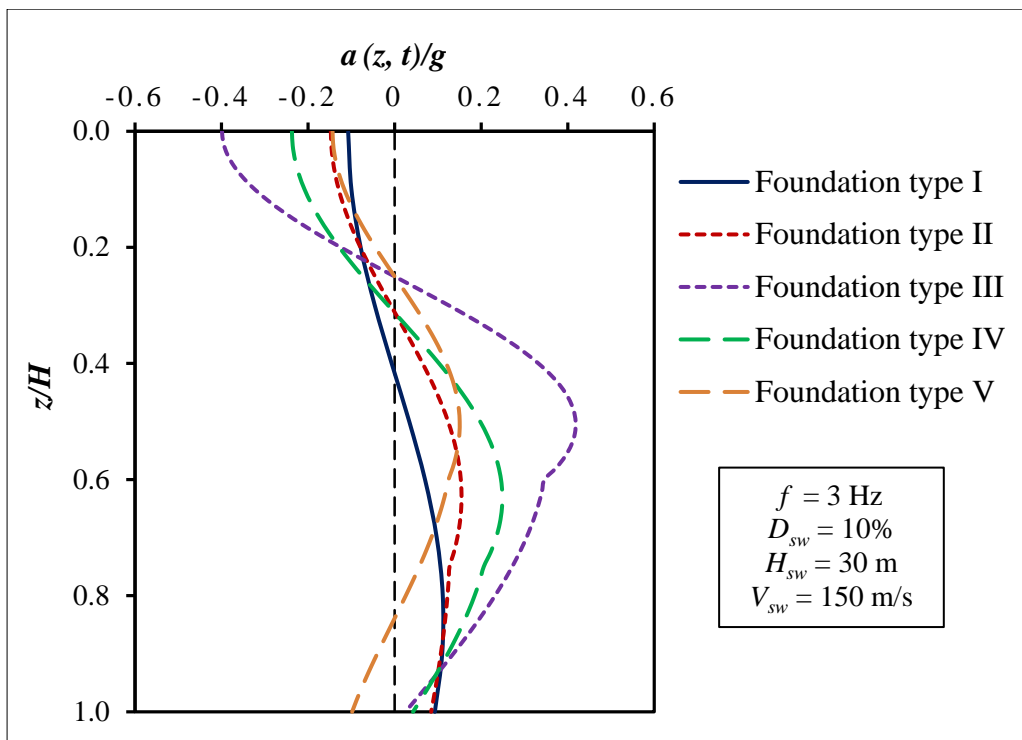
Fig. 5.9 Acceleration profiles for five different foundation types, using present linear analysis

The *FS* values for different normalized frequencies are computed using the present method and are given in Table 5.1. For lower normalized frequencies the *FS* values are lower compared to higher normalized frequencies. This can be attributed to the mode change behavior of the landfill. At lower normalized frequencies the landfill is vibrating in first mode where the seismic inertial forces for entire height of the landfill act in same direction. As a

result the net amount of seismic inertial force acting on the landfill is more, is the reason for lower *FS*. But, whereas at higher normalized frequencies the landfill is vibrating in higher modes where some part of seismic forces along the height of the landfill act in one direction and the remaining part act in the opposite direction. As a result, the net amount of seismic inertial force acting on the landfill is less, is the reason for higher *FS*. Table 5.1 also gives the *FS* values for different seismic acceleration coefficients. With the increase in seismic acceleration coefficient the *FS* is decreased. This is because increase in the seismic acceleration coefficient will increase the amount of seismic inertial force as a result *FS* gets decreases. The *FS* values for $k_h = 0.2$ are nearly 15 to 25 % lower than the values for $k_h = 0.1$.

Table 5.1: Factor of safety values computed for different normalized frequencies and different seismic acceleration coefficients using present linear analysis

$H_{sw} = 30$ m; $B = 20$ m; $k_h = 0.1$; $\alpha = 14°$; $\phi_{sw} = 30°$; $\beta = 18.4°$; $D_{sw} = 10\%$; $D_{fs} = 5\%$; $\delta_a = \delta_p = 20°$; $\gamma_{sw} = 10.5$ kN/m³; $C_a = C_p = 10$ kN/m²; $C_{sw} = 3$ kN/m²; $V_{sw} = 100$ m/s; Foundation type II			
Normalized frequency, $\frac{\omega H_{sw}}{V_{sw}}$	Present study ($k_h = 0.0$)	Present study ($k_h = 0.1$)	Present study ($k_h = 0.2$)
0	2.21	1.52	1.15
1	2.21	1.31	0.92
2	2.21	1.63	1.29
3	2.21	2.05	1.91
4	2.21	1.75	1.45
5	2.21	1.71	1.39
6	2.21	2.04	1.89

Fig. 5.10 shows the variation of *FS* for different values of interface cohesion, *C*. Increase in the interface cohesion results a higher *FS*. Fig 5.10 also shows the *FS* values for two different normalized frequencies and for two different seismic acceleration coefficients. When $k_h = 0.1$ the *FS* values for $\omega H_{sw}/V_{sw} = 3$ are nearly 35% higher than the values for $\omega H_{sw}/V_{sw} = 1$. Similarly, when $k_h = 0.2$ the *FS* values for $\omega H_{sw}/V_{sw} = 3$ are nearly 51% higher than the values for $\omega H_{sw}/V_{sw} = 1$. This can be explained with the help of Fig. 5.11. When $k_h = 0.1$ and for $\omega H_{sw}/V_{sw} = 1$ the landfill is in first mode and for $\omega H_{sw}/V_{sw} = 3$ the landfill is in second mode as

shown in Fig. 5.11, is the reason for higher FS values when $\omega H_{sw}/V_{sw} = 3$. For $\omega H_{sw}/V_{sw} = 1$, the FS values for $k_h = 0.1$ are nearly 29% higher to the values of $k_h = 0.2$ and it is 6.5 % for $\omega H_{sw}/V_{sw} = 3.0$.
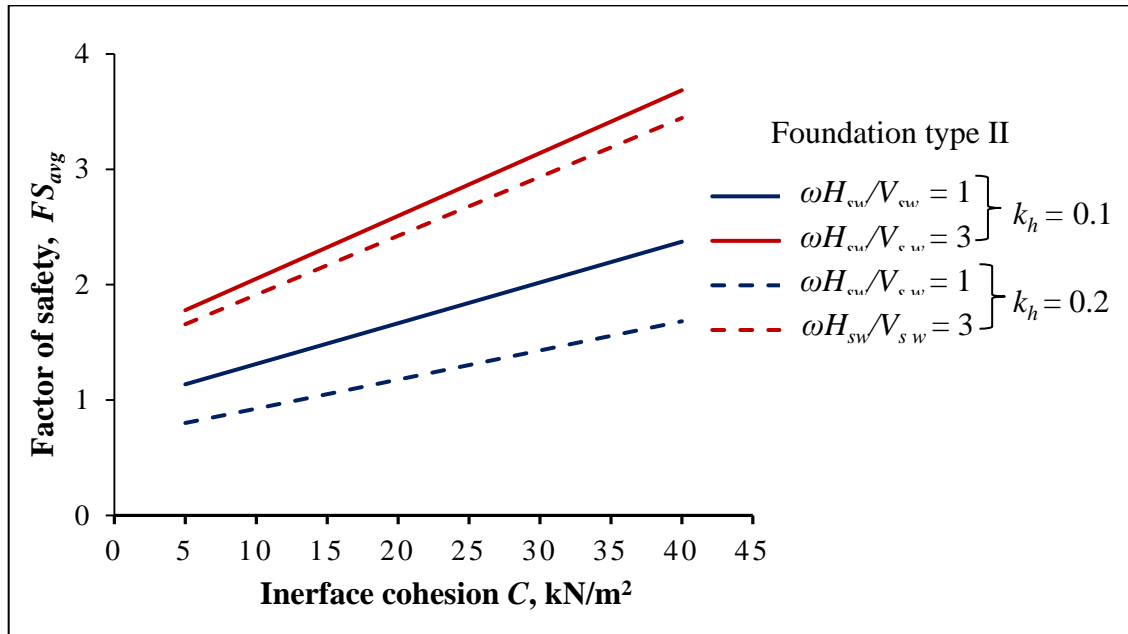

Fig. 5.10 Variation of factor of safety with the minimum interface cohesion of liner materials for $\omega H_{sw}/V_{sw} = 1$ and 3 and for $k_h = 0.1$ and 0.2 using present linear analysis
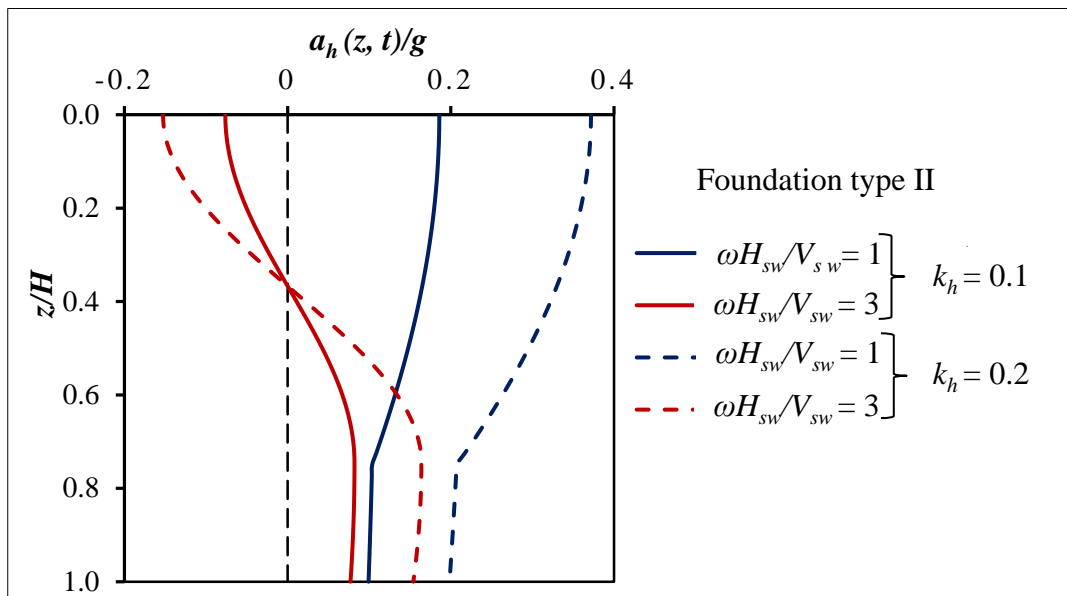
Fig. 5.11 Acceleration profiles for $\omega H_{sw}/V_{sw} = 1$ and 3 and for $k_h = 0.1$ and 0.2, using present linear analysis

5.2.4 Comparison of Results

In the following section, results obtained using present method is compared with the pseudo-dynamic analysis of Savoikar and Choudhury (2012) for similar landfill configuration and with same input parameters. On comparing the results of present study with the existing pseudo-dynamic method shows the similar trends.

Fig. 5.12 shows the comparison of *FS* values from present linear analysis with the results of pseudo-dynamic analysis for different values of minimum interface friction angle of liner materials, $\delta°$. From Fig. 5.12 it is noted that increase in interface friction angle results in higher *FS*. For the given input parameters the *FS* values from the present method are higher than the pseudo-dynamic values. This could be attributed to the mode change behavior which has been already explained in the previous sections. The *FS* values for foundation type I are nearly 17 to 18% higher than the pseudo-dynamic values. Similarly for foundation type II, nearly 13 to 14% higher and for foundation type IV, nearly 3 to 5% higher than the pseudo-dynamic values.

Fig. 5.13 shows the comparison of *FS* values from present linear analysis with the results of pseudo-dynamic analysis for different values of minimum interface cohesion of liner materials, *C*. From Fig. 5.13 it is noted that increase in interface cohesion results in higher *FS*. For the given input parameters the *FS* values from the present method are higher than the pseudo-dynamic values. The *FS* values for foundation type I are nearly 18% higher than the pseudo-dynamic values. Similarly for foundation type II, nearly 13 to 14% higher and for foundation type IV, nearly 4% higher than the pseudo-dynamic values.

Table 5.2 gives the comparison of *FS* values from the present study with the pseudo-dynamic values for different values of top width-to-height, *B/H$_{sw}$*. For the given input parameters, with the increase in *B/H$_{sw}$* the *FS* values are first decreased and then increased as shown in table 5.2.The *FS* values for foundation type I are nearly 10 to 13% higher at low and nearly 17% higher at high *B/H$_{sw}$* values compared to pseudo-dynamic values. Similarly for foundation type II, nearly 4 to 5% and 13% higher at low and high *B/H$_{sw}$* values respectively. For foundation type IV, nearly 3 to 8% lower and 3 to 4% higher at low and high *B/H$_{sw}$* values respectively.
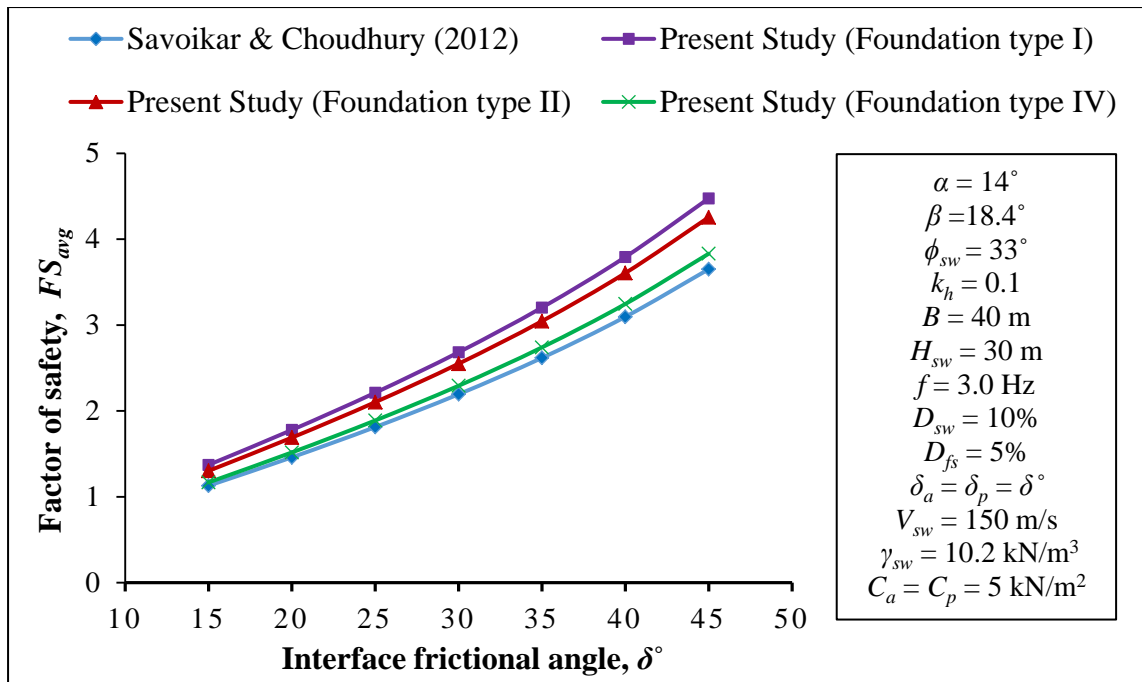
Fig. 5.12 Comparison of factor of safety values from present linear analysis with the pseudo-dynamic values for different interface friction angles and for different foundation types
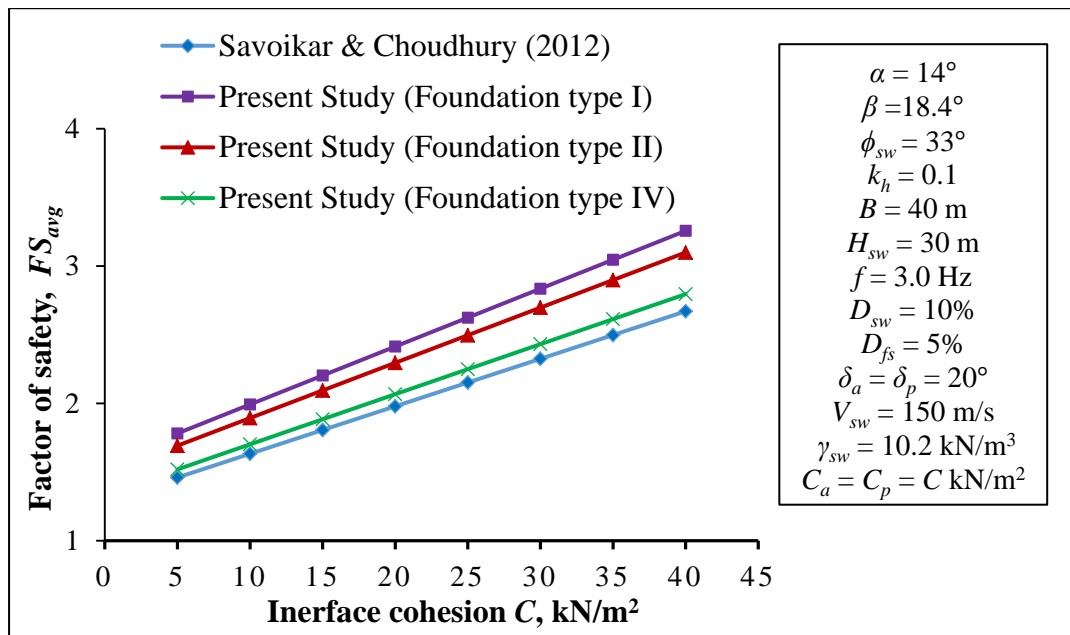
Fig. 5.13 Comparison of factor of safety values from present linear analysis with the pseudo-dynamic values for different interface cohesion and for different foundation types

Table 5.2: Comparison of factor of safety values from present linear analysis with the pseudo-dynamic values for different B/H_{sw} values and for different foundation types

H_{sw} = 30 m; k_h = 0.1; α = 14°; ϕ_{sw} =33°; β = 18.4°; D_{sw} = 10%; D_{fs} = 5%; $\delta_a = \delta_p$ = 20°; γ_{sw}=10.2 kN/m³; $C_a = C_p$ = 10 kN/m²; C_{sw} = 3 kN/m²; f = 3 Hz; V_{sw} = 150 m/s				
Top width-to-Height ratio, B/H_{sw}	Savoikar and Choudhury (2012) (Pseudo-dynamic analysis)	Present study (Foundation type I)	Present study (Foundation type II)	Present study (Foundation type IV)
0.25	1.74	1.94	1.82	1.60
0.50	1.64	1.90	1.79	1.59
0.75	1.60	1.90	1.80	1.61
1.00	1.60	1.92	1.83	1.64
1.25	1.62	1.97	1.87	1.68
1.50	1.66	2.03	1.93	1.73
1.75	1.73	2.10	1.99	1.79
2.00	1.82	2.18	2.07	1.86

Table: 5.3 Comparison of factor of safety values from present linear analysis with the pseudo-dynamic values for different internal friction angle of solid waste values and for different foundation types

H_{sw} = 30 m; B = 40 m; k_h = 0.1; α = 14°; β = 18.4°; D_{sw} = 10%; D_{fs} = 5%; $\delta_a = \delta_p$ = 20°; γ_{sw}=10.2 kN/m³; $C_a = C_p$ = 5 kN/m²; C_{sw} = 3 kN/m²; f = 3 Hz; V_{sw} = 150 m/s				
Internal friction angle of solid waste, $\phi_{sw}°$	Savoikar and Choudhury (2012) (Pseudo-dynamic analysis)	Present study (Foundation type I)	Present study (Foundation type II)	Present study (Foundation type IV)
15	1.441	1.77	1.68	1.51
20	1.45	1.77	1.68	1.51
25	1.45	1.77	1.69	1.52
30	1.46	1.78	1.69	1.52
35	1.46	1.78	1.69	1.52
40	1.47	1.79	1.70	1.52

Table 5.3 gives the comparison of *FS* values from the present study with the pseudo-dynamic values for different values of internal friction angle of solid waste, ϕ_{sw}°. From table 5.3 it is noted that increase in internal friction angle results in slightly higher *FS*. For the given input parameters the *FS* values from the present method are higher than the pseudo-dynamic values. The *FS* values for foundation type I are nearly 18% higher than the pseudo-dynamic values. Similarly for foundation type II, nearly 14% higher and for foundation type IV, nearly 3 to 5% higher than the pseudo-dynamic values.

5.3 Equivalent Linear Analysis

5.3.1 Proposed Methodology

In the linear analysis low-strain shear modulus and constant damping properties of MSW, sand and clay have been used to evaluate the seismic stability of MSW landfill resting on five different foundation types. But in reality, the shear strain generated during a seismic event is significantly large. So, in the present equivalent linear strain-dependent shear modulus and damping ratio have been used to compute acceleration profiles, *FS* and yield acceleration coefficient of a MSW landfill.

Expression for the calculation of shear strain generated in the landfill mass may be obtained from the partial derivative of equation (5.12) with respect to z_{sw}. The expression for shear strain (γ_{s1}) in the landfill mass as a function of depth (z_{sw}) and time (t) is as follows;

$$
\begin{aligned}
\gamma_{s1}(z_{sw},t) &= \frac{\partial u_{sw}(z_{sw},t)}{\partial z_{sw}} \\
&= \frac{u_{ho}}{M^2+N^2}\left[\cos \omega t \left(MA_{sw}+NB_{sw}\right)+\sin \omega t \left(MB_{sw}-NA_{sw}\right)\right]
\end{aligned}
\tag{5.23}
$$

Where

$$
A_{sw} = y_{sw_2} C_{s_1} - y_{sw_1} C_{s_2}
\tag{5.24a}
$$

$$
B_{sw} = y_{sw_1} C_{s_1} + y_{sw_2} C_{s_2}
\tag{5.24b}
$$

where

$$
C_{s_1} = \frac{1}{H_{sw}}\left[\cos\left(\frac{y_{sw_1} z_{sw}}{H_{sw}}\right)\sinh\left(\frac{y_{sw_2} z_{sw}}{H_{sw}}\right)\right]
\tag{5.25a}
$$

$$C_{s_2} = \frac{1}{H_{sw}}\left[\cosh\left(\frac{y_{sw_2} z_{sw}}{H_{sw}}\right)\sin\left(\frac{y_{sw_1} z_{sw}}{H_{sw}}\right)\right]$$

(5.25b)

Similarly, expression for the calculation of shear strain generated in the foundation soil may be obtained from the partial derivative of equation (5.13) with respect to z_{fs}. The expression for shear strain (γ_{s2}) in the foundation as a function of depth (z_{fs}) and time (t) is as follows;

$$\gamma_{s2}(z_{fs},t) = \frac{\partial u_{fs}(z_{fs},t)}{\partial z_{fs}}$$

$$= \frac{-u_{ho}}{M^2 + N^2}\left[\cos \omega t\left(MA_{fs} - NB_{fs}\right) + \sin \omega t\left(MB_{fs} + NA_{fs}\right)\right]$$

(5.26)

where,

$$A_{fs} = \begin{bmatrix} D_{c1}\chi\left(y_{fs_1}C_{f_1}S_{h_1} - y_{fs_2}C_{f_1}S_{h_2} + y_{fs_1}C_{f_2}S_{h_2} + y_{fs_2}C_{f_2}S_{h_1}\right) + \\ D_{c2}\chi\left(y_{fs_1}C_{f_1}S_{h_2} + y_{fs_2}C_{f_1}S_{h_1} - y_{fs_1}C_{f_2}S_{h_1} + y_{fs_2}C_{f_2}S_{h_2}\right) + \\ y_{fs_1}C_{f_3}S_{h_3} - y_{fs_2}C_{f_4}S_{h_3} + y_{fs_1}C_{f_4}S_{h_4} + y_{fs_2}C_{f_3}S_{h_4} \end{bmatrix}$$

(5.27a)

$$B_{fs} = \begin{bmatrix} D_{c1}\chi\left(y_{fs_1}C_{f_1}S_{h_2} + y_{fs_2}C_{f_1}S_{h_1} - y_{fs_1}C_{f_2}S_{h_1} + y_{fs_2}C_{f_2}S_{h_2}\right) - \\ D_{c2}\chi\left(y_{fs_1}C_{f_1}S_{h_1} - y_{fs_2}C_{f_1}S_{h_2} + y_{fs_1}C_{f_2}S_{h_2} + y_{fs_2}C_{f_2}S_{h_1}\right) + \\ y_{fs_1}C_{f_4}S_{h_3} + y_{fs_2}C_{f_3}S_{h_3} - y_{fs_1}C_{f_3}S_{h_4} + y_{fs_2}C_{f_4}S_{h_4} \end{bmatrix}$$

(5.27b)

where,

$$C_{f_1} = \frac{1}{H_{fs}}\left[\cos\left(\frac{y_{fs_1} z_{fs}}{H_{fs}}\right)\cosh\left(\frac{y_{fs_2} z_{fs}}{H_{fs}}\right)\right]$$

(5.27a)

$$C_{f_2} = \frac{1}{H_{fs}}\left[\sin\left(\frac{y_{fs_1} z_{fs}}{H_{fs}}\right)\sinh\left(\frac{y_{fs_2} z_{fs}}{H_{fs}}\right)\right]$$

(5.27b)

$$C_{f_3} = \frac{1}{H_{fs}}\left[\cosh\left(\frac{y_{fs_1} z_{fs}}{H_{fs}}\right)\sin\left(\frac{y_{fs_2} z_{fs}}{H_{fs}}\right)\right]$$

(5.27c)

$$C_{f_4} = \frac{1}{H_{fs}}\left[\cos\left(\frac{y_{fs_1} z_{fs}}{H_{fs}}\right)\sinh\left(\frac{y_{fs_2} z_{fs}}{H_{fs}}\right)\right]$$

(5.27d)

$$S_{h_1} = \sin\left(y_{sw_1}\right)\cosh\left(y_{sw_2}\right) \tag{5.28a}$$

$$S_{h_2} = \cos\left(y_{sw_1}\right)\sinh\left(y_{sw_2}\right) \tag{5.28b}$$

$$S_{h_3} = \cos\left(y_{sw_1}\right)\cosh\left(y_{sw_2}\right) \tag{5.28c}$$

$$S_{h_4} = \sin\left(y_{sw_1}\right)\sinh\left(y_{sw_2}\right) \tag{5.28d}$$

The modulus reduction and damping ratio curves of MSW, sand and clay are required for the present solution. These two curves could be developed by conducting cyclic tri-axial tests on MSW, sand and clay. In the absence of case specific data, curves available in the literature may be used. In the present study, the modulus reduction and damping ratio curves proposed by Choudhury and Savoikar (2009b) have been used for MSW. The mathematical expressions for these curves are given in section 3.3.1 of chapter 3 (equation (3.47a) and (3.47b)).

For sand, mean curve proposed by Seed and Idriss (1991) have been used. The mathematical expressions for these curves are obtained by using the modified hyperbolic model of Matasovic (1993). The model parameters are obtained using best curve-fit technique.

The expression for modulus reduction curve of sand used in the present study is;

$$\left(\frac{G_{\text{sec}}}{G_{\max}}\right)_{sand} = \frac{1}{1 + 8\left(\dfrac{\gamma_{u_2}}{0.37}\right)^{0.92}} \tag{5.29a}$$

The expression for damping ratio curve of sand used in the present study is;

$$\left(D_{fs}\right)_{sand} = 28\left(1 - e^{-2.5\gamma_{u_2}^{0.51}}\right) \tag{5.29b}$$

Similarly for clay, curves proposed by Vucetic and Dobry (1991) have been used. The modulus reduction and damping curves for clay having both low (PI = 15%) and high (PI = 30%) plasticity are used in the present study. The mathematical expressions for these curves are obtained in the similar way for clay.

The expression for modulus reduction curve of clay having low plasticity is;

$$\left(\frac{G_{\text{sec}}}{G_{\text{max}}}\right)_{PI=15\%} = \frac{1}{1+5.7\left(\dfrac{\gamma_u}{0.44}\right)^{0.9}} \tag{5.30a}$$

The expression for damping ratio curve of clay having low plasticity is;

$$\left(D_{fs}\right)_{PI=15\%} = 24\left(1-e^{-1.9\gamma_u^{0.48}}\right) \tag{5.31b}$$

The expression for modulus reduction curve of clay having high plasticity is;

$$\left(\frac{G_{\text{sec}}}{G_{\text{max}}}\right)_{PI=15\%} = \frac{1}{1+4.8\left(\dfrac{\gamma_u}{0.8}\right)^{0.85}} \tag{5.32a}$$

The expression for damping ratio curve of clay having high plasticity is;

$$\left(D_{fs}\right)_{PI=30\%} = 23\left(1-e^{-1.3\gamma_u^{0.47}}\right) \tag{5.32b}$$

The following four different foundation types are studied in the present equivalent linear based analysis:

Foundation type I: Shallow sand deposit underlain by a rigid base

Foundation type II: Deep sand deposit underlain by a rigid base

Foundation type III: Shallow clay deposit underlain by a rigid base

Foundation type IV: Deep clay deposit underlain by a rigid base

The procedure for the computation of strain-dependent dynamic properties and *FS* is coded using MATLAB program.

The following are the programming steps:

1. Develop modulus reduction and damping curves of MSW and foundation soil from laboratory tests. In the absence of those, curves available in the published literature may be used.
2. Assign low strain values of shear modulus (G) and damping ratio (ξ) for both the layers (i.e., solid waste and foundation soil).

3. At a particular time step use shear modulus (G) and damping ratio (ξ) to compute the maximum shear strain in the landfill and foundation soil using equation (5.23) and (5.26), respectively.

4. Compute the effective shear strain from maximum shear strain using,

$$\gamma_{eff}^i = R_\gamma * \gamma_{max}^i$$

where the superscript (i) indicates the iteration number and R_γ is the ratio of effective shear strain and maximum shear strain. In the present study R_γ is treated as one.

5. Use the effective shear strain to compute a new set of values ($G^{(i+1)}$ and $\xi^{(i+1)}$) using the modulus reduction and damping ratio curves for the next iteration.

6. Repeat the steps 3 to 5 until the difference between the computed shear modulus and damping ratio in two successive iterations is less than 15%.

7. The shear modulus and damping ratio corresponding to the last iteration are the equivalent linear values. Use the equivalent linear values to compute the acceleration profiles along the depth at that particular time step.

8. Use the acceleration profiles to compute seismic inertial forces at the same time step.

9. Use the seismic inertial forces to compute the *FS* values for the same time step using the proposed equations.

10. Repeat the steps 2 to 9 for the next time step.

5.3.2 *Validation of Acceleration Profiles from Equivalent Linear Analysis using DEEPSOIL*

In the DEEPSOIL linear analysis, small strain value of shear wave velocity is used and a fixed damping ratio value is assigned to MSW material. But in reality, significantly large amount of shear strain will generate during a seismic event. And it is well established in geotechnical earthquake engineering that the shear modulus decreases significantly with the increase in the shear strain and at the same time damping ratio value increases. Equivalent linear approach of ground response analysis uses two curves namely modulus reduction curve and damping ratio curve to arrive a strain dependent shear modulus and damping ratio value. It is an iterative process. In the present study, the modulus reduction curve and damping ratio curve proposed by Choudhury and Savoikar (2009) are used for MSW in the DEEPSOIL equivalent linear analysis. The mean curves proposed by proposed by Seed and Idriss (1991) are used for sand. The curves proposed by Vucetic and Dobry (1991) are used for clay. Unit weight, boundary condition and input motion are kept same as in the linear analysis. Acceleration ratio is also

computed for the equivalent linear approach. The acceleration profiles obtained from the present study are validated using DEEPSOIL equivalent linear analysis results. The acceleration ratios obtained from the present equivalent linear analysis are in good agreement with the DEEPSOIL results.

Fig. 5.14 shows the validation of acceleration ratios computed for foundation type I and II with the results of DEEPSOIL equivalent linear analysis. For an input frequency of $f = 0.3$ Hz ($\omega = 2\pi f = 1.885$ rad/s), the acceleration ratio from the present method for foundation type I is 1.185 and from the DEEPSOIL equivalent linear analysis is 1.176, the percentage difference is 0.77%. At the same input frequency the acceleration ratio from the present method for foundation type II is 1.221 and from the DEEPSOIL is 1.224, the percentage difference is 0.26%. At the same input frequency, the acceleration ratio for foundation type II is nearly 4% higher than the value for foundation type I. Similarly, for another input frequency of $f = 1.75$ Hz ($\omega = 2\pi f = 10.995$ rad/s), the acceleration ratio from present method for foundation type I is 1.212 and from DEEPSOIL is 1.068, the percentage difference is 13.4%. At the same input frequency the acceleration ratio from the present method for foundation type II is 1.373 and from the DEEPSOIL is 1.452, the percentage difference is 5.41%. At the same input frequency the acceleration ratio for foundation type II is nearly 26% higher to foundation type I.

Fig. 5.15 shows the validation and comparison of acceleration ratios computed for foundation type III when PI = 15% and PI = 30%, with the results of DEEPSOIL. For an input frequency of $f = 0.2$ Hz ($\omega = 2\pi f = 1.256$ rad/s), the acceleration ratio from the present method for foundation type III when PI = 15% is 1.093 and from the DEEPSOIL equivalent linear analysis is 1.104, the percentage difference is 0.967%. At the same input frequency the acceleration ratio from the present method for foundation type III when PI = 30% is 1.085 and from the DEEPSOIL is 1.088, the percentage difference is 0.20%. Similarly, for another input frequency of $f = 0.75$ Hz ($\omega = 2\pi f = 4.712$ rad/s), the acceleration ratio from present method for foundation type III when PI = 15% is 2.638 and from DEEPSOIL is 2.644, the percentage difference is 0.23%. At the same input frequency the acceleration ratio from the present method for foundation type III when PI = 30% is 3.070 and from the DEEPSOIL is 3.283, the percentage difference is 6.50%.

Fig. 5.14 Validation graph of acceleration ratio for foundation type I and II using present equivalent linear analysis and DEEPSOIL equivalent linear analysis

Fig. 5.15 Validation graph of acceleration ratio for foundation type III when PI = 15% and 30% using present equivalent linear analysis and DEEPSOIL equivalent linear analysis

Fig. 5.16 shows the validation of acceleration ratios computed for foundation type III and IV when PI = 30%, with the results of DEEPSOIL equivalent linear analysis. For an input

frequency of $f = 0.3$ Hz ($\omega = 2\pi f = 1.885$ rad/s), the acceleration ratio from the present method for foundation type III is 1.232 and from the DEEPSOIL equivalent linear analysis is 1.217, the percentage difference is 1.25%. At the same input frequency the acceleration ratio from the present method for foundation type IV is 1.328 and from the DEEPSOIL is 1.353, the percentage difference is 1.82%. At this input frequency, the acceleration ratio for foundation type IV is nearly 10% higher than the value for foundation type III. It is also observed from Fig. 5.16 the peak amplification in foundation type III is nearly 18% higher than in foundation type IV.
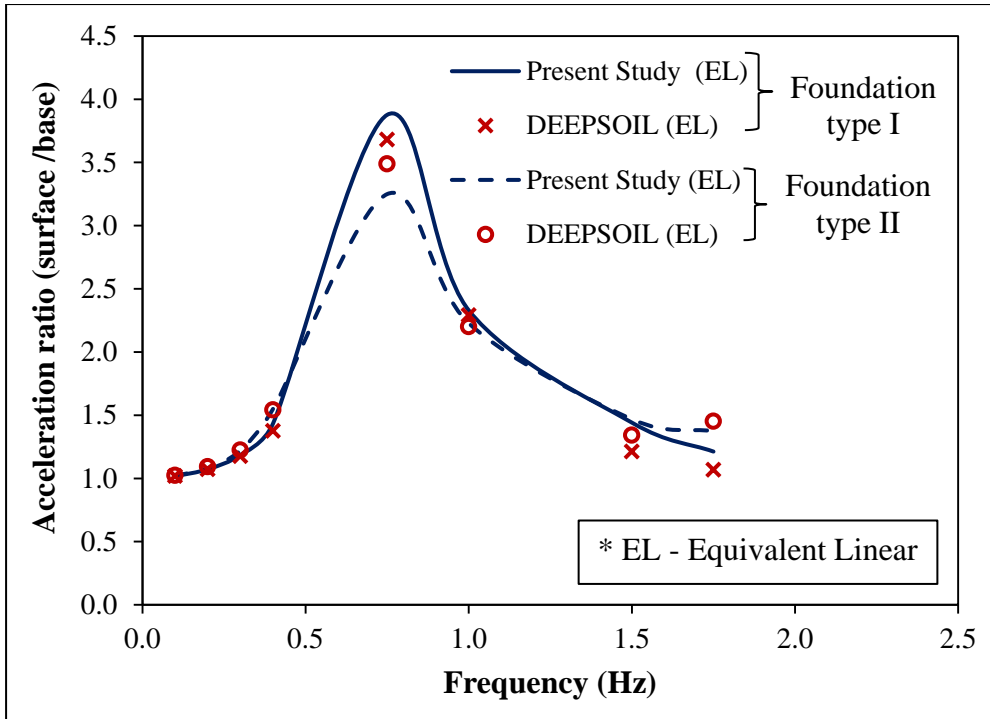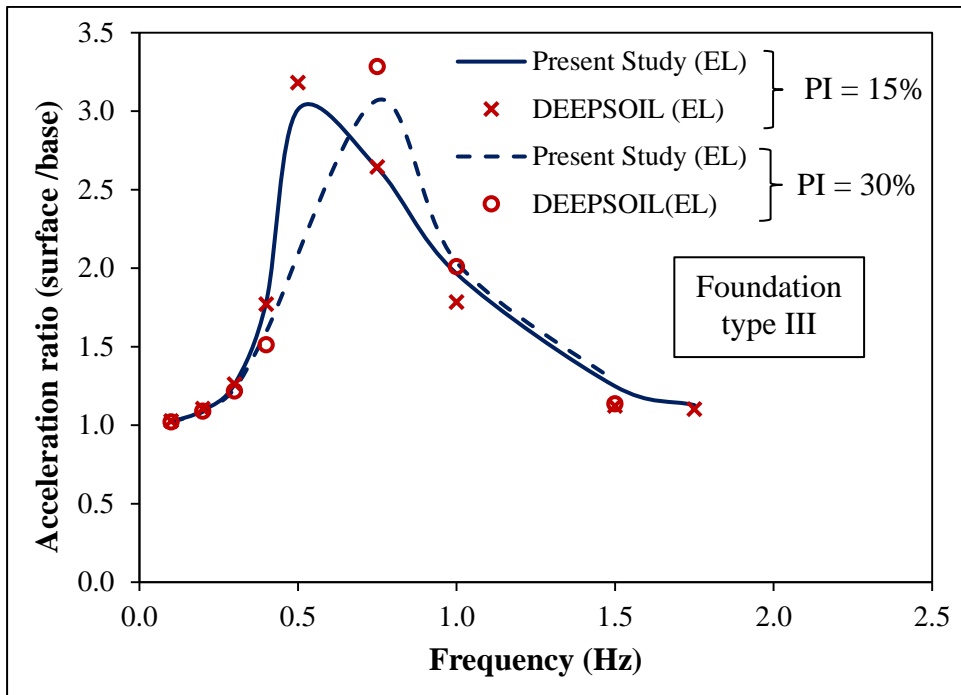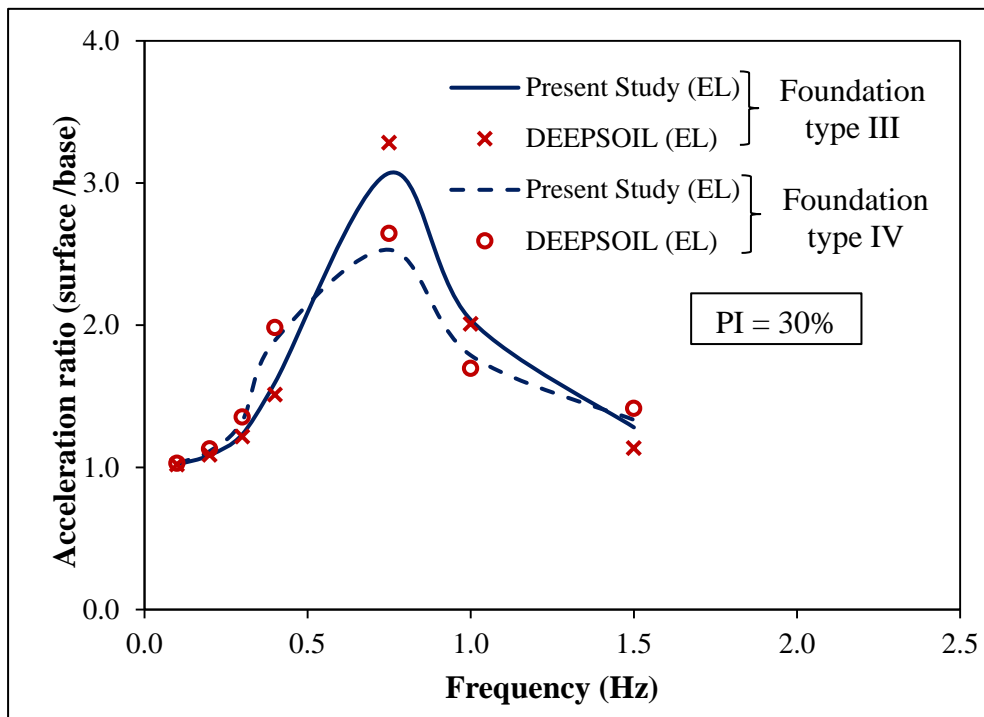

Fig. 5.16 Validation graph of acceleration ratio for foundation type III and IV when PI = 30% using present equivalent linear analysis and DEEPSOIL equivalent linear analysis

5.3.3 Parametric Study

In the present parametric study, the following variation of parameters is used: $H_{sw} = 30$ m, $B/H_{sw} = 0.5$ to 2, $\alpha = 14°$, $\beta = 18.4°$, $\phi_{sw} = 15$ to $45°$, $\delta_a = \delta_p = 15$ to $45°$, $\gamma_{sw} = 10.5$ kN/m^3, $k_h = 0.1$, $V_{sw} = 150$ m/s, $f = 1.75$ Hz, $t/T = 0$ to 1, $D_{sw} = 10\%$ and $D_{fs} = 5\%$. The unit weight and shear wave velocity of sand and clay are kept same.

Fig. 5.17 shows the variation of FS for different values of minimum interface friction angle of liner materials, δ. From Fig. 5.17, it is noted that increase in interface friction angle results a higher FS. Fig. 5.17 also shows the variation of FS for the given foundation type. For the

given input parameters, foundation type I is having the least *FS* in comparison to other foundation types. The *FS* values for foundation type III and IV are having negligible difference and are nearly 25% higher compared to foundation type I. The *FS* values for foundation type II are nearly 19% higher compared to foundation type I. For the given input parameters, the value of PI for clay is having negligible effect on the *FS* values.
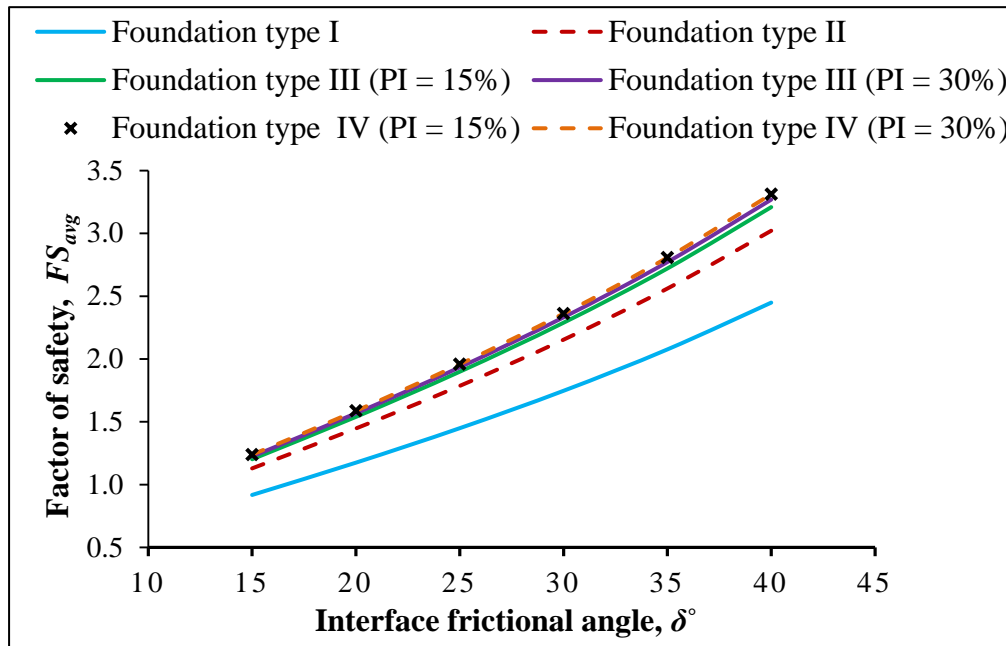
Fig. 5.17 Variation of factor of safety with the interface friction angle of waste mass for five different foundation types, using present equivalent linear analysis

The *FS* values for different values of minimum interface cohesion of liner materials, C are computed using the present method and are presented in table 5.4. It is observed from table 5.4 increase in interface values results a higher *FS* values. Table 5.1 also gives the *FS* values for different foundation types. . For the given input parameters, foundation type I is having the least and foundation IV is having the highest *FS* in comparison to other foundation types. The *FS* values for foundation type IV are nearly 25 to 26% higher compared to foundation type I. The *FS* values for foundation type III are nearly 23to 24% higher compared to foundation type I. Similarly, the *FS* values for foundation type II are nearly 18 to 19% higher compared to foundation type I.

Table 5.4: Factor of safety values computed for different interface cohesion values and different foundation types using present equivalent linear analysis

H_{sw} = 30 m; k_h = 0.1; α = 14°; ϕ_{sw} =33°; β = 18.4°; D_{sw} = 10%; D_{fs} = 5%; $\delta_a = \delta_p$ = 20°; γ_{sw}=10.5 kN/m³; $C_a = C_p$ = C kN/m²; C_{sw} = 3 kN/m²; V_{sw} = 150 m/s; f = 3 Hz; PI = 15%				
Interface Cohesion, C kN/m²	Present study (Foundation type I)	Present study (Foundation type II)	Present study (Foundation type III)	Present study (Foundation type IV)
0	0.99	1.22	1.30	1.34
5	1.17	1.44	1.54	1.58
10	1.36	1.67	1.77	1.83
15	1.54	1.89	2.01	2.07
20	1.72	2.12	2.25	2.32
25	1.91	2.34	2.48	2.56
30	2.09	2.57	2.72	2.81
35	2.28	2.79	2.96	3.05

Fig. 5.18 shows the variation of *FS* for different values of top width-to-height ratio, B/H_{sw}. From Fig. 5.18, it is noted that increase in B/H_{sw} results a higher *FS*. Fig. 5.18 also shows the variation of *FS* for the given foundation type. For the given input parameters, foundation type II is having the least and foundation III is having the highest *FS* in comparison to other foundation types. The *FS* values for foundation type III are nearly 5 to 8% higher compared to foundation type II.
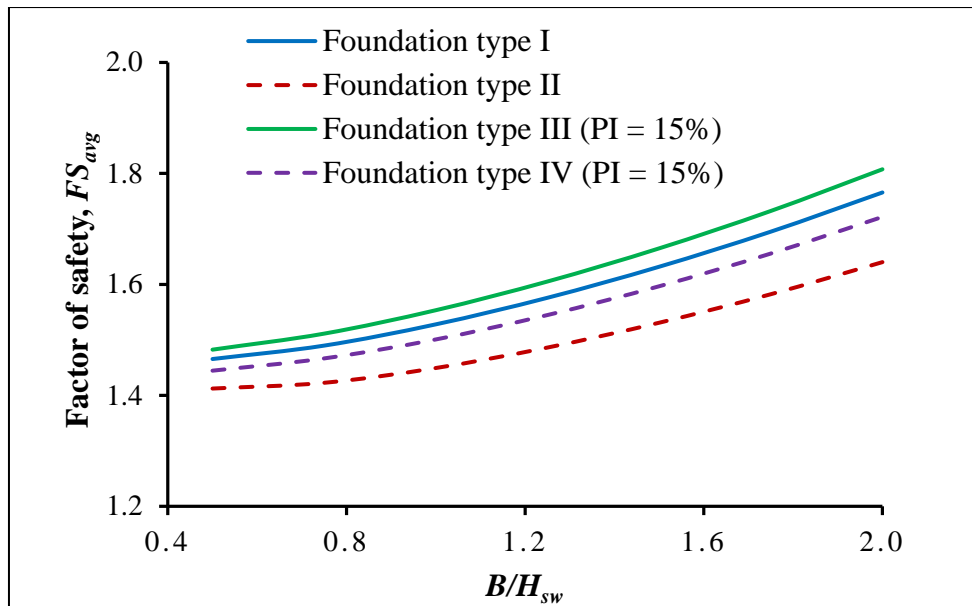
Fig. 5.18 variation of factor of safety with the top width-to-height ratio of a landfill for four different foundation types, using present equivalent linear analysis

5.3.4 Comparison of Results

In the following section, results obtained using present equivalent linear method is compared with the pseudo-dynamic analysis of Savoikar and Choudhury (2012) and the present linear analysis for similar landfill configuration and with same input parameters. On comparing the results of present study with the existing pseudo-dynamic method and present linear analysis shows the similar trends.

Fig. 5.19 shows the comparison of *FS* values from present equivalent linear analysis with the results of pseudo-dynamic analysis and present linear analysis for different values of minimum interface cohesion of liner materials, *C*. From Fig. 5.19 it is observed that increase in interface cohesion results in significantly higher *FS*. For the given input parameters, from the present linear analysis, foundation type I has nearly 13 to 14% higher *FS* than the pseudo-dynamic analysis. But from the present equivalent linear analysis, foundation type I has nearly 6 to 8% lower *FS* than the pseudo-dynamic analysis. From the present linear analysis, foundation type III has nearly 3 to 4% higher *FS* than the pseudo-dynamic analysis. But from the present equivalent linear analysis, foundation type III has nearly 7 to 8% higher *FS* than the pseudo-dynamic analysis.

Fig. 5.19 Comparison of factor of safety values from present equivalent linear analysis with the pseudo-dynamic analysis and present linear analysis for different interface cohesion values and for different foundation types

Fig. 5.20 shows the comparison of *FS* values from present equivalent linear analysis with the results of pseudo-dynamic analysis and present linear analysis for different values of internal friction angle, ϕ_{sw}°. From Fig. 5.20 it is observed that increase in internal friction angle results in slightly higher *FS*. For the given input parameters, from the present linear analysis, foundation type I has nearly 13 to 14% higher *FS* than the pseudo-dynamic analysis. But from the present equivalent linear analysis, foundation type I has nearly 6 to 7% lower *FS* than the pseudo-dynamic analysis. From the present linear analysis, foundation type III has nearly 4 to 5% higher *FS* than the pseudo-dynamic analysis. But from the present equivalent linear analysis, foundation type III has nearly 7 to 8% higher *FS* than the pseudo-dynamic analysis.

Fig. 5.20 Comparison of factor of safety values from present equivalent linear analysis with the pseudo-dynamic analysis and present linear analysis for different internal friction angles and for different foundation types

The *FS* for different values of interface friction angle are computed using present equivalent linear analysis and are compared with the existing pseudo-dynamic analysis and present linear analysis. The *FS* values are present in table 5.5. It is observed from table 5.5 the increase in interface friction angle results in significantly higher *FS*. For the given input parameters, for foundation type I, the *FS* values from the present linear analysis are nearly 13 to 14% higher than the pseudo-dynamic analysis. But from the present equivalent linear analysis, foundation type I has nearly 7 to 8% 1ower *FS* than the pseudo-dynamic analysis. From the present linear analysis, foundation type III has nearly 3 to 4% higher *FS* than the pseudo-dynamic analysis. But from the present equivalent linear analysis, foundation type III has nearly 7% higher *FS* than the pseudo-dynamic analysis.
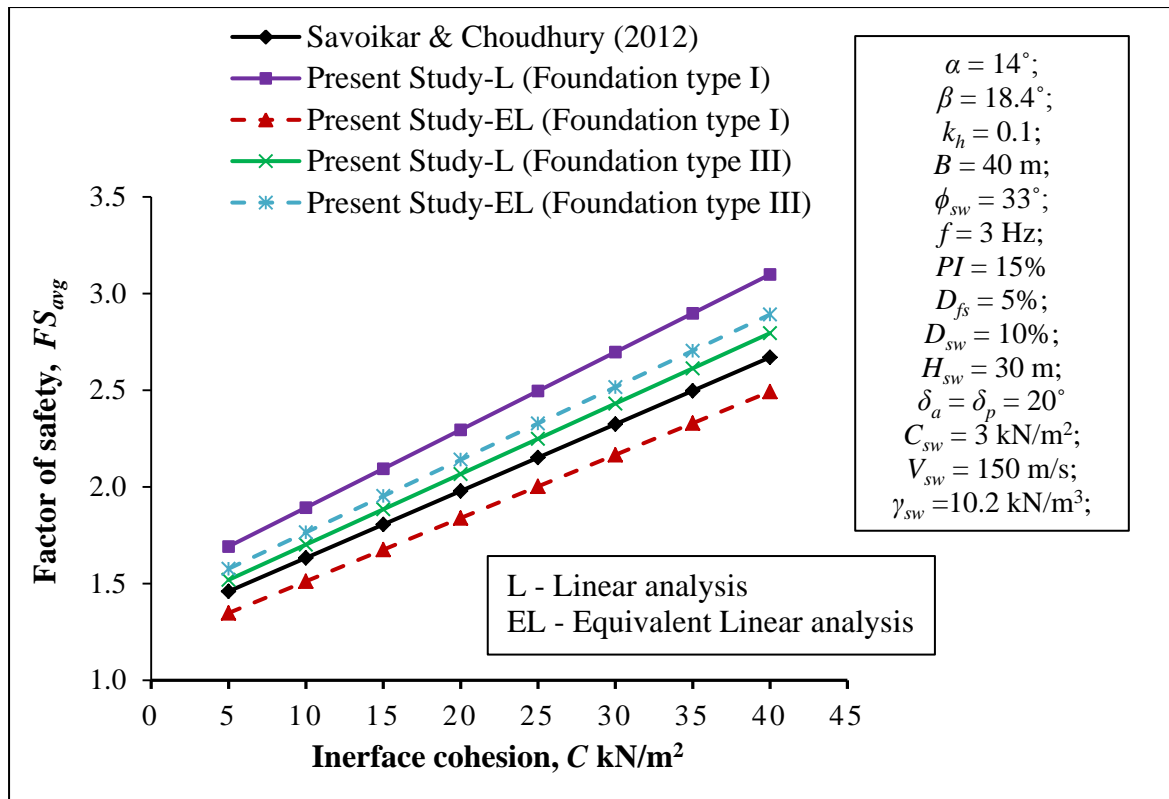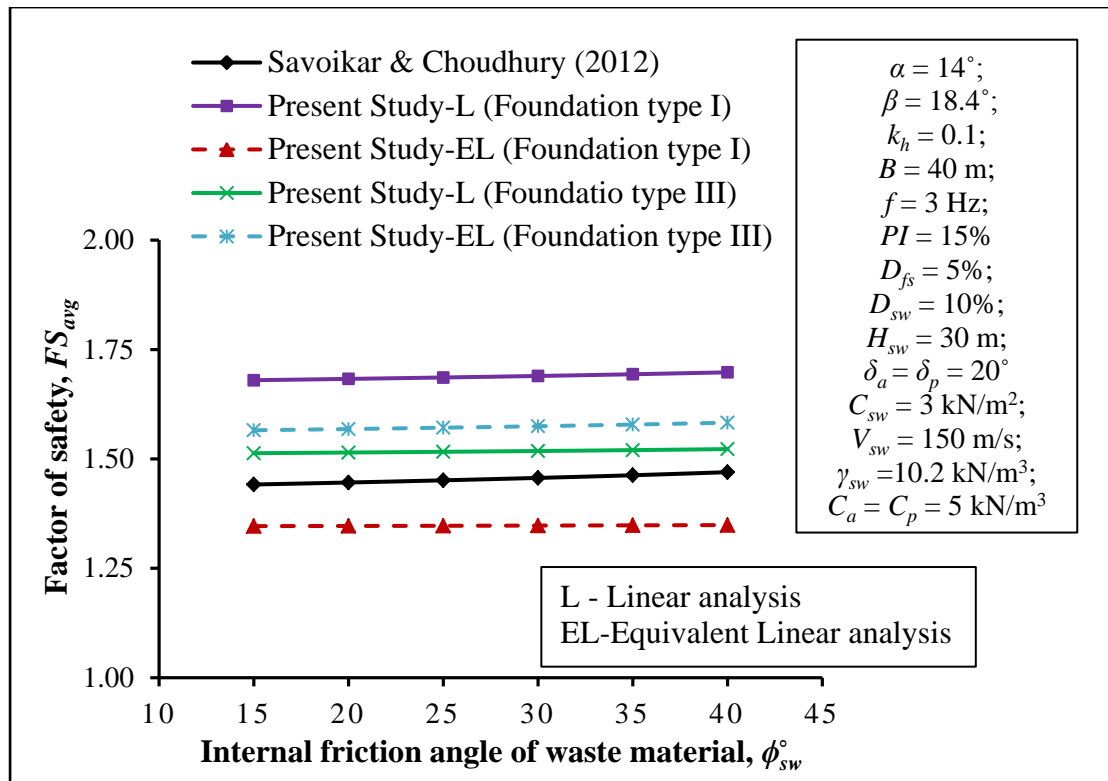
Table 5.5: Comparison of factor of safety values from present equivalent linear analysis with the pseudo-dynamic analysis and present linear analysis for different interface friction angles and for different foundation types

$H_{sw} = 30$ m; $B = 40$ m; $k_h = 0.1$; $\alpha = 14°$; $\phi_{sw} = 33°$; $\beta = 18.4°$; $D_{sw} = 10\%$; $D_{fs} = 5\%$; $\gamma_{sw} = 10.2$ kN/m^3; $C_a = C_p = 5$ kN/m^2; $C_{sw} = 3$ kN/m^2; $V_{sw} = 150$ m/s; $f = 3$ Hz; $PI = 15\%$					
Interface friction angle, $\delta°$	Savoikar and Choudhury (2012)	Present study-L* (Foundation type I)	Present study-EL# (Foundation type I)	Present study-L* (Foundation type III)	Present study-EL# (Foundation type II)
15	1.12	1.30	1.03	1.16	1.21
20	1.46	1.68	1.34	1.51	1.57
25	1.81	2.10	1.67	1.88	1.96
30	2.19	2.55	2.03	2.29	2.37
35	2.61	3.04	2.43	2.74	2.84
40	3.09	3.60	2.88	3.24	3.36
45	3.65	4.25	3.40	3.83	3.96

* L – Linear Analysis   # EL – Equivalent Linear Analysis

5.4 Summary

The acceleration ratios and *FS* values for the model MSW landfill resting on different foundation types are computed using present method linear and equivalent linear analysis. The acceleration ratios are validated using DEEPSOIL linear and equivalent linear analysis. The *FS* values are compared with the similar existing literature. And detailed parametric study is carried out.

6.1 General

In this chapter, the major conclusions drawn from the present study are highlighted. Future scope of work is also reported at the end of this chapter.

6.2 Major Conclusions

The following are the major conclusions drawn based on the present research work carried out:

- Amplification of acceleration is highly depends on the characteristics of input motion.

- Acceleration distribution is found to be found to be time dependent and is non-linear in nature.

- The Acceleration ratio computed using the proposed linear and equivalent linear based approach is very much comparable with DEEPSOIL linear and equivalent linear results.

- Front and back slope angles, height and top width of the landfill, internal friction angle of MSW, minimum interface friction angles at the base of active and passive wedges, frequency of input motion, and material damping of MSW have significant influence on the stability of landfill.

- For low frequency input motions the landfill is vibrating in first mode and for high frequency input motions it is vibrating in higher modes. Consideration of this phenomenon in the seismic stability analysis of MSW landfills results in a safe and economic design.

- The factors of safety values obtained from the present method are found to be higher than the existing pseudo-static methods for high frequency input motions and found to be lower for low frequency input motions.

- The *FS* values for low frequency input motions are found to be critical for landfills.

- The maximum shear strain computed for low frequency input motion is significantly higher as compare to high frequency input motion.

- The *FS* values computed using the proposed equivalent linear based approach are lower than the values of linear analysis but, it is still higher than the values of pseudo-static and pseudo-dynamic analysis for a given set of input parameters.

- Use of characteristic profiles for unit weight and shear wave velocity in the calculation of seismic *FS* may give the better results.

- The types of foundation soil significantly affect the seismic *FS* of MSW landfills.

- For the given input parameters, landfill resting on the deep sand deposit underlain by a rigid base is having the least *FS* out of five different foundation types used in the present study.

6.3 Limitations of the Present Study

- The present solution is valid for dry conditions only. The solution needs improvement to consider the effect of excess pore water pressure generated during earthquake on the *FS* value.
- The present solution is applicable for the landfills lined with the impermeable materials like Geosynthetics.
- The present solution is applicable for the design of typical side-hill type landfills.

6.4 Future Scope of Work

➢ The equivalent shear modulus and damping are considered in the present study. The results may improve if the actual non-linear behavior of shear modulus and damping are considered in the present solution.

➢ The proposed method may extend for the design of expanded landfills.

➢ In the present study, solid waste is modelled as a Kelvin-Voigt (KV) material for dry condition. The solution may be extended for the solid waste with the presence of water using Kelvin-Voigt-Maxwell-Biot (KVMB) model (Rajesh and Choudhury, 2016). That solution will be applicable for the design of bioreactor landfills.

➢ In the present study, the landfill rests on single layer foundation soil is considered. The solution may extend for the landfill resting on multiple layers of foundation soil.

➢ In the present study, typical side-hill type model landfill is considered. The solution may be extended for other landfill configurations such as hill type and canyon type.

Abreu, A. E. S., Gandolfo, O. C. B. and Vilar, O. M. (2016). "Characterizing a Brazilian sanitary landfill using geophysical seismic techniques." *Waste Management*, **53**, 116–127.

Akai, K., Bray, J. D., Christian, J. T. and Boulanger, R. W. (1997). *Geotechnical reconnaissance of the effects of the January 17, 1995, Hyogoken-Nanbu earthquake, Japan*. 1st ed. DIANE Publishing; pp. 130.

Anbazhagan, P., SivakumarBabu, G., Lakshmikanthan, P. and VivekAnand, K. (2016). "Seismic characterization and dynamic site response of a municipal solid waste landfill in Bangalore, India." *Waste Management & Research*, **34**(3), 205–213.

Athanasopoulos, G., Vlachakis, V., Zekkos, D. and Spiliotopoulos, G. (2013) The December 29th 2010 Xerolakka Municipal Solid Waste landfill failure. In: *Proc. of the 18th international conference on soil mechanics and geotechnical engineering*; Paris.

Augello, A. J., Matasovic, N., Bray, J. D., Kavazanjian Jr, E. and Seed, R. B. (1995). "Evaluation of solid waste landfill performance during the Northridge earthquake." *Earthquake Design and Performance of Solid Waste Landfills*, GSP (ASCE), **54**, 17-50.

Bellezza, I. (2014). "A New Pseudo-dynamic Approach for Seismic Active Soil Thrust." *Geotechnical and Geological Engineering*, **32**(2), 561-576.

Bellezza, I. (2015). "Seismic Active Earth Pressure on Walls Using a New Pseudo-Dynamic Approach." *Geotechnical and Geological Engineering*, **33**(4), 795-812.

Blight, G. (2008). "Slope failures in municipal solid waste dumps and landfills: a review." *Waste Management & Research*, **26**(5), 448-463.

Blight, G. E. (2004) A flow failure in a municipal solid waste landfill–the failure at Bulbul, South Africa. In: *Proc. of a three day conference on advances in geotechnical engineering*; London (U.K), pp. 777-788.

Bray, J. D. and Rathje, E. M. (1998a). "Earthquake-Induced Displacements of Solid-Waste Landfills." *Journal of Geotechnical and Geoenvironmental Engineering*, **124**(3), 242–253.

Bray, J. D., Rathje, E. M., Augello, A. J. and Merry, S. M. (1998b). "Simplified Seismic Design Procedure for Geosynthetic-Lined, Solid-Waste Landfills." *Geosynthetics International*, **5**(1-2), 203-235.

Bray, J. D., Zekkos, D., Kavazanjian, E., Athanasopoulos, G. A. and Riemer, M. F. (2009). "Shear Strength of Municipal Solid Waste." *ASCE Journal of Geotechnical and Geoenvironmental Engineering*, **135**(6), 709–722.

Brink, D., Day, P. W. and Du Preez, L. (1999) Failure and remediation of bulbul drive landfill: Kwazulu-Natal, South Africa. In: *Proc. of the 7th International Waste Management and Landfill Symposium*; Cagliari (Italy), pp. 4-8.

Chang, M. (2005). "Three-dimensional stability analysis of the Kettleman Hills landfill slope failure based on observed sliding-block mechanism." *Computers and Geotechnics*, **32**(8), 587-599.

Choudhury, D. and Savoikar, P. (2009a). "Equivalent-linear seismic analyses of MSW landfills using DEEPSOIL." *Engineering Geology*, **107**(3–4), 98–108.

Choudhury, D. and Savoikar, P. (2009b). "Simplified method to characterize municipal solid waste properties under seismic conditions." *Waste Management*, **29**(2), 924–933.

Choudhury, D. and Savoikar, P. (2011). "Seismic yield accelerations of MSW landfills by pseudo-dynamic approach." *Natural Hazards*, **56**(1), 275–297.

Chouksey, S. K. and Babu, G. L. S. (2015). "Constitutive Model for Strength Characteristics of Municipal Solid Waste." *International Journal of Geomechanics*, **15**(2), 1–14.

Dvirnoff, A. H. and Munion, D. W. (1986) Stability failure of a sanitary Landfill. In: *proc. of International symposium on environmental geotechnology*; pp. 26-34.

Eid, H. T., Stark, T. D., Evans, W. D., and Sherry, P. E. (2000). "Municipal solid waste slope failure. I: Waste and foundation soil properties." *Journal of Geotechnical and Geoenvironmental Engineering*, **126**(5), 397-407.

Erdogan, H., Sadat, M. M. and Hsieh, N. N.(1986) Stability Analysis of Slope Failures in Landfills: A Case Study. In: *Proc. of 9 th Madison Waste Conforence*; Univ. of Wisconsin-Madison, pp. 168-177.

Feng, S. J. and Gao, L. Y. (2010). "Seismic analysis for translational failure of landfills with retaining walls." *Waste Management*, **30**(11), 2065–2073.

Feng, S. J. and Li, X. (2014). "Three-dimensional Seismic Stability Analysis and Permanent Displacement of MSW landfills." *Geoenvironmental Engineering*, GSP **241**, 149–159.

Hashash, Y. M. A., Musgrove, M. I., Harmon, J. A., Groholski, D. R., Phillips, C. A., and Park, D. (2015). "DEEPSOIL 6.1, User manual." *Board of Trustees of University of Illinois at Urbana-Champaign*, Urbana.

Houston, W. N., Houston, S. L., Liu, J. W., Elsayed, A., and Sanders, C. O. (1995) In-situ testing methods for dynamic properties of MSW landfills. In: *proc. of Earthquake Design and Performance of Solid Waste Landfills*, pp. 73-82

Huang, Y. and Fan, G. (2016). "Engineering geological analysis of municipal solid waste landfill stability." *Natural Hazards*, **57**(2), 217-221.

Hudson, M., Idriss, I. M. and Beikae, M. (1994). "User's manual for QUAD4M." *Center for Geotechnical Modeling, Department of Civil and Environmental Engineering University of California*, USA.

Idriss, I. M. and Sun, J. L. (1993). "User's manual for SHAKE91." *Center for Geotechnical Modeling, Department of Civil and Environmental Engineering University of California*, USA.

Kavazanjian, E. (2001) Mechanical properties of municipal solid waste. In: *Proc. of Sardinia*, **8**(1), 415-424.

Kavazanjian, E., Matasovic, N., Bonaparte, R. (1995). "Evaluation of MSW properties for seismic analysis." *Geoenvironment 2000*, GSP (ASCE), **46**(2), 1126–1141.

Kocasoy, G. and Curi, K. (1995). "The Ümraniye-Hekimbaşi open dump accident." *Waste management & research*, **13**(4), 305-314.

Koelsch, F., Fricke, K., Mahler, C. and Damanhuri, E. (2005) Stability of landfills -The Bandung dumpsite disaster. In: *Proc. of the 10th International Landfill Symposium*; Sardinia.

Koerner, R. M. and Soong, T. Y. (2000) Stability assessment of ten large landfill failures. In: *proc. of advances in transportation and geoenvironmental systems using geosynthetics*, pp. 1-38.

Kramer, S. L. (1996). *Geotechnical earthquake engineering*. 2nd ed. Prentice Hall, 527 Upper Saddle River, NJ.

Matasovic, N., Kavazanjian, E., and Anderson, R. L. (1998). "Performance of solid waste landfills in earthquakes." *Earthquake Spectra*, **14**(2), 319-334.

MATLAB (2011). *Programming, version 7.13*. The Math Works Inc.

Mitchell, J. K., Seed, R. B. and Seed, H. B. (1990). "Kettleman Hills waste landfill slope failure. I: Liner-system properties." *Journal of Geotechnical Engineering*, **116**(4), 647-668.

Ordonez, G. A. (2000). "SHAKE2000: A computer program for the 1D analysis of geotechnical earthquake engineering problems. " *GeoMotions*, LLC.

Pain, A., Choudhury, D. and Bhattacharyya, S. K. (2015). "Seismic stability of retaining wall-soil sliding interaction using modified pseudo-dynamic method." *Geotech. Lett*, **5**(1), 56-61.

Pain, A., Choudhury, D. and Bhattacharyya, S. K. (2016). "Seismic Uplift Capacity of Horizontal Strip Anchors Using a Modified Pseudodynamic Approach." *International Journal of Geomechanics*, **16**(1), 04015025. DOI: 10.1061/(ASCE)GM.1943-5622.0000471

Pain, A., Choudhury, D. and Bhattacharyya, S. K. (2017). "Seismic rotational stability of gravity retaining walls by modified pseudo-dynamic method." *Soil Dynamics and Earthquake Engineering*, **94**, 244-53.

Psarropoulos, P. N., Tsompanakis, Y. and Karabatsos, Y. (2007). "Effects of local site conditions on the seismic response of municipal solid waste landfills." *Soil Dynamics and Earthquake Engineering*, **27**(6), 553-63.

Qian, X. and Koerner, R. M. (2004). "Effect of Apparent Cohesion on Translational Failure Analyses of Landfills." *Journal of Geotechnical and Geoenvironmental Engineering*, **130**(1), 71–80.

Qian, X. and Koerner, R. M. (2009). "Stability analysis when using an engineered berm to increase landfill space." *Journal of geotechnical and geoenvironmental engineering*, **135**(8), 1082-1091.

Qian, X. and Koerner, R.M. (2010). "Modification to translational failure analysis of landfills incorporating seismicity." *Journal of geotechnical and geoenvironmental engineering*, **136**(5), 718-727.

Qian, X., Koerner, R.M. and Gray, D.H. (2003). "Translational failure analysis of landfills." *Journal of Geotechnical and Geoenvironmental Engineering*, **129**(6), 506-519.

Rajesh, B. G. and Choudhury, D. (2016). "Generalized Seismic Active Thrust on a Retaining Wall with Submerged Backfill Using a Modified Pseudodynamic Method." *International Journal of Geomechanics*, 06016023. DOI: 10.1061/(ASCE)GM.1943-5622.0000750

Rajesh, B. G. and Choudhury, D. (2017). "Seismic Passive Earth Resistance in Submerged Soils Using Modified Pseudo-Dynamic Method with Curved Rupture Surface." *Marine Georesources & Geotechnology*. DOI:10.1080/1064119X.2016.1260077

Ramaiah, B. J., Ramana, G. V. and Bansal, B. K. (2016a). "Dynamic Properties of Municipal Solid Waste from a Dump Site in Delhi, India." *Geo-chicago,* GSP **241**, 121–130.

Ramaiah, B. J., Ramana, G. V. and Bansal, B. K. (2017). "Field and large scale laboratory studies on dynamic properties of emplaced municipal solid waste from two dump sites at Delhi, India." *Soil Dynamics and Earthquake Engineering*, **90**, 340–357.

Ramaiah, B. J., Ramana, G. V. and Kavazanjian, E. (2014). "Undrained Response of Municipal Solid Waste Collected from a Waste Site in Delhi, India." *Geo-Shanghai*, GSP **214**, 130–139.

Ramaiah, B. J., Ramana, G. V., Kavazanjian, E., Matasovic, N. and Bansal, B. K. (2016b). "Empirical Model for Shear Wave Velocity of Municipal Solid Waste In Situ." *Journal of Geotechnical and Geoenvironmental Engineering*, **142**(1), 101-106.

Rathje, E. M. and Bray, J. D. (2001). "One-and two-dimensional seismic analysis of solid-waste landfills." *Canadian Geotechnical Journal*, **38**(4), 850-62.

Reddy, K. R. and Munwarbasha, B. (2014) Slope Stability of Waste Dumps and Landfills : State-of-the- Art and Future Challenges. In: *Proc. of Indian Geotechnical Conference;* Kakinada (India). December 18-20, 2014.

Ruan, X. and Lin, H. (2015). "Relationship Between Shear Wave Wavelength and Pseudo-Dynamic Seismic Safety Factor in Expanded Landfill." *Arabian Journal for Science and Engineering*, **40**(8), 2271–2288.

Ruan, X., Sun, S. and Liu, W. (2013). "Effect of the amplification factor on seismic stability of expanded municipal solid waste landfills using the pseudo-dynamic method." *Journal of Zhejiang University SCIENCE* , **14**(10), 731–738.

Savoikar, P. and Choudhury, D. (2010). "Effect of cohesion and fill amplification on seismic stability of municipal solid waste landfills using limit equilibrium method." *Waste management & research : the journal of the International Solid Wastes and Public Cleansing Association, ISWA*, **28**(12), 1096–113.

Savoikar, P. and Choudhury, D. (2012). "Translational Seismic Failure Analysis of MSW Landfills Using Pseudodynamic Approach." *International Journal of Geomechanics*, **12**(2), 136–146.

Seed, R. B., Mitchell, J. K. and Seed, H. B. (1990). "Kettleman hills waste landfill slope failure. II: stability analyses." *Journal of Geotechnical Engineering*, **116**(4), 669-690.

Stark, T. D., Huvaj-Sarihan, N. and Li, G. (2008). "Shear strength of municipal solid waste for stability analyses." *Environmental Geology*, **57**(8), 1911–1923.

Sun, S. L. and Ruan, X. B. (2013). "Seismic stability for landfills with a triangular berm using pseudo-static limit equilibrium method." *Environmental Earth Sciences*, **68**(5), 1465–1473.

Xuede, Q. (2008). "Limit equilibrium analysis of translational failure of landfills under different leachate build-up conditions." *Water Science and Engineering*, **1**(1), 44-62.

Yuan, P., Kavazanjian, E., Chen, W. and Seo, B. (2011). "Compositional effects on the dpynamic properties of municipal solid waste." *Waste Management*, **31**(12), 2380–2390.

Zekkos, D., Sahadewa, A., Woods, R. D. and Ii, K. H. S. (2014). "Development of Model for Shear-Wave Velocity of Municipal Solid Waste." *Journal of Geotechnical and Geoenvironmental Engineering,* **140**(3), 1–14.

Zekkos, D., Bray, J. D., Kavazanjian, E., Matasovic, N., Rathje, E. M., Riemer, M. F. and Stokoe, K. H. (2006) "Unit Weight of Municipal Solid Waste." *Journal of Geotechnical and Geoenvironmental Engineering*, **132**(10), 1250–1261.

Zekkos, D., Bray, J. D. and Riemer, M. F. (2008). "Shear modulus and material damping of municipal solid waste based on large-scale cyclic triaxial testing." *Canadian Geotechnical Journal*, **45**(GEOBASE), 45–58.

Zhan, T. L. T., Chen, Y. M. and Ling, W. A. (2008). "Shear strength characterization of municipal solid waste at the Suzhou landfill , China." *Waste Management*, **97**, 97–111.

The following papers are accepted or communicated for publication, based on the results and analyses presented in this thesis:

Annapareddy, V. S. R., Pain, A. and Sarkar, S. (2017). "Seismic Translational Failure Analysis of MSW Landfills Using Modified Pseudo-dynamic Approach." *International Journal of Geomechanics ASCE*. Ms. No. GMENG-2342R2. (Accepted, in press for publication)

Pain, A., Annapareddy, V. S. R. and Sarkar, S. (2017). "A simplified approach to compute translational factor of safety of MSW landfills using strain dependent dynamic properties under seismic condition." *Natural Hazards*. (Submission ID: NHAZ-D-17-00686)

Pain, A., Annapareddy, V. S. R. and Sarkar, S. (2017). "Effect of local site condition on the seismic stability of municipal solid waste landfills." *Geotechnical Earthquake Engineering and Soil Dynamics V 2018 (GEESDV 2018) conference, ASCE*. (Submission ID: 0069_0101_000050)